

GIS BASED TSUNAMI INUNDATION MAPS; CASE STUDIES
FROM MEDITERRANEAN

DERYA İTİR DİLMEN

JULY 2009

GIS BASED TSUNAMI INUNDATION MAPS; CASE STUDIES
FROM MEDITERRANEAN

A THESIS SUBMITTED TO
THE GRADUATE SCHOOL OF NATURAL AND APPLIED
SCIENCES
OF
MIDDLE EAST TECHNICAL UNIVERSITY

BY

DERYA ITIR DİLMEN

IN PARTIAL FULLFILLMENT OF THE REQUIREMENTS
FOR
THE DEGREE OF MASTER OF SCIENCE
IN
CIVIL ENGINEERING

JULY 2009

I hereby declare that all information in this document has been obtained and presented in accordance with academic rules and ethical conduct. I also declare that, as required by these rules and conduct, I have cited all material and results that are not original to this work.

Name, Last name : Derya Itir Dilmen

Signature :

ABSTRACT

GIS BASED TSUNAMI INUNDATION MAPS; CASE STUDIES FROM MEDITERRANEAN

Dilmen, Derya İtir

MS., Department of Civil Engineering

Supervisor: Prof. Dr. Ahmet Cevdet Yalçın

July 2009, 149 pages

In this thesis, detailed tsunami numerical modeling study was applied to the selected case studies, Fethiye town (Turkey) and Kiparissia-Zakintos-Pylos (Greece) in Mediterranean, using rupture-specific tsunami sources which can generate tsunamis in Mediterranean. As a first step of the study, the general database of Fethiye and Kiparissia-Zakintos-Pylos were integrated to GIS-based environment to organize, analyze and display reliable data from different sources. Secondly, for each earthquake scenario, the tsunami propagation and coastal amplifications were computed by TUNAMI N3 to evaluate the coastal amplifications of tsunamis and understand the tsunami propagation for the cases. As the final step, a study of inundation areas of probable tsunamis in these regions was performed. Available results were used to understand the effects of tsunamis and assist in developing mitigation strategies. Methods and results were presented and discussed.

Keywords: Tsunami, Fethiye, GIS, TUNAMI N3, Inundation

ÖZ

CBS- TABANLI TSUNAMI BASKIN HARITALARININ HAZIRLANMASI; AKDENİZ UYGULAMALARI

Dilmen, Derya İtir

Yüksek Lisans, İnşaat Mühendisliği Bölümü

Tez Yöneticisi: Prof. Dr. Ahmet Cevdet Yalçınır

Temmuz, 2009, 149 sayfa

Bu tezde, TUNAMI N3 benzetim/canlandırma programı, seçilen çalışma alanları Fethiye ve Kiparissia-Zakintos-Pylos Bölgesi'nde kullanılarak depreşim dalgalarının (tsunamiler) oluşumu ve hareketi araştırılmış, bu araştırmanın sonuçlarının kullanıcılar tarafından daha kolay anlaşılıp youmlanabilmesine olanak sağlamak amacıyla, CBS tabanlı baskın haritaları oluşturulmuş, sonuçlar görsel ve işlenebilir biçimde sunulmaya çalışılmıştır.

İlk aşamada, Fethiye ve Kiparissia-Zakintos-Pylos Bölgesi için çeşitli kaynaklardan veriler toplanarak bir veritabanı oluşturulmuştur. İkinci aşamada hem deniz taban topoğrafyası hem de kıyı alanı kara topoğrafyasına ait sayısal veriler kullanılarak benzetim içalışmaları için ayrıntılı sayısal veri tabanı oluşturulmuştur. Üçüncü aşamada ise olası deprem senaryolarından en çok tehlike yaratabilecek olanlar seçilerek benzetim ve canlandırma modelleri yapılmış ve tsunaminin hareketleri modellenmiştir. Sonuçlar CBS tabanlı uygulamalara aktarılarak örnek tsunami baskın haritaları hazırlanmıştır. Yürütülen yöntem ve sonuçlar anlatılarak tartışılmış, tsunami konusunda afet etkilerinin azaltılması için önlem ve stratejiler geliştirilmesine katkı sağlanmıştır

Anahtar kelimeler: Tsunami, Fethiye, GIS, TUNAMI N3, Baskın Haritası

to my nephew Yücel...

ACKNOWLEDGEMENTS

The author wishes to express her deepest gratitude to her beloved, supervisor Prof. Dr. Ahmet Cevdet Yalçınır not only for his great knowledge and experiences he shared but also for his understanding, patience and encouragement throughout her Ms. studies.

Special thanks to the staff of the Coastal Engineering Research Center, especially to Prof. Dr. Ayşen Ergin, and Dr. Işıkhan Güler for enlightening the author with their great knowledge in coastal engineering.

The author would also like to thank Işıl İnel for her friendship and supports and express deep appreciation to Cihan Gürcay who always motivated and helped the author with steadiness at every subject.

The great scientist Prof. Dr. Fumihiko Imamura, has contributed this thesis with his developments in tsunami modeling program, TUNAMI N3.

Assoc. Prof. Dr. Zuhale Akyürek and Serkan Kemeç have contributed this thesis in GIS based applications.

The author's family members Saliha, Hayri, Işıl, Tarkan and Yücel have supported this thesis with their endless love and encouragement throughout the years.

This study is partly supported by European Union Projects, TRANSFER (Tsunami Risk and Strategies for the European Region) and SEHELLARC (Seismic and Tsunami Risk Assessment and Mitigation Scenarios in Western Hellenic Arc).

TABLE OF CONTENTS

ABSTRACT.....	iv
ÖZ.....	v
DEDICATION.....	vi
ACKNOWLEDGEMENTS.....	vii
TABLE OF CONTENTS.....	viii
CHAPTERS	
1. INTRODUCTION.....	1
2. LITERATURE SURVEY.....	3
3. METHODOLOGY	13
4. GIS-BASED TSUNAMI INUNDATION MAPPING FOR FETHIYE ...	18
4.1 Geological Background of the Study Region (Fethiye)	18
4.2 Data Processing applied to the Fethiye Bay	25
4.3 Estimation of Tsunamigenic Data and Simulations	31
4.3.2 Tsunami Simulations for the case study Fethiye	36
5. SUMMARY OF TSUNAMI SOURCE AND SIMULATIONS	69
6. INUNDATION MAPPING FOR THE CASE STUDY “FETHIYE”	71
7. DISCUSSION OF RESULTS AND CONCLUSION FOR “FETHIYE”. 74	
8. GIS-BASED TSUNAMI INUNDATION MAPPING FOR THE ZAKINTOS, KIPARISSIA AND PYLOS TOWNS (TURKEY)	75
8.1 Geological History of Zakintos-Kiparissia-Pylos Region.....	75
8.2 Data Processing.....	77
8.3 Estimation of Tsunamigenic Data and Simulations	79
8.3.1 Estimation of Probable Tsunami Source Mechanisms for the Kiparissia-Pylos-Zakintos region.....	80
8.3.2 Tsunami Simulation for the Zakintos-Kiparrisia-Pylos.....	86
8.3.2.1 Tsunami Simulation of P01	99

8.3.2.2 Tsunami Simulation of P04	104
9. SUMMARY OF THE SIMULATIONS P01 AND P04 SCENARIOS ...	119
10. DISCUSSION OF RESULTS AND CONCLUSION FOR THE PYLOS- ZAKINTOS-KIPARISSIA.....	124
11.SUGGESTIONS FOR THE FUTURE.....	126
REFERENCES	127

LIST OF TABLES

Table 1: Boundaries of the study area (Fethiye).....	19
Table 2: Tsunamis along the Fethiye Bay, from BC 1410 to 2002.....	20
Table 3: The characteristics of the data used.....	25
Table 4: The characteristics of the data used.....	26
Table 5: Selected Sources taken from FORTH,METU-OERC and NOAGI.....	34
Table 6: Selected Sources taken from FORTH,METU-OERC and NOAGI (cont.).....	35
Table 7: Coordinates of the selected gauges in the Domain C and Domain D.....	48
Table 8: Summary of rupture specific simulations performed for the Fethiye.....	70
Table 10: Boundaries of the study area (Pylos-Zakinthos-Kiparissia).....	77
Table 11: Characteristics of the data used.....	78
Table 12: Estimated rupture parameters for the Western Greece.....	81
Table 12: Study Domains.....	87
Table 14: Summary of the P01 Scenario-Input Values.....	119
Table 15: Summary of the P04 Scenario-Input Values.....	120
Table 16: Summary of the water surface elevations at selected gauge point.....	120
Table 16: Summary of the water surface elevations at selected gauge point.....	121

LIST OF FIGURES

Figure 1: Flow chart.....	14
Figure 2: Google Earth (left) and Quickbird (right) images of the Fethiye.....	19
Figure 3: Tsunami triggered earthquakes in the Eastern Mediterranean.....	24
Figure 4: DEM of the Fethiye Region.....	28
Figure 5: Closer view to GIS based layer.....	30
Figure 6: Layers and DEM along the coastal zone of the Fethiye Bay.....	31
Figure 7: The sources in the Eastern Mediterranean estimated by Kandilli and OERC	38
Figure 8: Estimated source, WCS1 Scenario.....	39
Figure 9: The source of WCS3 Scenario.....	39
Figure 10: The source of WCS4 Scenario.....	40
Figure 11: The source of Z26-2 Scenario.....	41
Figure 12: The source of Z29-1 Scenario.....	41
Figure 13. The Scenario 1 from NOAGI.....	42
Figure 14. The scenario 2 from NOAGI	43
Figure 15: The structure of nested Domains (Domain B, Domain C and Domain D) for the simulation of the Fethiye Region.....	44
Figure 16: The sea state at different time steps, distribution of max. (+) and max. (-) tsunami wave amplitudes	45
Figure 17: The sea state at different time steps, distributions of max. (+) and max. (-) tsunami wave amplitudes	46
Figure 18: The sea state at different time steps, max. (+) and max. (-) tsunami wave amplitudes in the Domain D.....	47
Figure 19: Gauge location in the domain c and time histories of water surface elevations for gauges j and k	48
Figure 20: Gauge locations in the Domain D and time histories of water surface elevations for gauges	50
Figure 21: The sea state at different time steps (t=0, 60, 120 and 180 min), and max. (+) and max. (-) tsunami wave amplitudes in the Domain B.....	52
Figure 22: The sea state at different time steps (t=0, 60, 120 and 180 min), and max. (+) and max. (-) tsunami wave amplitudes in the Domain C.....	53
Figure 23: The sea state at different time steps (t=0, 60, 120 and 180 min), tsunami amplitudes in the Domain D.....	54
Figure 24: Gauge locations at Domain C and time histories for the gauges j and k.	55
Figure 25: Gauge locations at Domain D and time histories for the gauge SovalyeW.....	56
Figure 26: The sea state at different time steps, max. (+) and max. (-) tsunami wave amplitudes in the Domain B.....	58
Figure 27: The sea state at different time steps (t=0, 60, 120 and 180 min), max. (+) and max. (-) tsunami wave amplitudes in the Domain C.....	59

Figure 28: The sea state at different time steps, max. (+) and max. (-) tsunami wave amplitudes in the Domain D.	60
Figure 29: Gauge locations at Domain C and time histories for the gauges j and k	61
Figure 30: Gauge locations at Domain D and time histories for the gauge SovalyeW	62
Figure 31: The sea state at different time steps and max. (+) and max. (-) tsunami wave amplitudes in the Domain B.	64
Figure 32: The sea state at different time steps max. (+) and max (-) tsunami wave amplitudes in the Domain C.	65
Figure 33: The sea state at different time steps (t=0, 60, 120 and 180 min), max. (+) and max (-) tsunami wave amplitudes in the Domain D	66
Figure 34: Gauge locations at Domain C and time histories for the gauges j and k.	67
Figure 35: Gauge locations at Domain D of Z26-2 and time histories for the gauges	68
Figure 36: Brief Summary of the applied processes	69
Figure 37: Inundated areas overlayed with Quickbird image in a raster format.....	72
Figure 38: Inundation areas as a result of simulation Z26-2	73
Figure 39: Surficial Seismic Zones. Main faults (red lines), and earthquakes ($M_w \geq 6$) in the SEHELLARC project. (Slejko, 2009)	80
Figure 40: Estimated rupture parameters for the zones p01, p02, p03.....	82
Figure 41: Estimated rupture parameters for the zones p04, p05, p06.....	83
Figure 42: Estimated rupture parameters for the zones p10, p11, p12.....	84
Figure 43: Estimated rupture parameters for the zones p13, p14, p18.....	85
Figure 44: The structure of nested Domains (Domain B, Domain C and Domain D) for the simulation of Kiparissia-Philiatra Region	87
Figure 45: The structure of nested Domains (Domain B, Domain C and Domain D) for the simulation of Pylos Region.....	88
Figure 46: The structure of nested Domains (Domain B, Domain C and Domain D) for the simulation of Zakynthos Region.....	88
Figure 47. The sea state at different time steps and maximum positive and maximum negative tsunami amplitudes in the Domain B (Kiparissia-Philiatra).....	89
Figure 48: The time histories of water surface elevations (in hours) at selected gauge points at Domain C.....	91
Figure 49: The sea state at different time steps and maximum positive and maximum negative tsunami amplitudes in the Domain D (Kiparissia-Philiatra).....	92
Figure 50: Time histories of water surface elevations at selected gauges at Domain D	94
Figure 51: The time histories of water surface elevations (in hours) at selected gauge points at Domain C.....	96
Figure 52: Propagation of tsunami for specific times (t=16, 32, 48 and 80 min), max (+) and max (-) tsunami wave amplitudes	97
Figure 53: The time histories of water surface elevations (in hours) at selected gauge points at Domain D, Pylos	99
Figure 54: The time histories of water surface elevations (in hours) at selected gauge points at Domain C, Zakynthos.....	101
Figure 55: Propagation of tsunami for specific times, maximum positive and maximum negative wave amplitude in the Domain D.....	102

Figure 56: The time histories of water surface elevations (in hours) at selected gauge points at Domain D, Zakynthos	104
Figure 57: The time histories of water surface elevations (in hours) at selected gauge points at Domain C.....	106
Figure 58: The Sea State at Different Time Steps and max (+) and max (-) tsunami amplitudes in the Domain D.....	107
Figure 59: The time histories of water surface elevations at selected gauge points at Domain D	109
Figure 60: The time histories of water surface elevations (in hours) at selected gauge points at Domain C.....	111
Figure 61: Propagation of tsunami for specific times. Distributions of max. (+) and max. (-) tsunami wave amplitude.	112
Figure 62: The time histories of water surface elevations (in hours) at selected gauge points at Domain D, Pylos	114
Figure 63: The time histories of water surface elevations (in hours) at selected gauge points at Domain C, Zakynthos.....	116
Figure 64: Propagation of tsunami for specific times. Max (+) and max (-) wave amplitude.	117
Figure 65: The time histories of water surface elevations (in hours) at selected gauge points at Domain D, Zakynthos	118
Figure 66: Flow depth distribution from 0.5 to 4.5 for the simulation of P01 in Western Greece	122
Figure 67: Flow depth distributions between 4.5 and 5	123
Figure 68 : Flow depth distributions greater than 4.5	123

CHAPTER 1

INTRODUCTION

The word “Tsunami” first introduced to the literature by Japanese after the Meiji Tsunami occurred in 1896. Shallow focus earthquakes in subduction zones, landslides, volcanic or nuclear explosions and meteorites are the most frequently tsunami generated reasons. Among tsunami generated reasons, in the case of earthquake generated tsunamis, the energy of the rupture is transferred to the water and causes displacements in the sea level over the affected region. This transmitted energy results in tsunami generation and propagates from the source region as long period waves.

Coastal communities can face with the tragic loss of lives and extensive property damages by tsunamis. The damage of a tsunami can be summarized as i) deaths and injuries ii) property damages in different levels iii) environmental pollution from drifting materials, oil, or other substances iv) spread of disease.

In recent years, the earthquake with a magnitude of 9.3 in the northwest coast of Sumatra on December, 26, 2004 triggered such a tsunami that engenders deaths, injuries and property damages along the Indian Ocean coastline. This event became a pioneer for the scientific studies based on the exchange and enhancement of existing data, development and utilization of available computational tools to abate the losses of tsunamis.

Overall world, tsunamis occur most frequently in Pacific Ocean. Despite tsunamis’ low frequency of occurrence, there are numerous tsunamis encountered in the Mediterranean basin due to earthquakes or/and submarine ground failures and volcanic eruptions of volcanoes found in this region.

The aim of this thesis is to numerically model a rupture specific tsunami by articulating TUNAMI N3 tsunami simulation tool and ArcGIS 9.3 mapping and analysis tool along the Fethiye (Turkey) and Pylos, Zakintos, Kiparissia Towns (Kiparrissia Gulf, Greece) regions to be able to comprehend the behavior of tsunami, develop GIS-based tsunami inundation maps and estimate the damages caused by the tsunami to assist in establishing mitigation strategies

Incorporation of the information generated from the inundation maps provides geocoding of the potentially affected areas which affords policy makers an additional level of preparedness.

In this thesis, the computational capabilities of TUNAMI N3 numerical model were combined with graphical abilities of GIS in spatially organizing, analyzing and displaying modeling results of TUNAMI N3. The general data was collected from different sources and a study of inundation areas of probable tsunamis in Fethiye town (Turkey) and Kiparissia-Zakintos-Pylos (Greece) regions was done by given appropriate computational tools. These regions will be directly affected from tsunamis that can be triggered by the rupture of earthquakes in Mediterranean. The final product is the map of inundated areas for maximum amplitudes of waves throughout these regions and the estimation of risk due to tsunami in the inundation zone.

A literature survey was given in Chapter 2. In Chapter 3, object, scope and methodology of the thesis were explained. Data processing for the case study Fethiye was stated in Chapter 4. Chapter 5 is the analysis of the results and summary for this case study. Chapter 6 includes the discussion and conclusion. Chapter 7 is explaining data processing for the case study Kiparissia-Zakintos-Pylos. Chapter 8 is the analysis of the results and summary for this case study and the last chapter is the general discussion and conclusion of the thesis studies.

CHAPTER 2

LITERATURE SURVEY

The scientific investigations on GIS-based tsunami inundation mapping in Mediterranean can be divided into i) Analytical and Experimental Studies on Tsunamis ii) Numerical simulation of tsunamis and iii) GIS-based mapping applications of tsunamis

The analytical and experimental studies on tsunamis since 1967 were given by taking the article “Amplitude Evolution and runup of Solitary Waves on a Sloping Plane” as a reference. Studies were done by Shuto (1967), Gjevik & Pedersen (1981), Pedersen and Gjevik, (1983), Kim et. al., (1983), Synolakis (1987), Pelinovsky and Mazova (1992), Synolakis and Skjelbreia (1993), Titov (1995), Pelinovsky et al. (1996), Kanoglu (1996), Kanoglu and Synolakis (1997), Lin et. al. (1999), Carrier and Yeh (2002). Experimental studies of solitary waves were investigated by Hall and Watts (1953), Pedersen and Gjevik (1983) and Synolakis (1987), Shankar and Jayaratne (2002), Lee and Raichlen, (2002).

Numerical simulations of tsunamis are essential in fundamental and applied research activities to accomplish basic aspects of wave generation, propagation and inundation. They are commonly based either on the Boussinesq or on the nondispersive shallow water equations Tinti, (1994). Titov (1995), Synolakis, (1995a, 1995b, 1998), Imamura (1995), Yalciner et al. (2001), Dodd (2002), Lynett et. al. (2002), Lee and Raichlen (2002), Maiti and Sen (1999) are some references of numerical studies on tsunamis. The combination for graphical user interface with geospatial data capabilities linked with numerical modeling software of tsunamis has provided modelers a new platform to transfer numerical modeling results into a spatially referenced, digital environment.

There are several types of numerical models done for estimating numerical simulation of non-linear waves of tsunamis. Fifteen of these models were explained briefly. These are: TSUNAMI CEA/DASE, TsunamiClaw, Coulwave, COMCOT, UBO-TSUFD&UBO-TSUFD-VB, UBO-TSUFE, TSUNAMI-SKREDP, 1HD, H2D DPWAVES, GLOBOUSS, C3 Tsunami Model, MOST, TUNAMI N1, N2, N3 and lastly NAMI DANCE. The following information about numerical models were adapted from the report of EU Funded TRANSFER Project Work Package 5, Deliverable 5.8

TSUNAMI CEA/DASE[®] is developed by *Atomic Energy Commissariat (CEA)* and *France's Geophysical Laboratory (LDG)* for operational and research purposes. The model is certified, fully tested. In the model, nonlinear shallow water wave equations are used and finite difference method are used. Okada elastic dislocation and any surface deformation can be generated. It is observed that it can include as many sub faults as necessary. The model is developed in FORTRAN language and it is being applied for the scenarios in French Polynesia, Pacific Ocean, Indian Ocean and Mediterranean Sea.

The model TsunamiClaw[®] is developed by *University of Washington (USA)*. The model uses nonlinear shallow water equations as equation type; finite volume, Riemann solvers as numerical schemes and 2D+1 rectangular mesh with adaptive refinement. It allows wetting & drying. The source for the model is multi segment fault model and any surface deformation in space and time. The model can use up to six nested levels and adaptive mesh refinement is observed. The programming language is Fortran 77 and operating systems are Unix, Linux. The model is applied to Sumatra for tsunami propagation, run-up and inundation.

The model Coulwave[®] is developed by *Texas A&M University (USA)* and is validated through benchmark problems. The model uses finite volumes, fourth order, implicit, domain decomposition of Boussinesq equations as equation type, MPI as numerical schemes and cartesian, structured as mesh/grid type. It allows wetting & drying. Wave breaking can be observed in the model. The programming language is Fortran 90 with a command driven/batch run user interface.

The model is used by Inundation Science & Engineering Cooperative and TRANSFER partners. Cox(2008) compared the physical and numerical tsunami model simulations for Seaside, Oregon using the Lidar-measured laboratory beach and Coulwave and STOC numerical models to see the effect of macro- roughness and sharp topographic changes.

COMCOT[®] is a model developed in *Cornell University*, USA. It is tested (compared with both experiments and field data). The model uses shallow water equations, finite difference method and leap-frog scheme method. Cartesian or spherical coordinate systems can be chosen and grid system is staggered, nested grids. The generation can be caused from a submarine landslide, elastic fault model and any surface deformation. The model is observed as fast, balanced between efficiency and accuracy. The multi generation mechanism is also an advantage. The programming language is FORTRAN 90. The model is applied to tsunami propagation, run-up and inundation, tsunami mitigation fields.

The models UBO-TSUFDF & UBO-TSUFDF-VB[®] are developed for research purposes by *Università di Bologna, Dip. di Fisica, Settore Geofisica*, Italy. The equations used in this model are shallow water wave equations. As the numerical scheme, finite difference and leap frog scheme methods are used with a rectangular constant grid domain and with cartesian and geographical coordinates. Multi-fault vertical co- seismic displacements computed through Okada's formulas and corrected for bathymetric effects. The model is developed in Fortran 90/95 programming language with a command line interface. It is being applied for the scenarios in the Mediterranean Sea, 2004 Sumatra tsunami, 2006 Java tsunami, and scenario tsunamis in the Indian Ocean.

UBO-TSUFDF[®] is other model developed by *Università di Bologna, Dip. di Fisica, Settore Geofisica, Italy* for research purposes. The equation type used in this model is shallow water wave equations. As the numerical scheme, finite element method and two step time integration methods are used. Triangular elements and cartesian coordinate system on a fixed boundary grid are used as mesh/grid type.

In the model, multi-fault vertical co-seismic displacements are computed through Okada's formulas and corrected for bathymetric effects in the case of an earthquake source. Impulses are computed through UBO-TSUIMP[®] in case of moving body. Loss of energy due to the interaction with the boundaries and with sea bottom is observed. Coriolis force can be included in the model. The model is developed in Fortran 77 programming language with a command line interface. The program is being applied for the scenarios in the Mediterranean Sea (simulation of historical events in the Adriatic Sea, Ionian Sea, Tyrrhenian Sea, 1999 Izmit bay earthquake-induced tsunami, and scenarios in the Gulf of Corinth and of Mediterranean-wide tsunamis), and in the Indian Ocean (2004 Sumatra, 2006 Java, and several scenarios).

The model TSUNAMI-SKREDP[®] is developed by *Norwegian Geotechnical Institute/ ICG*, Norway. The model is certified and fully tested (grid refinement, comparison with analytic solutions, comparison with results from independent codes, careful assessment of features). The equations used in this model are shallow water wave equations. As the numerical scheme, finite difference, second order, explicit methods are used. Any initial sea surface deformations, prescribed source functions for slides and earthquakes or input from files are the generation input for this model. The model is developed in FORTRAN 77 programming language with a Norwegian command driven interface. The model has been applied to North East Atlantic, Arctic Ocean, Norwegian Fjords, Mediterranean, Indian Ocean, South China Sea, hydropower reservoirs in Norway and The Philippines.

The model IHD[®] is developed by *Department of Mathematics, University of Oslo/ ICG*, Norway. It is fully tested (grid refinement, careful assessment of features, inter-comparison of models, check against analytical solutions, benchmarks). The model uses various Boussinesq formulations & full potential theory as equation type; finite difference and element method, boundary integral method, Eulerian and Lagrangian coordinates as numerical schemes and adaptive mesh as mesh/grid type. But assessment of grid resolution is required. It includes the dispersive effects and non-linear effects in tsunami generation and propagation. The programming language is Fortran 77 and operating systems are Unix, Linux with a command driven and mixed

language interface. The model is used by University of Oslo, NGI, and ICG. The model is applied to North East Atlantic, Arctic Ocean, Norwegian Fjords, Indian Ocean, and Mediterranean.

The model H2D[®] is developed by *Universidad de Cantabria*, Spain. The shallow water wave equations are used in calculations. Numerical scheme of the program is finite difference, implicit alter direction. Upwind for the advective methods are used.

The coordinate system is Cartesian and the grid type is rectangular quadratic cells. The generation model is Gaussian hump. The model accounts for Coriolis, non linear advection, bottom friction, horizontal eddy viscosity and wetting and drying. The model is developed in FORTRAN 77 programming language with a command driven interface. The model has been applied to Mediterranean Sea, Algerian tsunami simulation, Alboran sea.

The model DPWAVES[®] is developed by *Norwegian Geotechnical Institute/ ICG*, and is validated through basin oscillations, and solitary waves. The model uses implicit second order finite elements as numerical schemes and regular or irregular finite elements and adaptive mesh as mesh/grid type. It does not allow wetting & drying. The model is flexible with respect to type of elements of adaptive meshes. The programming language is Diffpack (C++ library) and operating systems are Unix, Linux with a command-driven user interface. NGI applied the model to Indian Ocean, Paleo Barents Sea for research and to Norwegian fjords commercially for risk assessment.

The model GLOBOUSS[®] is being developed by *Department of Mathematics, University of Oslo/ ICG Norway*. It is thoroughly tested (analysis of properties, grid refinement, inter-comparison of models, analytical solutions). The model uses various Boussinesq equations with Coriolis terms as equation type; finite differences, implicit method and ADI iteration for implicit equations as numerical schemes and Arakawa C grid, geographical and Cartesian coordinates as mesh/grid type. Wetting & drying is not allowed as DPWAVES. The model is suitable code for dispersive transoceanic propagation. The programming language is again Fortran 77 and operating systems are Unix and Linux with a command driven interface in

English. The model is used by University of Oslo, NGI, and ICG and applied in most oceanic regions with major fault zones worldwide.

C3 Tsunami Model is developed by *Universidad de Cantabria*, Spain. It is validated through benchmark problems. The model uses shallow water wave equations as equation type; finite difference method with leap-frog scheme method (FD), finite Volumes (VOF) applied in flooding areas (near coast as numerical schemes and Cartesian or spherical coordinate system and embedded grids as mesh/grid types. It allows wetting & drying. The generation model is Okada 1985 for co-seismic tsunamis. C3 model takes advantages of the best capabilities of COMCOT model and TSUNAMICLAW model. C3 is a hybrid finite difference-finite volume method which balances between efficiency and accuracy. The programming language is Fortran 90 and operating systems are Windows, Linux. The users can input parameter files. The model is applied in the Cadiz test site for TRANSFER project

In 1997, Method of Splitting Tsunamis (MOST) was developed by *National Oceanographic Atmospheric Administration NOAA/Pacific Marine Environmental Laboratory*. MOST model was used for the Pacific Ocean for real time tsunami forecasting. The model's database contains 246 model scenarios for unit sources that cover historically most active subduction zones around the Pacific. It stores all simulation data for each unit solution, including amplitudes and velocities for each offshore location (Titov, 2005).

In this model, seismic parameter estimates and tsunami measurements are used to analyze a pre-computed generation/propagation database and select a linear combination of scenarios that most closely matches the observational data. This produces estimates of tsunami characteristics in deep water which then can be used as initial conditions for a site-specific inundation algorithm

Borrero et. al. (2006) computed tsunami propagation and inundation areas and flow depths with MOST model for Sunda megathrust for two tsunamis occurred in 1797 and 1833 and for four plausible scenarios. According to Synolakis et. al. (2009), the inundation distance is highly dependent on bathymetry and topography. In their articles, they presented the inundation maps developed for Southern California by

using MOST numerical model.

In 1991, Numerical Analysis Model for Investigation of Near-field tsunamis No.1. , TUNAMI-N1[®], was developed by Prof. Fumihiko Imamura et.al. in *Disaster Control Research Center in Tohoku University, Japan*, for Tsunami Inundation Modeling Exchange (TIME) Project using Fortran Program. It continued to be enhanced and TUNAMI-N2, TUNAMI-N3 were developed for the simulation of the propagation of long waves. The computer program TUNAMI N2[®] determines the tsunami source characteristics from earthquake rupture characteristics. It is one of the key tools for developing studies for propagation and coastal amplification of tsunamis in relation to different initial conditions. It computes all necessary parameters of tsunami behavior in shallow water and in the inundation zone allowing a better understanding of the effect of tsunamis. It solves nonlinear form of long-wave equations and depth averaged velocities with bottom friction by finite difference technique for the basins of irregular shape and bathymetry and provides us a very convenient tool to simulate tsunamis. Shuto, Goto and Imamura (1990), Goto and Ogawa (1992), Imamura (1995), Goto et. al. (1997), Yalciner et. al. (2001,2002), are some of the studies that used TUNAMI-N2.

NAMI DANCE is one of these computational tools developed in C⁺⁺ programming language between Russian and Turkish Scientists in combination of identical computational procedures and TUNAMI-N2. Non-linear shallow water equations are used as numerical model since it gives results in less time and less error. The model solves the governing equations by the finite difference technique with leap-frog scheme. It can compute the wave propagation at all locations, even at shallow and land regions within the limitations of grid size (Zahibo et.al., 2003)

TUNAMI-N3 is developed by *Disaster Control Research Center, Tohoku University, Japan and Ocean Engineering Research Center, Middle East Technical University (METU), Turkey*, for operational and research purposes. The equation type used in this model is shallow water wave equations. The numerical schemes are finite difference method and leap frog scheme. Model is generated for fault dislocation based on Okada, Mansinha & Smyle. The main feature of the model is tsunami

propagation and tsunami run-up in nested grids. The model is developed with FORTRAN language and can be used in operating systems Dos, Windows or UNIX. The model has been applied to 1833 Sumatera (Bengkulu) Tsunami, 1996 Toli-toli (Sulawesi) Tsunami, 1883 Krakatau Tsunami, 1996 Biak Tsunami, 1935 North Sumatera Tsunami, 2000 Banggai Tsunami, 1992 Flores Tsunami, 2004 Aceh Tsunami, 1994 East Java Tsunami, 2006 South Java Tsunami, Scenarios for Fethiye and Pylos and Caribbean Sea. As for the use of GIS based tsunami inundation applications, the following investigations were performed:

A history of GIS constitutes a collaboration of different disciplinarians starting from 1960s with Howard Fisher's creation of SYMAP (Synaptic Mapping System). Prior to the advent of GIS, inundation maps were developed with computer aided drafting software in the form of water surface elevations overlaid onto topographic maps. The transition from manual map preparation to automated delineation procedures is becoming more practice. Through 1970, with the developments in computer science, the computer handling of geographic information increased and the new ideas and principles were created (Foresman, 1998). In 1981, Environmental Systems Research Institute (ESRI) published ArcInfo, and in 1992 ESRI released ArcView which initiated the use of GIS in all fifty states.

GIS allows maps to be used in interchangeable platforms and subsequently by many agencies. Inundation areas from multiple tsunami scenarios can be overlaid within GIS allowing for graphical comparison of scenario output. Furthermore, with the incorporation of additional geospatial datasets (buildings, population etc.) both risk and damage assessments associated with a tsunami can be easily assessed.

According to Zerger (2002), modeling of inundation for risk management strategies is important for evacuation planning, developing urban zoning that accounts for inundation, using as an educational tool to inform citizens of the risks present in their community, identifying risk for possibly establishing insurance premiums, Developing building codes to minimize the impacts, cost-benefit analysis for developing mitigation strategies and managing post-disaster recovery. GIS provides opportunity the emergency and risk management to be identified prior to an incident.

Disaster events, can be modeled and displayed in GIS. In all stages of emergency management, the appropriate data has to be gathered, organized, and displayed logically to determine the size and scope of emergency management programs. During an actual emergency it is critical to have the right data, at the right time, displayed logically, to respond and take appropriate action. By utilizing a GIS, all departments can share information through databases on computer-generated maps in one location. (Johnson, 2000)

The integration of GIS and tsunamigenic earthquake data can be done in three ways: tsunamigenic earthquake data can be input for a model independent form GIS. The results of model can be integrated with spatial and thematic data of the selected region. The data can be input to GIS. Both input and output can be integrated into GIS. In Zbindens et. al. (2003), the hazard modeling was done by taking input from WIZMAP and imported to ArcGIS environment.

Wood and Good (2004) claim that GIS is an ideal tool to integrate natural, socioeconomic and hazards information. Because of this property, it is also ideal for supporting community hazard planning efforts. Therefore in their articles they assessed the vulnerability of an Oregon port and harbor community to earthquake and tsunamis. Joy Sanyal and Xi Lu (2009) make a qualitative hazard intensity study of Gangetic West Bengal, India by using GIS in flood hazard mapping to show the flood prone areas in the region. According to results of this study, using GIS is a simple and cost effective way to create flood hazard map.

Chandrasekar et.al. (2007) investigates tsunami inundated areas for Kanyakumari district, India using GIS techniques to determine the effect of tsunami on coastal environment. Inundation distances were carried out by combining cadastral data and satellite images. Tsunami height was measured manually along coastline by collecting data with GPS, leveling and surveying equipment. These data were added to superimpose cadastral data and satellite image of the region. Tsunami inundation was higher in shallow near shore bathymetry and flat onshore topography since such regions are not unable to resist tsunami impact.

“Human life and other values (property, habitat, wildlife, etc.) at risk from emergencies can be quickly identified and targeted for protective action. Once information is mapped and data is linked to the map, emergency management planning can begin. GIS allows emergency management needs to be identified prior to an incident. Disaster events, such as wildfires, tsunamis, floods, earthquakes, hurricanes, epidemics, chemical cloud dispersion, and oil spills, can be modeled and displayed in GIS. Emergency management personnel can use modeling for training, for actual tactical deployment during a disaster, or to analyze the consequences of a possible disaster. The use of this technology takes emergency management planning information off the shelf for utilization by response personnel for real-world operations. In short, the thoughtful application of a GIS can take much of the panic and surprise out of emergencies”(Johnson,2000).

In this thesis, all stages of GIS-based tsunami inundation mapping was conveyed and given in the following sections for Fethiye (southwest of Turkey) and Pylos-Zakintos- Kiparissia (northwest of Greece) Towns.

CHAPTER 3

METHODOLOGY

Tsunami modeling and inundation mapping needs accurate, reliable data and computational tools. The necessary data consists of bathymetric/topographic data and rupture parameters. The computational tools must be valid and verified. The methodology was tried to be explained with flow charts and phases.

Flow chart of the GIS-based tsunami inundation mapping was shown in *Figure 1*. The spatial data processing, tsunamigenic earthquake data processing, model visualization and analysis results, satellite image processing, data integration and analysis, inundation mapping are the main components that will be discussed with the applications to different study areas in the following sections.

Since the most effective way to model, analysis and visualize the results of numerical models are by geographical position in GIS, in all stages of this thesis, GIS based applications were used. Input data were integrated into GIS based environment. The available results were incorporated to ArcGIS 9.3 to develop inundation maps and determine the level of impact and the vulnerable areas to improve the accuracy and effectiveness of decision making mechanisms for public safety in study regions.

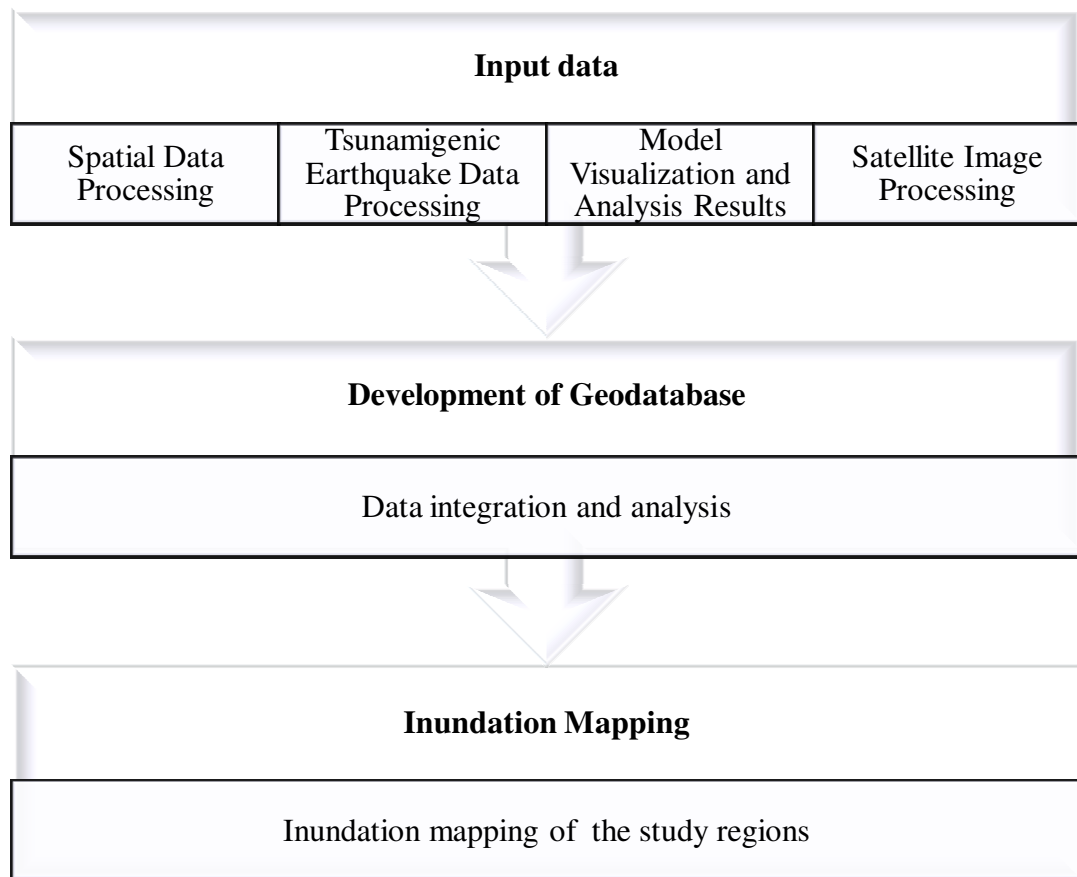


Figure 1: Flow chart

The following phases were considered during the thesis:

Phase 1: Catalogue and literature survey on the historical tsunamis

- i) The historical time for which tsunami reports and records covered
- ii) Evaluation of reliability of the historical documents of each event. This information can be taken from the respective catalogues or publications
- iii) Estimates of run-up heights and inundation distances of historical events from the collected data and information. The paleotsunami studies (coastal trench study) by the expert paleotsunami geologist(s) at the selected region(s) must be also kept in the agenda which may provide additional findings about the deposits of some historical tsunami events for comparison and assessment of the level of historical events.

Phase 2: Data Processing

The reliable bathymetric and topographic data in highest resolution are the most important parameter for accurate modeling efforts. This data must be collected from available navigational charts, conventional and multi beam bathymetric nearshore and offshore measurements (if available), digital elevation models, satellite images. Additionally, the coordinates of existing shoreline, nearshore bathymetry and land topography must be measured directly at site and to be added to the bathymetry topography database. The database must also be in sufficient resolution in GIS, especially nearshore and shallow regions. The digital form of bathymetry/topography data for a specified region must be developed

Phase 3: Development of the urban city plan

The distribution of land, coastal and marine structures must be located in the plans. An example list of important marine structures of each unit can be; residential, official building(s), social centers, reactor building(s), industrial plants, open areas, health services, fire station, communication center, coastal structures (piers, breakwaters, berthing structures, coastal protection structures, harbor, shelters), areas of solid wastes, treatment plants, etc.

Digital database of coastal, marine and other important structures in GIS must be covered.

Phase 4: Estimation of Tsunamigenic Data and Simulations

Characteristics, dimensions and locations of near field and far field submarine and/or coastal faults and landslide prone regions must be identified. This is a difficult task and needs consultation from marine geologists and earth scientists in international level since uncertainties in the underlying fault rupture and landslide processes are quite high. The fault maps, possible characteristics of each fault or segment of each fault must be covered.

Phase 5: Computation of the tsunami source parameters from estimated rupture characteristics

Some tsunami models directly compute the tsunami source (initial fluid displacements) and velocity fields. If the available code does not have the module to determine tsunami source, the user must compute the source from the rupture parameters separately by other codes. In any case, the tsunami source of any selected scenario must be described with figures.

Phase 7: Determination of study domain(s) for numerical modelling of tsunami

The borders of the nested study domains covering near field and far field must be determined. The spatial grid size of each domain must be obtained. It is suggested that the grid size of largest domain can be maximum 2 arc minute (~3700m) and smallest domain can be around 20 m.

Digital data of bathymetry and topography of each study domain in sufficient accuracy and required format must be covered in the report with discussions. It is strongly recommended that the shoreline data used in the model must fit well with the real shoreline.

Phase 8: Simulation and computation of all necessary tsunami parameters

Data of the initial conditions of tsunami source (i.e., initial fluid displacements and velocity fields) provided from Phase 7, will be used for the propagation of tsunamis in the open sea and their coastal amplification and run-up at shallower regions and

on land in the study regions. This phase is the most important phase of tsunami modeling, since it will give the base data of inundation mapping.

Phase 9: Inundation Mapping

The maps providing the information of the estimated hazard zones and must be prepared according to the numerical outputs of tsunami modeling coming from Phase 8. These maps provide information for the risk assessment and mitigation strategies.

CHAPTER 4

GIS-BASED TSUNAMI INUNDATION MAPPING FOR THE FETHIYE TOWN (TURKEY)

In this chapter, geological background of the study region, data process, estimation of tsunamigenic earthquake data and numerical tsunami simulations. The first four phases given in the methodology were applied and discussed in this chapter.

4.1 Geological Background of the Study Region (Fethiye)

Fethiye is situated in the eastern reaches of Mediterranean Coast of Turkey. Due to its proximity to the subduction zone of Euroasian plate and African plate, it is highly prone to earthquakes, volcanic activities and proceeding tsunamis which motivate this research and makes this study worthwhile for mitigation purposes along Fethiye Region. The boundaries of the study region (Fethiye) was given in *Table 1*.

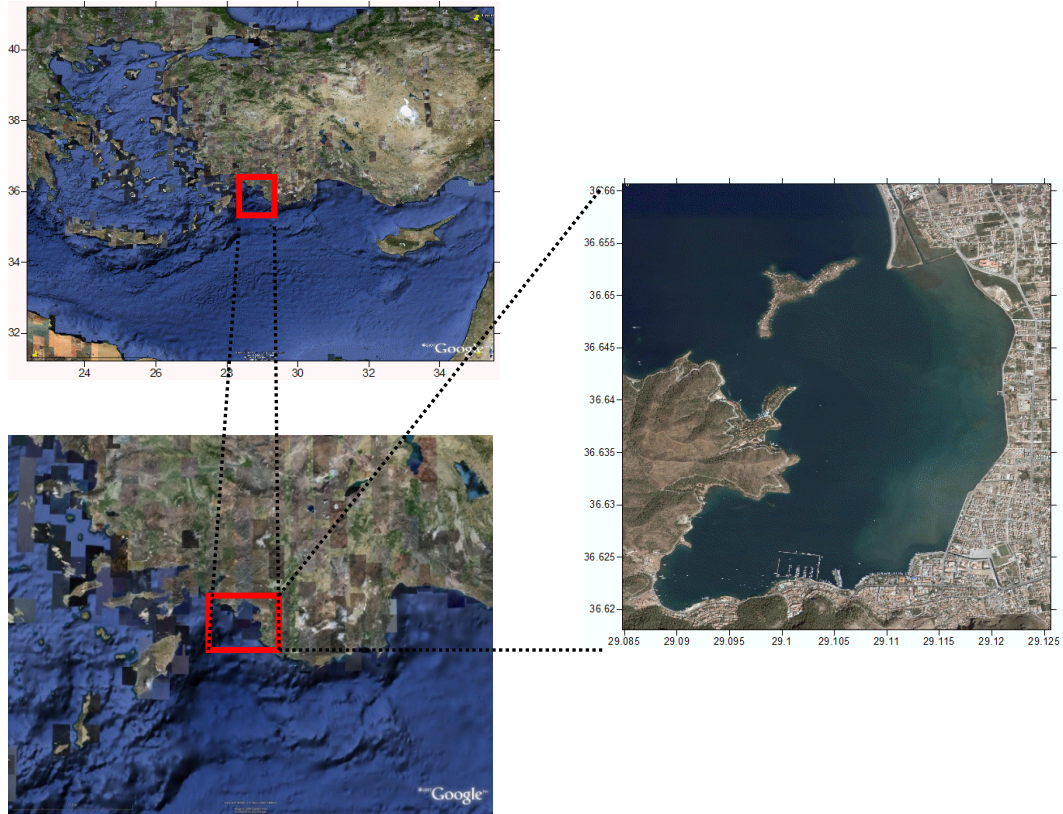


Figure 2: Google Earth (left) and Quickbird (right) images of the Fethiye

Table 1: Boundaries of the study area (Fethiye)

Coordinate System	GCS_WGS 84	
Longitude	29.08482348°E	29.12561811°E
Latitude	36.61809557°N	36.66064482°N

The investigation of historical tsunami events are necessary and effective tools for appropriate tsunami numerical modeling. Historical documents and geological investigations in the Eastern Mediterranean basin reveal that earthquakes, submarine landslides and tsunamis have been occurred because of the high seismicity, volcanic eruptions and steep slope in Mediterranean region over 3000 years. Evidences of tsunami deposits were found in Fethiye Bay by Cita et. al. (1996), Yalciner et.al. (2007), Papadopoulos et.al. (2009) as a result of geological investigations.

The compilation of reliable tsunami database especially for the Eastern Mediterranean region is essential in tsunami-related studies of wave numerical simulation, inundation mapping and risk assessment. Tsunamis in the Eastern Mediterranean were investigated by Soloviev (1989), Papazachos (1990), Cita and Rimoldi (1996), Cita et. al. (1996), Guidoboni (1997), Tinti and Maramai (1998), Yalciner et.al. (1999), Mckoy and Heiken (2000), Minoura et.al. (2000), Rebesco et.al (2000), Cita and Aloisi (2000), Altinok et.al. (2001), Papadoupulos et.al. (2001), Dawson et al. (2003), Salamon et.al (2007). Tsunami catalogues for the Mediterranean Sea were compiled by Galanopoulos (1960), Ambraseys (1962), Antonopoulos (1979), Papadopoulos and Chalkis (1984), Amiran et.al. (1994), Tinti and Maramai (1996), Soloviev et.al. (2000), Papadopoulos (2002), Tinti and Maramai (2004), Fokaefs and Papadopoulos (2005), Yolsal et.al. (2007). Recently, Altinok (2008) compiled historical documents in the Eastern Mediterranean between BC 1410-AC 1999 with inclusion of distant, local, volcanic and landslide generated tsunamis. It includes the list of them with date, region, cause, relevancy, approximate epicenter and magnitude of tsunamigenic earthquakes and other triggering mechanisms (Altinok(2000), Papadopoulos(2001), Papadopoulos(2007)). Altinok also modified the reliability level classification of a tsunami which was investigated by Iida (1984), Soloviev (1990) and, Tinti and Maramai (1996). Among 130 events, 65 events are well-documented and 44 events affected the Fethiye region. These 45 events were extracted from historical documents of Altinok (*Table 2*). Reliability levels were given according to studies of Modified Iida Scale (1984), Soloviev (1990), Tinti and Maramai (1996).

Table 2: Tsunamis along the Fethiye Bay, from BC 1410 to 2002

Time	Region	Reliability	Cause	Latitude	Longitude	EQ Magnitude
BC 1410	Aegean Sea, Northeast of Crete	3	VA	36.5	25.5	
B.C. 220/222/227	Rhodes, Cyprus, Corinth	2	ER	36.5	28	7.5

Table 2. Tsunamis along the Fethiye Bay (cont.)

		1	VA	36.5	25.5	6.5
53/62/66	Cnossos-Crete, Leban	4		34.8	25.5	7
68	Demre, Patara-Lycia	2	EA			
142	Fethiye Gulf, Rhodes, Kos, Seriphos, Syme Isl.	2	ER	36.3	28.6	7.6
261-262	Southern coasts of Anatolia	2	EA	36.5	27.8	
303/304	Sidon, Tyre- Syrian	2-3				
348-349	Beirut-Leban	1		33.8	35.5	
365	East Mediterranean, Crete, Greece, Adriatic coasts, Alexandria, West Anatolia	4	ER	35	23	8.3
551	Lebanese coast	4	EA+E L	33.8	35.1	
554	South west coasts of Anatolia, Kos Isl., Mandalya Gulf	4	ER	36.8	27.3	7
991	Damascus, Baalbek	2-3	EA+E L	33.45	36.3	
1068	Jerusalem	3	EA	32.57	35.28	6
1170	Damascus region	4	EA	34.40	35.8	7.7
1303	Eastern Mediterrenean, Rhodes, Crete, Peloponnesus	4	ER	35	27	8
1404	Aloppo-Tripoli	2-3	EA+E L	35.15	35.95	
1408	Syria-Cyprus	2-3	EL	35.67	36.17	6
1481	Rhodes, south-western coasts of Anatolia, Crete	4	ER	36.43	28.22	6.5
1494	Heraklion-Crete	3	ER	35.5	25.5	7.2
1546	Eastern Mediterrenean	4	EA			
1609	Rhodes, Eastern Mediterrenean	4	ER	36.4	28.3	7.2
1612	Northern Crete	2		35.5	25.5	
1650	Santorini, Patmos, Sikinos Isls., Northern Crete	4	VA	36.4	25.4	7
1672/1673	Santorini and Cyclades, Bozcada, Kos Isl.	2	ER	36.5	25.5	
1741	Rhodes	4	ER	36.2	28.5	7.3
1772	Chios, Foca	2	ER	38.8	26.7	6.4

Table 2. Tsunamis along the Fethiye Bay (cont.)

1846	Izmir, Aegean Sea	2	ER			
1851	Fethiye, Kaya-Mugla, Rhodes	4	ER	35.5	28.7	7.1
1851	Fethiye Gulf, Rhodes	3	ER	36.4	28.7	
1851	Rhodes	3	ER	36.4	28.7	
1855	Fethiye Gulf	4	ER	36.6	29.1	
1856	Rhodes, Crete, Chios	4	ER	35.6	26	8.2
1863	Rhodes	1	ER	36.5	28	
1866	Santorini Isl.	2	ER	36.4	25.3	6
1866	Chios	3	ER	38.25	26.25	
1867	Lesvos	4	ER	39.1	26.5	6.8
1926	Rhodes, Southeast of Turkey, Fethiye, Heraklion	4	ER			8
1933	Kos Island	2	ER	36.8	27.3	6.6
1948	Karpathos-Dodocanese	4	ER	35.5	27.2	7.1
1953	South coasts of Turkey	1	ER	35	32	6.3
1956	Greek Archipelago, Amargos, Astypalaea Isls., Fethiye	4	ER	36.64	25.96	7.5
1961	Marmaris, Rhodes, Izmir, Aegean Sea	3	ER	36.7	28.5	6.4
2002	City of Rhodes	4	GS	36.45	28.2	

Reliability levels are:

- (0) Occurrence Improbable: The event has been documented, but is impossible to confirm and there is no general agreement.
- (1) Doubtful credibility. Insufficient data or evidence for confirmation are available.
- (2) Probable tsunamis noted in various sources and catalogues, but with discrepancies, or confirmed in a single source of doubtful reliability.
- (3) Sources specific and reliable, but occurrence dates old. Discrepancies present in some sources and catalogues. Reliable report, but confirmed in only a limited number of sources.
- (4) The most reliable tsunamis which took place more recently. Multiple reliable

sources: historic documents, church manuscripts, manuscripts by various authors, state archives, biographies, essays, private letters, magazines and reports.

Since Altinok, (2009) study was the most recent one, it was also modified in this Thesis and a GIS based spatial database was prepared for the delineation of potential tsunami risk sites in the Eastern Mediterranean. The Eastern Mediterranean Sea tsunami triggered events were classified according to earthquake magnitudes overlaid with digital elevation model (DEM) generated from program GEBCO[®] in 1800m grid size were given in *Figure 3*. Totally 124 tsunamis were located in this figure.

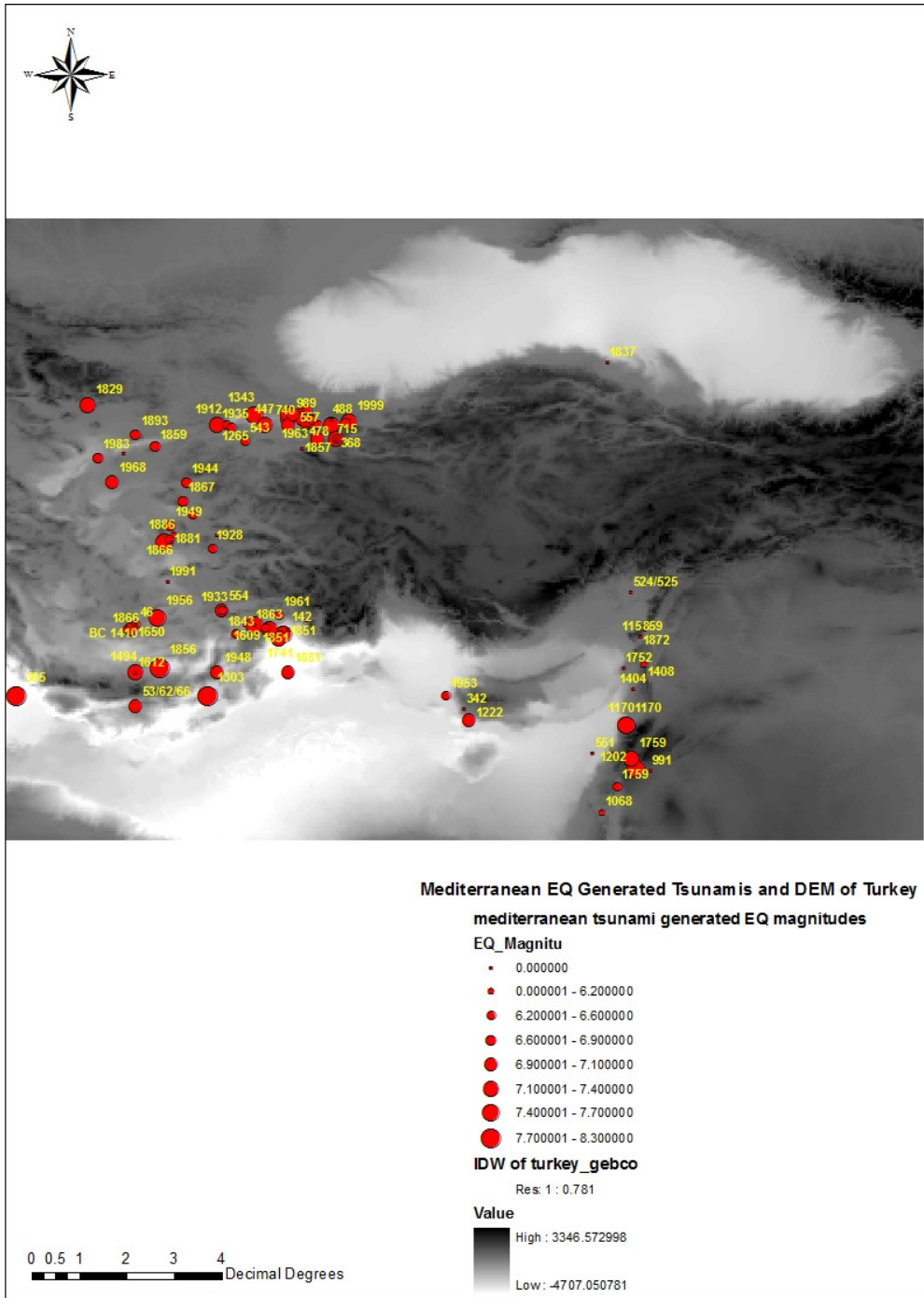


Figure 3: Tsunami triggered earthquakes in the Eastern Mediterranean

Figure 3 shows that Eastern Mediterranean is highly prone to tsunamis. Therefore future tsunamis may cause devastating damages in the coastal zones of Greece and Turkey.

4.2 Data Processing applied to the Fethiye Bay

The most challenging part of inundation mapping and tsunami assessment studies is data processing. In this study, Fethiye town is selected for one of the case studies. The main data for this work is bathymetric and topographic information, data of coastal utilization, marine structures, transportation, size and types of administrative, public and private structures. Therefore two different types of well defined data is necessary. They are spatial data and tsunamigenic data. The characteristics of the data are given in Table 3. The data are the combinations of the works of Fethiye Municipality, Korfez Haritacılık, Kandilli Observatory, NIK Systems (private firm), METU Geodetic and Geographic Information Technologies (GGIT) and Ocean Engineering Research Center (OERC).

The computational tools used are i) ArcGIS 9.3[®] for data management and processing, ii) TUNAMI- N3 for tsunami simulation and visualization iii) Surfer-8[®] for gridding and plotting program iv) GEBCO[®] for hydrographic and topographic data v) ERDAS[®] Imagine for the mosaic process of satellite images.

Table 3: The characteristics of the data used

Name	Date	Production Method	Source	Projection	Accuracy	
					Ó _p	Ó _n
DEM of the city center	2005	ARCGIS 9.3	Fethiye Municipality	GCS_WGS_1984 Transverse Mercator	20cm	20cm
Urban City Map	2005	Netcad	“Korfez Haritacılık”	GCS_WGS_1984- Transverse Mercator	0.3m	0.5m

Table 4: The characteristics of the data used

Quickbird multispectral image	13. Sep 2004	Erdas Imagine	NIK Systems	GCS_WGS_1984- Transverse Mercator	2.44m	3.66m
Shoreline Data	2007	GPS	METU GGIT and OERC	GCS_WGS_1984- Transverse Mercator	<1m	<1m
Historical Earthquake Data	2008	ARCGIS 9.3	Kandilli Observatory	GCS_WGS_1984	-	-
Inundation Data	2007	TUNAMI N3		GCS_WGS_1984- Transverse Mercator	-	-
Bathymetric Data	2007	GEBSCO, Direct Measurements, DEM	METU, OERC and “Korfez Haritacılık”	GCS_WGS_1984- Transverse Mercator	3.7km	5m
Buildings, Floor Height Values	2007	Direct Measurements	METU GGIT and OERC	GCS_WGS_1984- Transverse Mercator	0.3m	0.5m
Contour Data	1/25000	ARCGIS 9.3	General Command of Mapping	GCS_WGS_1984- Transverse Mercator	7.5m	5m

Spatial data must be spatially correct to ensure numerical modeling results and subsequent inundation files represent observed conditions. The uncertainty in the data will directly affect the risk assessment of the region. Therefore it is tried to be form a data which will be enough to evaluate risk assessments.

In the case of this thesis, high resolution airborne satellite imagery was used to generate a highly accurate, digital elevation model of Fethiye town. DEM provided information of the terrain, expressing geomorphologic features that might be related to tsunami propagation and run up. Field surveys were conducted to assess the vertical accuracy of the datasets. Spatial data used in this thesis, was acquired from Fethiye Municipality.

Horizontal Coordinate System of data taken from “Korfez Haritacılık” was “GCS_WGS_1984” Projection: ED 50 Transverse Mercator. Therefore the coordinate system of all layers was converted to same local projection system with the original data as “GCS_WGS_1984” Projection: ED 50 Transverse Mercator.

For accurate modeling of tsunami inundation and run-up, a detailed model of near shore bathymetry and coastal topography is preferable. Therefore the data were valuated, compared with aerial photography and manually adjusted as needed to reflect more accurately the coastal topography in the region of the Fethiye. Since the data acquired from “Korfez Haritacılık” has higher resolution at the residential areas of the Fethiye, the specific study was modeled with 946rows *728columns grid size, horizontal resolution of 20cm and vertical accuracy as 20cm.

The bathymetric and topographic data in digital format from available navigational charts, bathymetric measurements, contour maps, digital elevation models, satellite images, bathymetric /topographic data taken from ”Korfez Haritacılık” and previous studies performed for the Fethiye region for European Union (EU) funded Tsunami Risk and Assessment for European Region (TRANSFER) Project were combined and bathymetry/topography for the region were developed. The database was in sufficient resolution in GIS based format, especially at near shore and shallow regions. This formed “xyz” data of bathymetry and topography were in sufficient accuracy.

DEM acquired from “Korfez Haritacılık” was converted to regular points. The regular points and previously developed bathymetric data were gathered in ArcGIS 9.3[®]. Since the combined DEM does not include the elevations of the buildings in the Fethiye Region, the buildings elevation data were appended to it. From the new combination of spatial data, a new DEM of the study area was delineated in ArcGIS 9.3[®] with inverse distance weighted method and it is shown in *Figure 4*. At inland, the horizontal accuracy of the DEM is 7.5m and the vertical accuracy is 5m and in the sea, it is 3.7km and 5m respectively.

Figure 4 is the combination of all bathymetric/topographic data acquired from different sources with different resolution and accuracies. According to Figure 4, the water is about 30m deep in the middle of the bay and drops to 3-4m as it goes to coastal zones. The topography is nearly flat in the south eastern part of the Fethiye Bay.

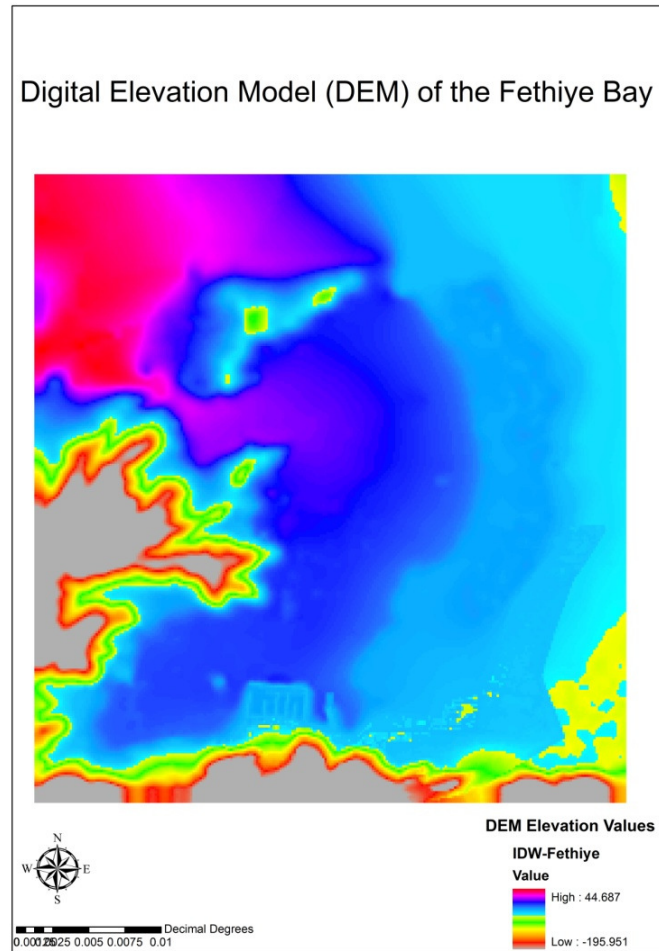


Figure 4: DEM of the Fethiye Region

ArcGIS offers several methods for creating surfaces. These methods include trend surfaces (TREND), inverse distance weighted (IDW), triangulation (CREATETIN), and kriging (KRIGING). Each of these methods has its own advantages and disadvantages in terms of data interpolation. No one method works universally as the

best for all data set. Selection of a particular method depends on the distribution of data points and the study objectives. In this thesis, in acquirement of DEM in ArcMAP 9.3[©] the inverse distance weighted method was used due to its simplicity of principle, the speed of calculation, and the ease of programming and reasonable results.

Urban city planning map of the Fethiye in NetCAD format were extacted in ArcMAP 9.3[©] and the Fethiye-specific layers were overlaid with DEM of the coastal zone. These layers are roads, coast, dock, monument, parks, pools, ruins, schools, sport centers, buildings, greenhouse, historical places, mosque, and autoparks were extracted and the attributes of the layers were modified. 655 buildings were integrated into the ArcMAP 9.3[©] with attribute information of floor heights. The hot spots can be identified with these layers in order to be used in emergency risk management.

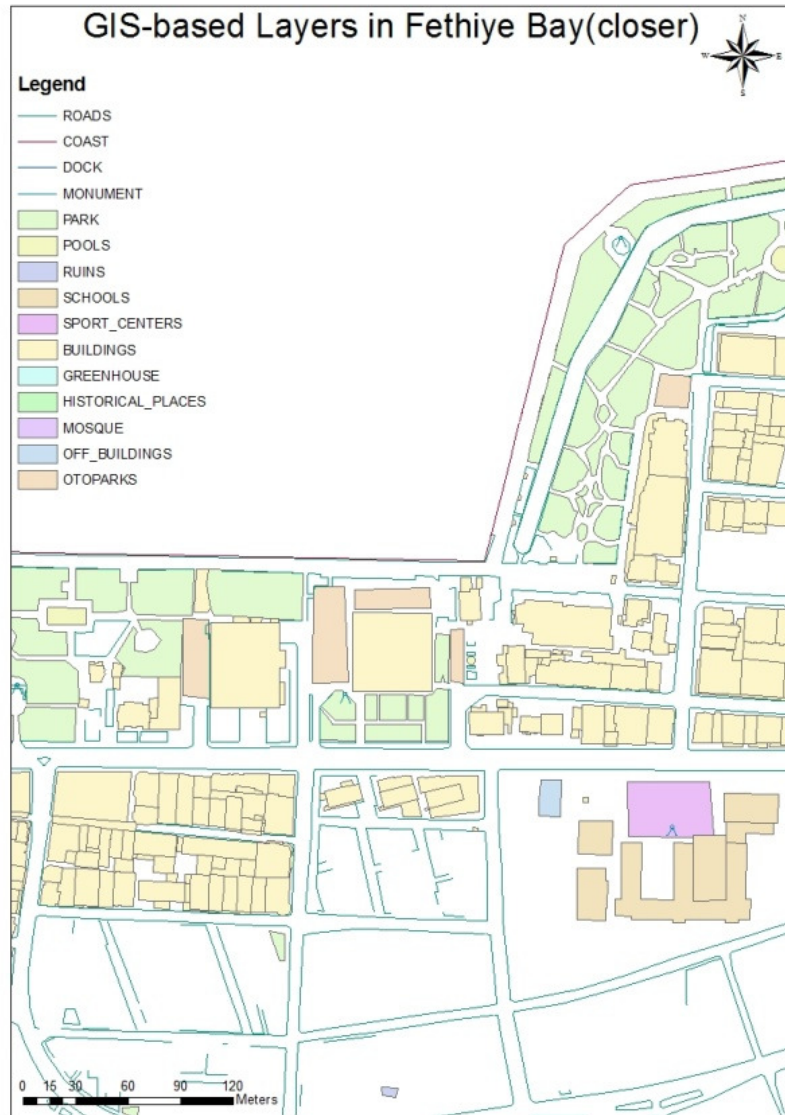


Figure 5: Closer view to GIS based layer

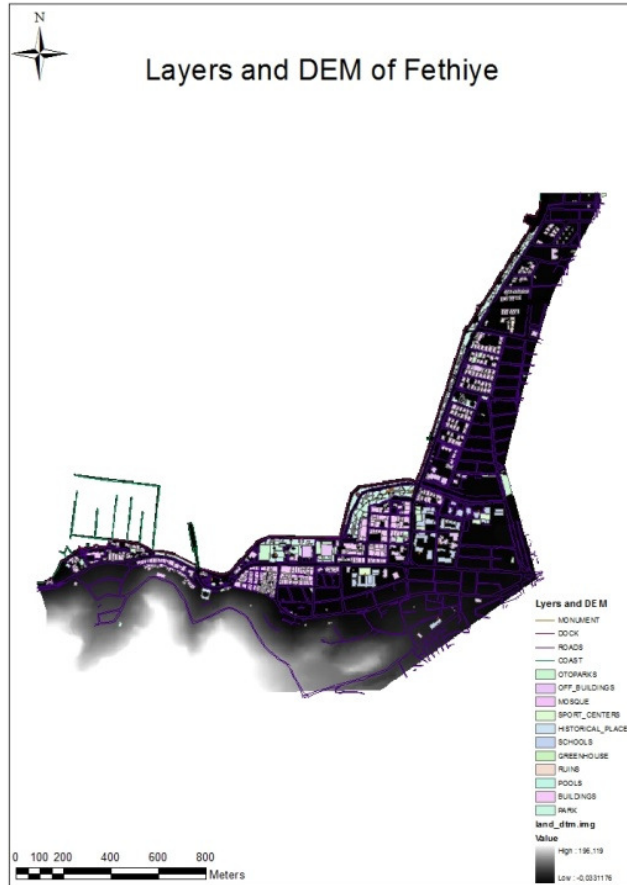


Figure 6: Layers and DEM along the coastal zone of the Fethiye Bay

The elevation values of the data were taken by direct measurements in the Fethiye Bay. Measurements were compared with the building elevation values given in 1/1000 city NetCAD urban city planning map.

4.3 Estimation of Tsunamigenic Data and Simulations

Since data from past tsunamis is usually insufficient, often the only way to determine the potential run ups and inundation from a local or distant tsunami is to use tsunami simulations together with the estimation of tsunamigenic data. It is one of the efficient procedures for tsunami assessments. In tsunami simulation, tsunami generation, propagation, coastal amplification and inundation can be modeled and visualized. Accurate and reliable applications in tsunami simulation need valid and

verified tsunami model and high resolution and reliable tsunamigenic data (tsunami source parameters, bathymetry and topography).

Numerical models usually solve similar equations but often employ different numerical techniques and are applied to different segments of the total problem of tsunami propagation from generation regions to distant areas of runup. For example, several numerical models have been used to simulate the interaction of tsunamis with islands. These models have used finite difference, finite element, and boundary integral methods to solve the linear long wave equations. These models solve these relatively simple equations and provide reasonable simulations of tsunamis for engineering purposes. The main equations in tsunami numerical modeling are non linear form of shallow water equations with friction term. Main equations were given below:

$$\frac{\partial \eta}{\partial t} + \frac{\partial M}{\partial x} + \frac{\partial N}{\partial y} = 0$$

$$\frac{\partial M}{\partial t} + \frac{\partial}{\partial x} \left(\frac{M^2}{D} \right) + \frac{\partial}{\partial y} \left(\frac{MN}{D} \right) + gD \frac{\partial \eta}{\partial x} + \frac{k}{2gD^2} M \sqrt{(M^2 + N^2)} = 0$$

$$\frac{\partial N}{\partial t} + \frac{\partial}{\partial x} \left(\frac{MN}{D} \right) + \frac{\partial}{\partial y} \left(\frac{N^2}{D} \right) + gD \frac{\partial \eta}{\partial y} + \frac{k}{2gD^2} N \sqrt{(M^2 + N^2)} = 0$$

η = water surface elevation

M and N = discharge fluxes in x and y direction respectively

D = total water depth,

h = undisturbed basin depth k is the bottom friction coefficient

4.3.1. Estimation of Probable Tsunami Source Mechanisms for the Fethiye Region

Tsunami source means point or area of tsunami origin, usually the site of an earthquake, volcanic eruption, or landslide that caused large-scale rapid displacement of the water to initiate the tsunami waves. Several parameters describe a tsunami source commonly used for tsunami simulations; epicenter of the fault axis, length and width of the fault, strike, dip and slip angles, focal depth etc.

Historical data are often very limited for most coastlines. Since the location of the sources is seldom accurately known, the sources were estimated as rupture specific worst case scenarios. Characteristics, dimensions and locations of near field and far field submarine and/or coastal faults and landslide prone regions was identified and i) inventory of near (<50 km) and far (>50 km) tsunamigenic sources, ii) characterization of tsunami faults, iii) characterization of identified unstable bodies, submarine landslides and possible tsunamigenic seafloor deformations were determined. This was a difficult task and it was needed much discussion among marine geologists and earth scientists, since uncertainties in the underlying fault rupture and landslide processes were large.

In this thesis, source parameters were estimated by METU, Ocean Engineering Research Center (OERC) and Foundation for Research and Technology – Hellas (FORTH) and National Observatory of Athens, Institute of Geodynamics (NOAGI). Since there is no sufficient information available about source parameters of the earthquake taken from the sources of the FORTH, the dip and slip angle of the faults were justified to give worst case conditions of tsunami sources. These sources were given in *Table 5*.

Table 5: Selected Sources taken from FORTH,METU-OERC and NOAGI

FORTH From 500 years events												
#	Name (Area)	Long. (E)	Lat. (N)	Dip(deg)	Rake(deg)	Strike(deg)	Depth(m)	Mw	L (km)	W (km)	U (m)	References
3	20	28.461755°	36.447044°	27	99	294	7.5	7.71	86	43	2.49	Moratto et. al. 2007, Papaioanou&Papazachos 2000
5	18	28.433966°	36.077436°	47	262	184	7.5	7.53	70	35	2.00	Moratto et. al. 2007, Papaioanou&Papazachos 2000
7	19	28.392994°	35.821452°	25	90	303	7.5	7.45	64	32	1.85	Moratto et. al. 2007, Papaioanou&Papazachos 2000
FORTH From 1000 years events												
3	20	28.461755°	36.447044°	27	99	294	7.5	8.04	126	63	3.65	Moratto et. al. 2007, Papaioanou&Papazachos 2000
5	18	28.433966°	36.077436°	47	262	184	7.5	7.84	100	50	2.90	Moratto et. al. 2007, Papaioanou&Papazachos 2000
7	19	28.392994°	35.821452°	25	90	303	7.5	7.76	91	45	2.70	
FORTH Worst Case Scenario												
1	-	28.400000°	35.500000°	20	90	55	7.5	8.35	190	90	5.00	E.Okal (Personal Communication)

Table 6: Selected Sources taken from FORTH,METU-OERC and NOAGI (cont.)

3	-	28.400000°	35.500000°	20	90	55	10	8.12	140	70	4.00	E.Okal (Personal Communication)
4	-	29.000000°	36.200000°	20	90	300	7.5	8.01	150	35	5.00	E.Okal (Personal Communication)
METU- OERC												
-	26-2	29.00°	36.66°	10	110	210	50	-	173.6	60	10	Yalciner et. al.(2008)
-	29-1	27.78°	34.2°	45	45	60	40	-	136.052	40	6	Yalciner et. al.(2008)
-	29-2	28.48	35.16	45	45	60	40	-	121.563	40	6	Yalciner et. al.(2008)
NOAGI												
1	-	28.2	36.0	20	90	135	20	7.5	86	25	1.3-2	Papadoupulos (2009)
2	-	28.5	36.35	20	90	285	20	7.5	86	25	1.3-2	Papadoupulos (2009)

4.3.2 Tsunami Simulations for the case study Fethyie

Models can be initialized with potential worst case scenarios for the tsunami sources or for the waves just offshore to determine corresponding worst case scenarios for runup and inundation. Models can also be initialized with smaller sources to understand the severity of the hazard for the less extreme but more frequent events. This information is then the basis for creating tsunami evacuation maps and procedures. At present, such modelling has only been carried out for a small fraction of the coastal areas at risk. Sufficiently accurate modelling techniques have only been available in recent years, and these models require training to understand and use correctly, as well as input of detailed bathymetric and topographic data in the area being modeled.

Consequently, numerical modelling may be the only way to estimate the tsunami propagation and the risk. Techniques now exist to carry out this assessment. Computer software and the training necessary to conduct this modelling are available through programmes such as the simulation tool TUNAMI N3, developed on the frame of IOC Tsunami Inundation Modelling Exchange (TIME) Programme. TUNAMI N3 uses the nonlinear shallow water equations. (Yalciner et. al, 2005)

In the stage of tsunami simulation of this thesis, TUNAMI N3 was used as propagation model and computed the sea state at different time steps. Time histories of water surface oscillations, the maximum positive and negative amplitudes at every grid point were determined and plotted by using GRAPHER and SURFER Programs. As a result of a 180 min tsunami simulation, snapshots were taken for the 1, 2 and 3 hours at Domain B, Domain C and at Domain D.

4.3.2.1 Rupture Specific Simulations

In this type of simulation, predefined earthquake source parameters were identified according to the reports of Foundation for Research and Technology – Hellas (FORTH) and National Observatory of Athens, Institute of Geodynamics (NOAGI)

prepared for the TRANSFER Project Work package 5 and METU-OERC about tsunamigenic earthquake sources estimated for the Eastern Mediterranean. The source parameters of FORTH, NOAGI and OERC given in *Table 4* were modeled to see and compare the initial source wave amplitudes and the location of the sources with respect to *Fethiye Bay*. *Figure 7* is the resource that was estimated as a consequence of the collaborated work done by METU-OERC and Bogazici University, Kandilli Observatory. The return periods of rupture parameters taken from FORTH are 500 and 1000 years. The worst case scenarios of the FORTH have a return period greater than 1000 years. METU and NOAGI followed a deterministic approach in determination of the initial source parameters.

This chapter briefly covers tsunami scenarios, simulation of predefined tsunami scenarios and their analysis and distribution of inundation distances.

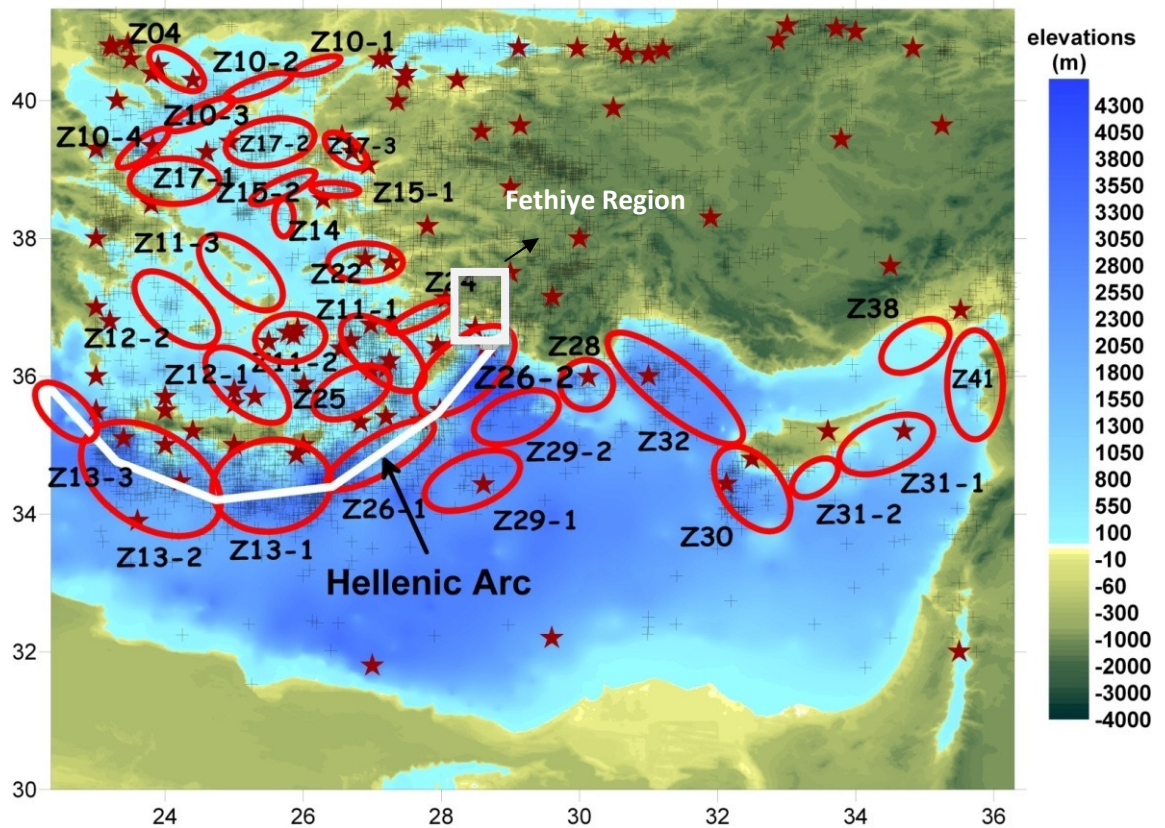


Figure 7: The sources in the Eastern Mediterranean estimated by Kandilli and OERC

From the given *Table 5*, six of the sources were selected as worst case scenarios and their parameters were taken from this table. These are worst case scenarios 1(WCS1), 3(WCS3) and 4(WCS4) from FORTH sources; Z26-2, Z29-1 and Z29-2 from METU and Scenarios 1 and 2 from NOAGI. The initial wave sources are given in *Figure 8, 9, 10 11, and 12, 13 and 14*. In these figures, the red color shows the positive wave amplitudes and blue color shows the negative wave amplitudes.

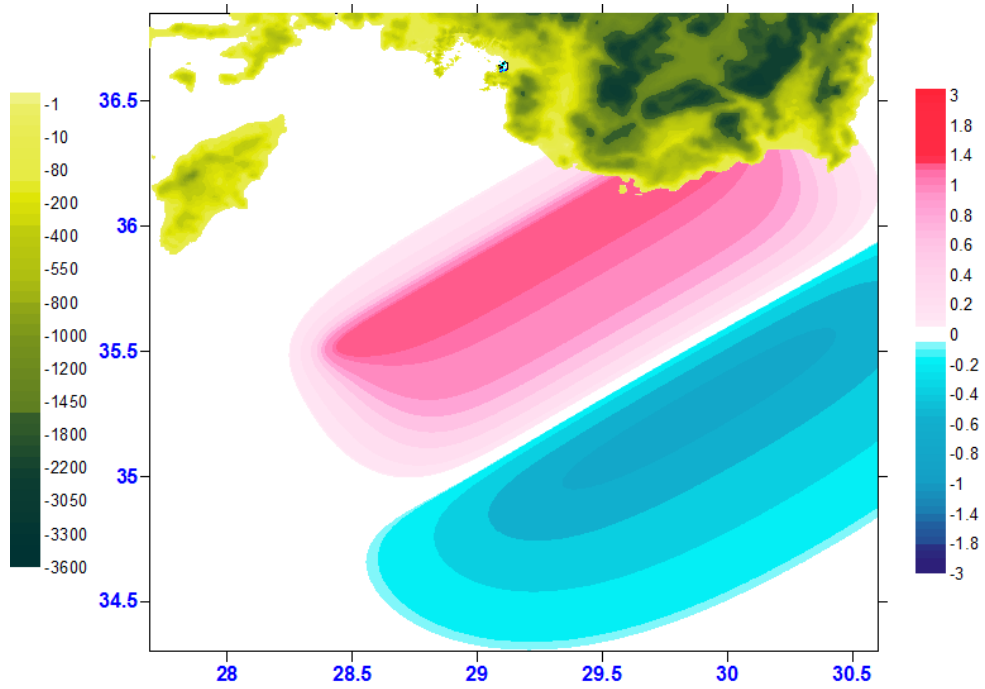


Figure 8: Estimated source, WCS1 Scenario

The initial maximum positive wave amplitude for the scenario WCS1 is **2.40m** and maximum negative wave amplitude is **-0.70m**.

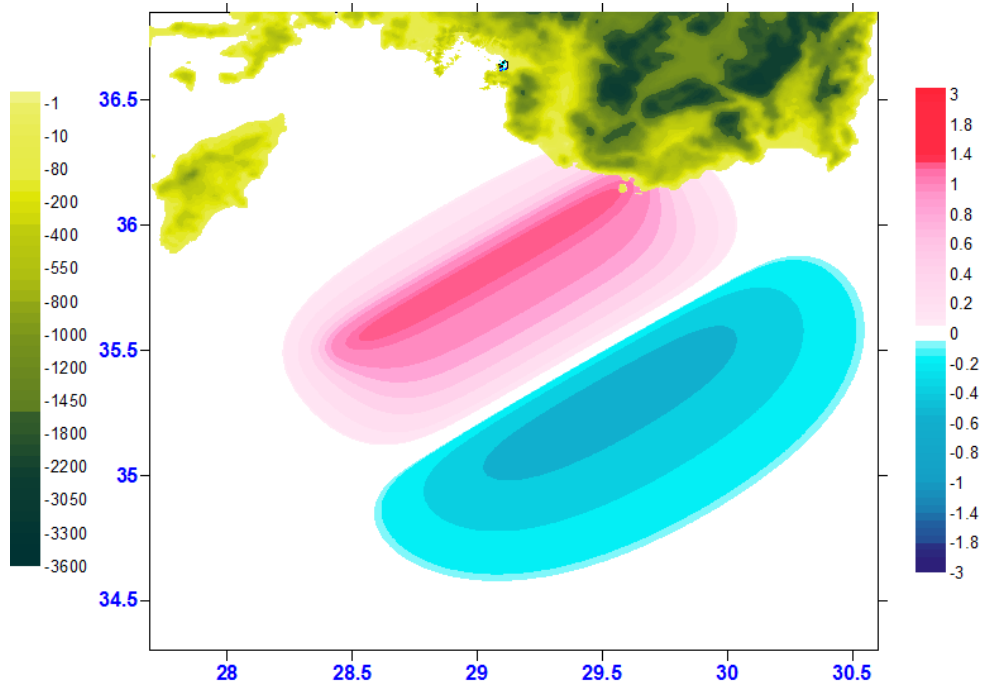


Figure 9: The source of WCS3 Scenario

The initial maximum positive wave amplitude for the WCS3 Scenario is **1.84m** and maximum negative wave amplitude is **-0.52m**.

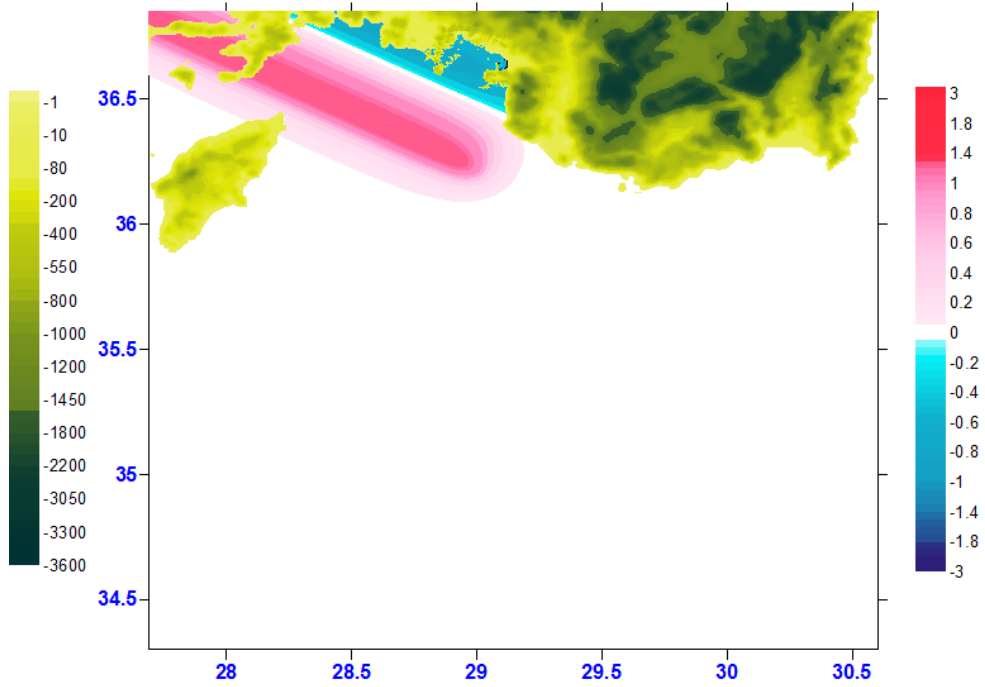


Figure 10: The source of WCS4 Scenario

The initial maximum positive wave amplitude is **2.14m** and maximum negative wave amplitude is **-0.7m**

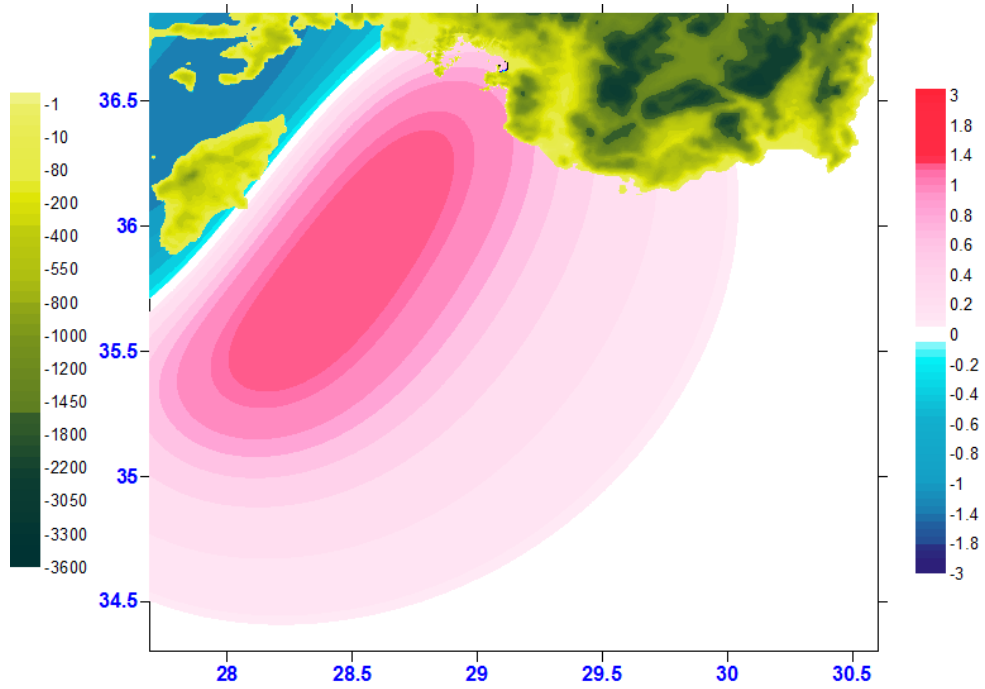


Figure 11: The source of Z26-2 Scenario

The initial maximum positive wave amplitude is for Z26-2 Scenario **2.12m** and maximum negative wave amplitude is **-1.24m** at the initial the source, Z26-2.

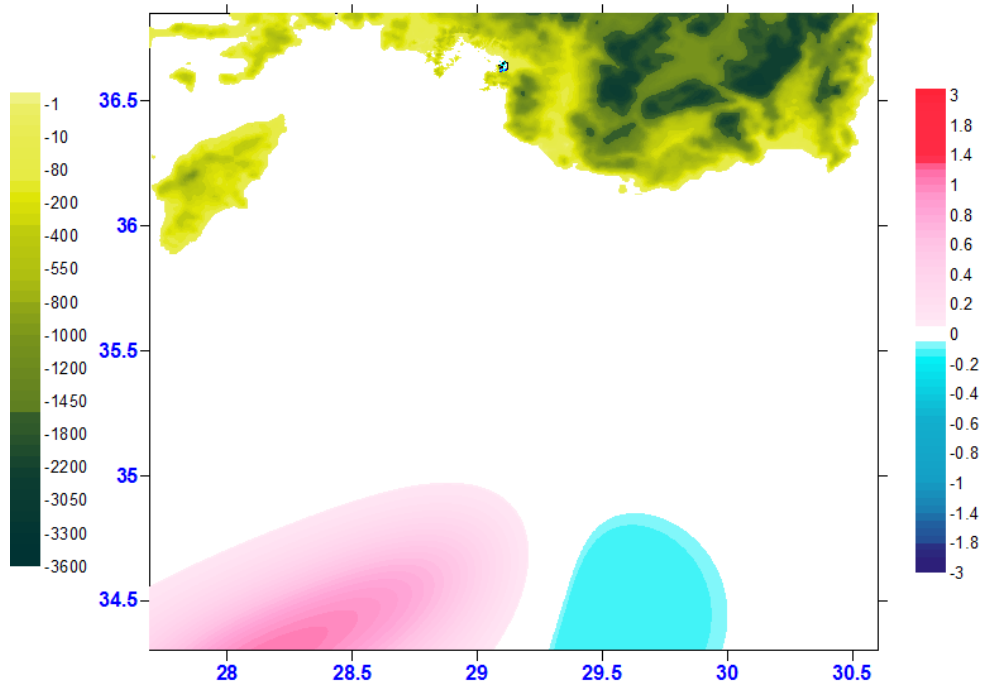


Figure 12: The source of Z29-1 Scenario

The initial maximum positive wave amplitude is **1.05m** and maximum negative wave amplitude is **-0.15m** at the initial source, Z29-1.

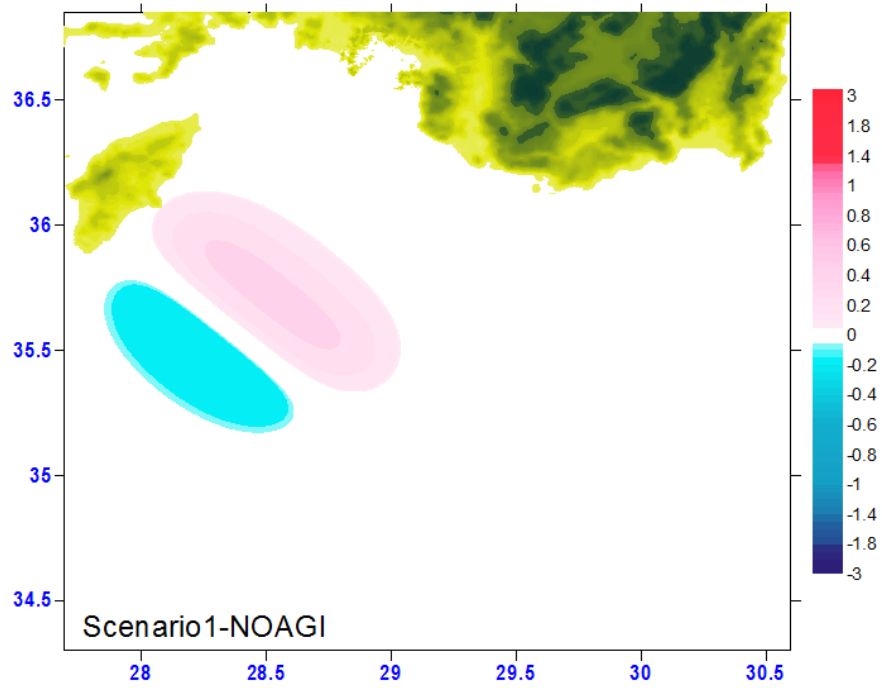


Figure 13. The Scenario 1 from NOAGI

The initial maximum positive wave amplitude is **0.51m** and maximum negative wave amplitude is **-0.17m** at the scenario 1 of NOAGI.

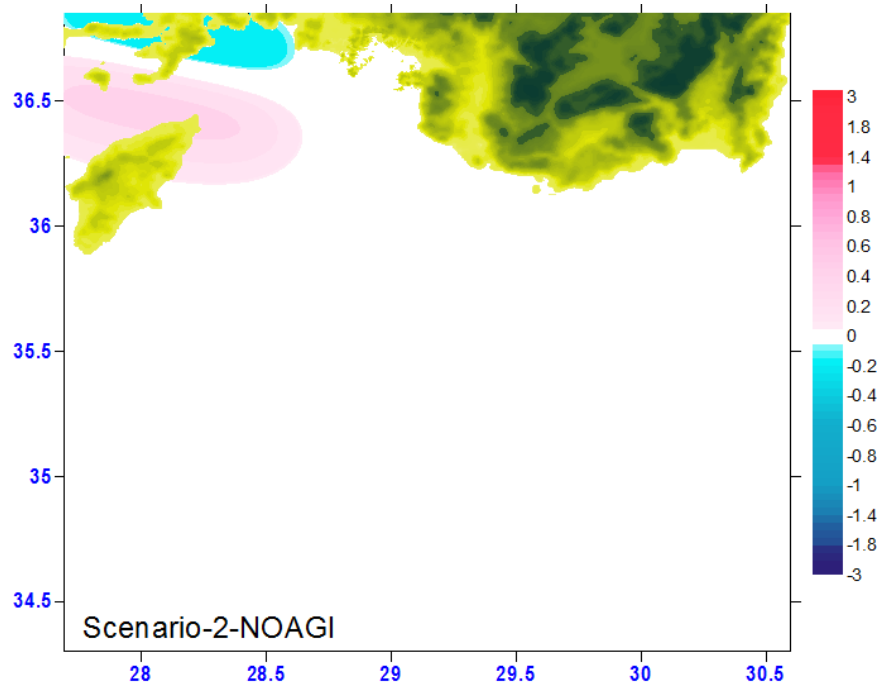


Figure 14. The scenario 2 from NOAGI

The initial maximum positive wave amplitude is **0.51m** and maximum negative wave amplitude is **-0.17m** at the scenario 2 of NOAGI.

From these eight events, the most critical and reliable sources were selected for tsunami propagation by looking the location and initial source parameters. The simulation of predefined selected most critical and reliable four tsunami scenarios, WCS1, WCS3, WCS4 and 26-2, and their analysis were done in TUNAMI N3.

4.3.2.1.1 Tsunami Simulation of WCS1

The rupture-specific simulation time of TUNAMI N3 was taken as 180 min of real-time computation for 135m 45m and 15m nested grid sizes in the Domains B, C and D respectively (*Figure 15*). This time was sufficient to see the maximum effect of the probable tsunamis in the Fethiye Bay. Same domains were used in tsunami simulations of WCS3, WCS4, Z26-2, Z29-1 and Z29-2. The maximum values for each grid were mapped in *SURFER 8*[®].

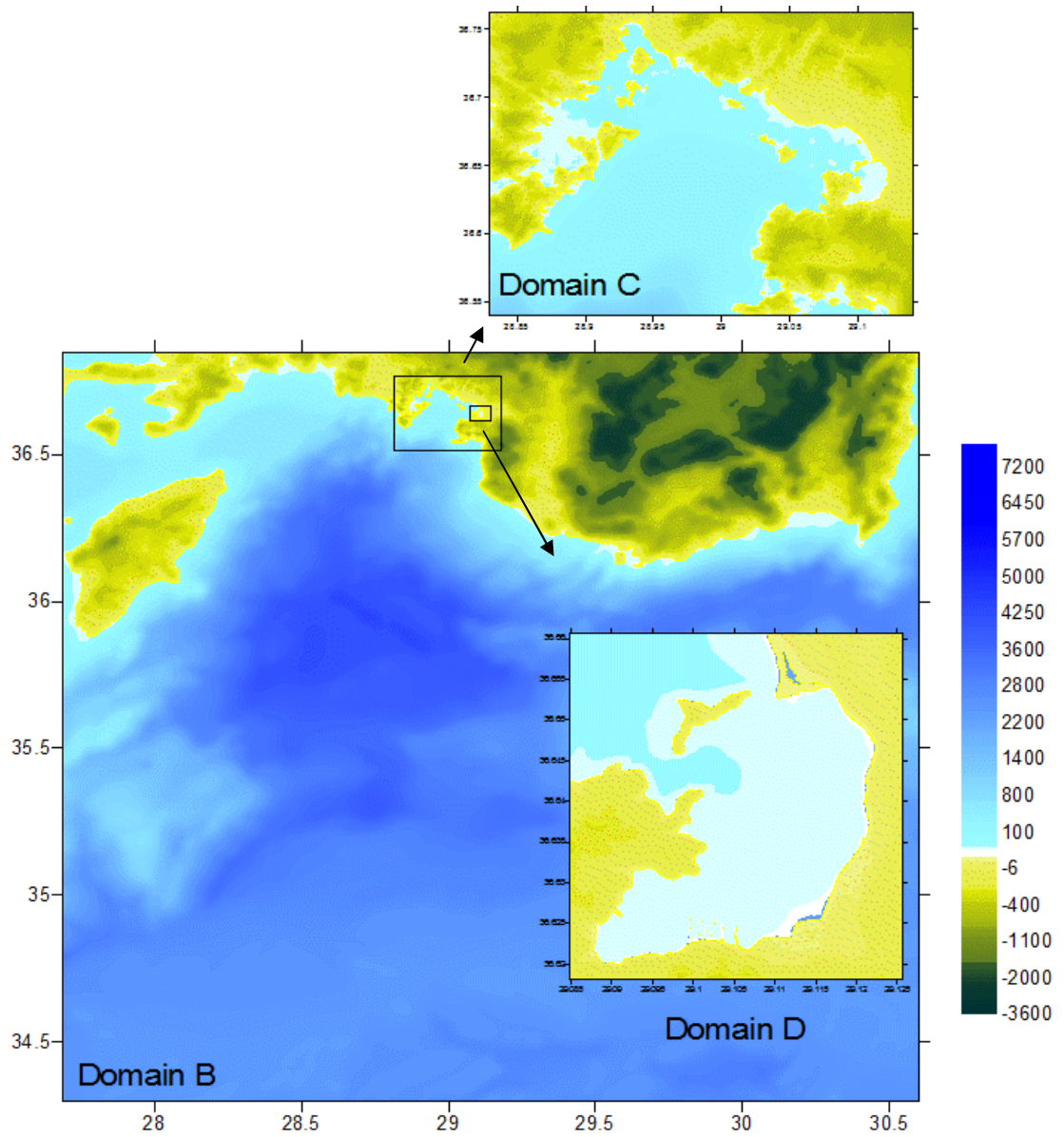


Figure 15: The structure of nested Domains (Domain B, Domain C and Domain D) for the simulation of the Fethiye Region

Propagation of the WCS1 Scenairo

Domain B

Wave propagation of the selected tsunami with estimated rupture parameters was simulated. The sea state at different time steps ($t=0, 60, 120$ and 180 min) were given in *Figure 16*. Maximum positive tsunami wave amplitude is **4.20m** and maximum negative tsunami wave amplitude is **-4.20min** in the Domain B at the point of 30m deep located in front of the “Sovalye” Island.

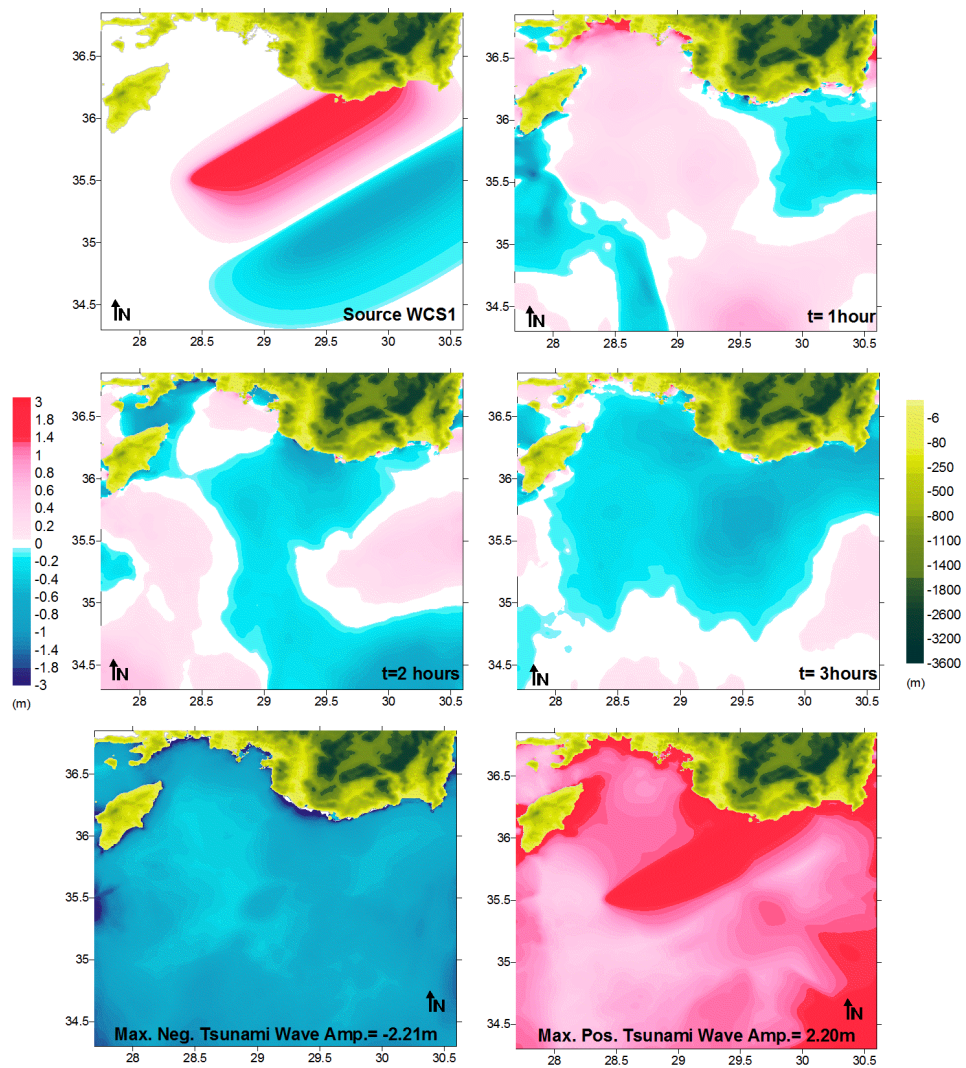


Figure 16: The sea state at different time steps, distribution of max. (+) and max. (-) tsunami wave amplitudes

Domain C

Distributions of wave propagations for different simulation time steps (0, 60, 120, 180min) and maximum positive and maximum negative tsunami amplitudes were given in *Figure 17*. Maximum positive and maximum negative tsunami amplitudes are **2.00m** and **-2.17m** respectively in the Domain C in front of the “Sovalye” Island.

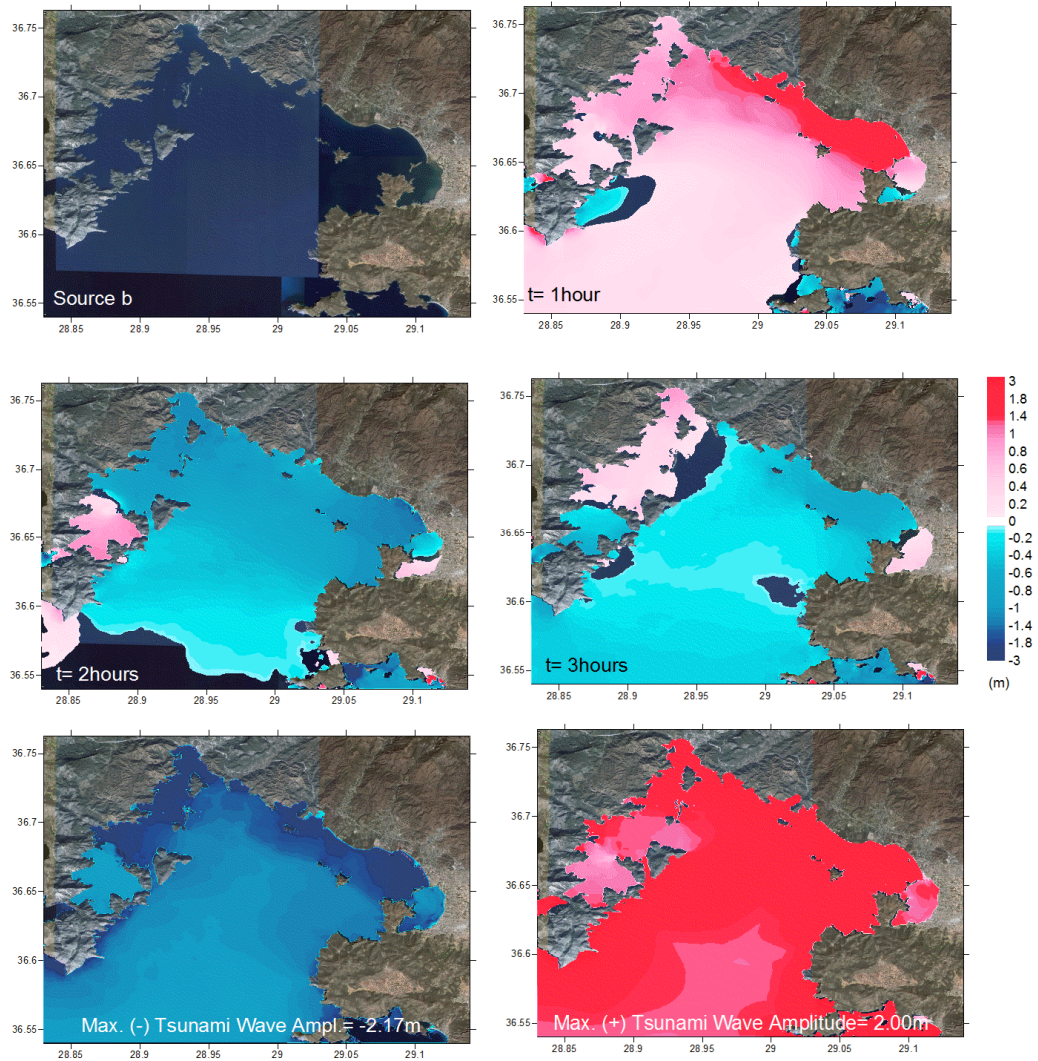


Figure 17: The sea state at different time steps, distributions of max. (+) and max. (-) tsunami wave amplitudes

Domain D

Distributions of wave propagations for different simulation time steps and maximum positive and maximum negative tsunami amplitudes were given in *Figure 18*. Maximum positive and maximum negative tsunami amplitudes are **1.81m** and **-1.95m** respectively in the Domain D at the gauges in front of “Sovalye” Island.

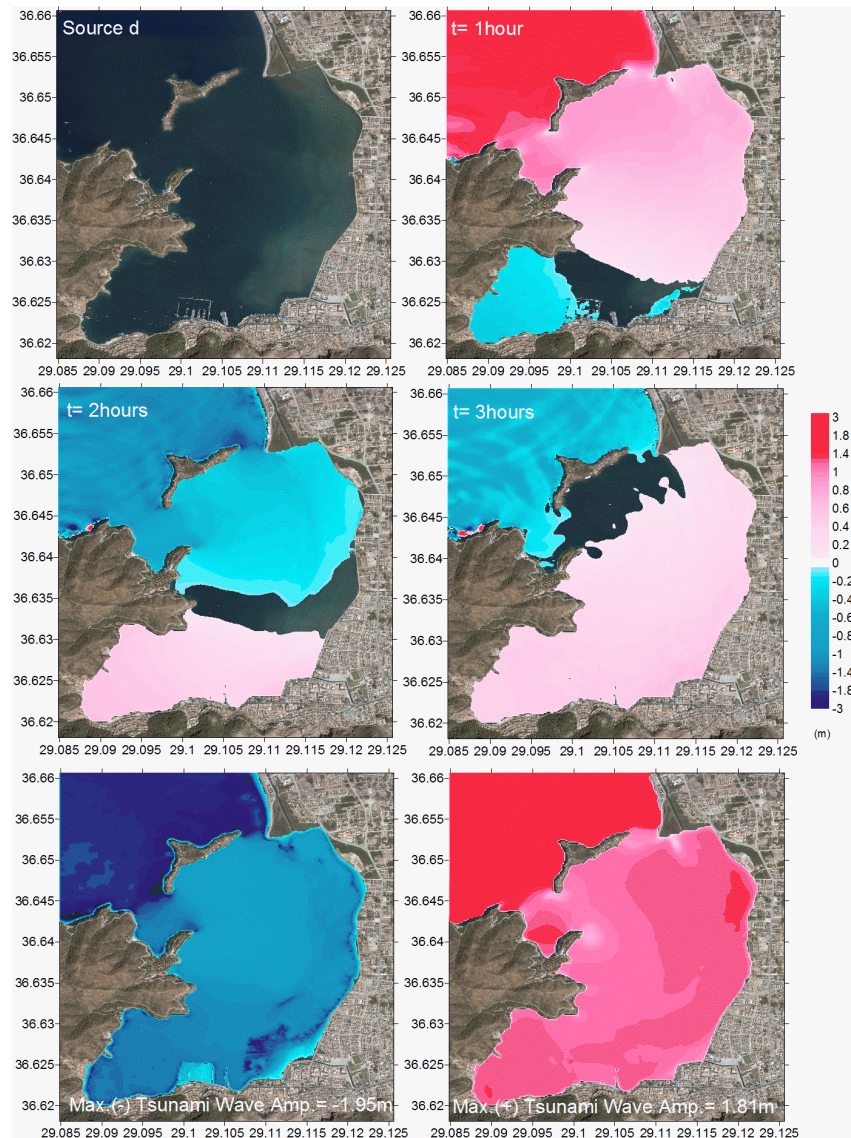


Figure 18: The sea state at different time steps, max. (+) and max. (-) tsunami wave amplitudes in the Domain D

Gauge Locations

Gauge locations were identified to store the water surface fluctuations and understand the arrival time and magnitude of the tsunami waves affecting Fethiye Bay. Coordinates of the selected gauges were given in *Table 5*. *Figure 19* and *Figure 20* are showing the gauges j, k and SovalyeW in the Domains C and D respectively.

Table 7: Coordinates of the selected gauges in the Domain C and Domain D

Domains	Domain C		Domain D
Gauges	j	k	SovalyeW
Longitude (degree)	29.0801883777E	29.0902779384E	29.0903934386E
Latitude (degree)	36.6529221356N	36.6525966683N	36.6589043074N

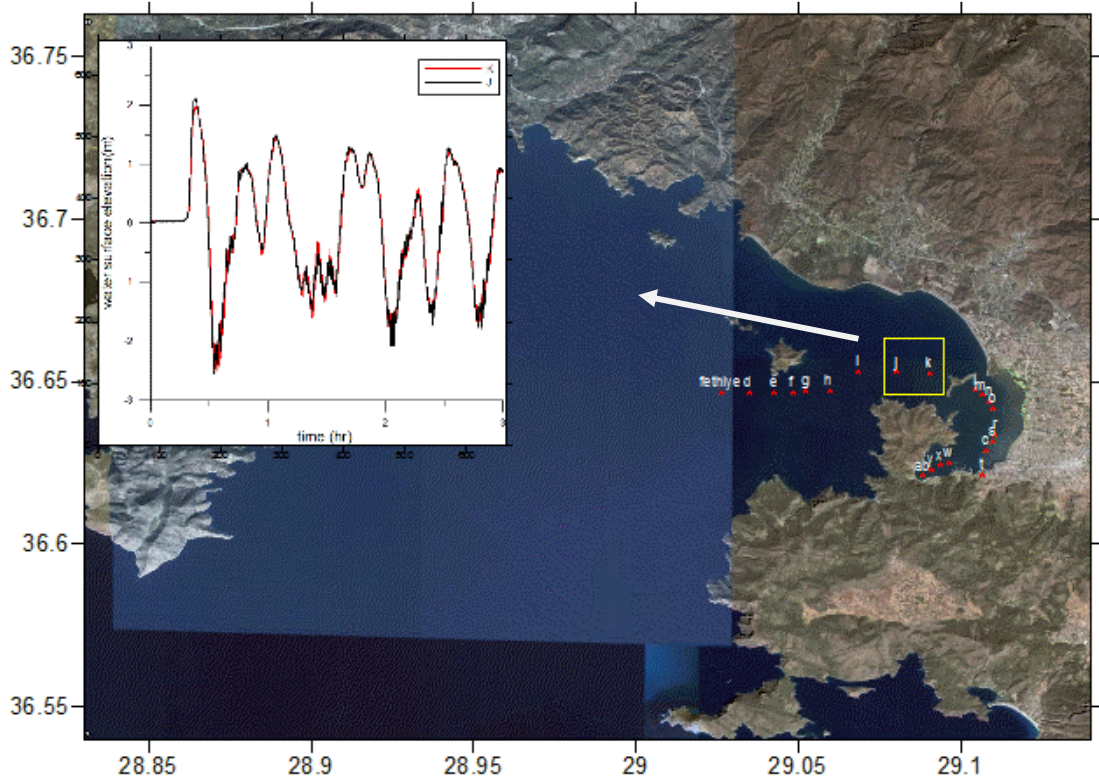


Figure 19: Gauge location in the domain c and time histories of water surface elevations for gauges j and k

As it is seen in *Figure 19*, at the entrance of the bay, in Domain C, the maximum positive and maximum negative water surface elevations for the gauges **j** and **k** are **2.10m**, **1.968m**, and **-2.55m**, **-2.54m** respectively. First wave arrives to the Fethiye Bay in 7min after tsunami occurred.

Since the locations of the gauges selected in the Domain D is different, there is a decrease in water surface elevations depending on bathymetric conditions. At the gauges in the Domain D, the maximum water surface elevation at the selected gauges in the bay are **1.2m**. The maximum positive and maximum negative water surface elevations for the gauge SovalyeW are **1.81m** and **-1.90m** respectively.

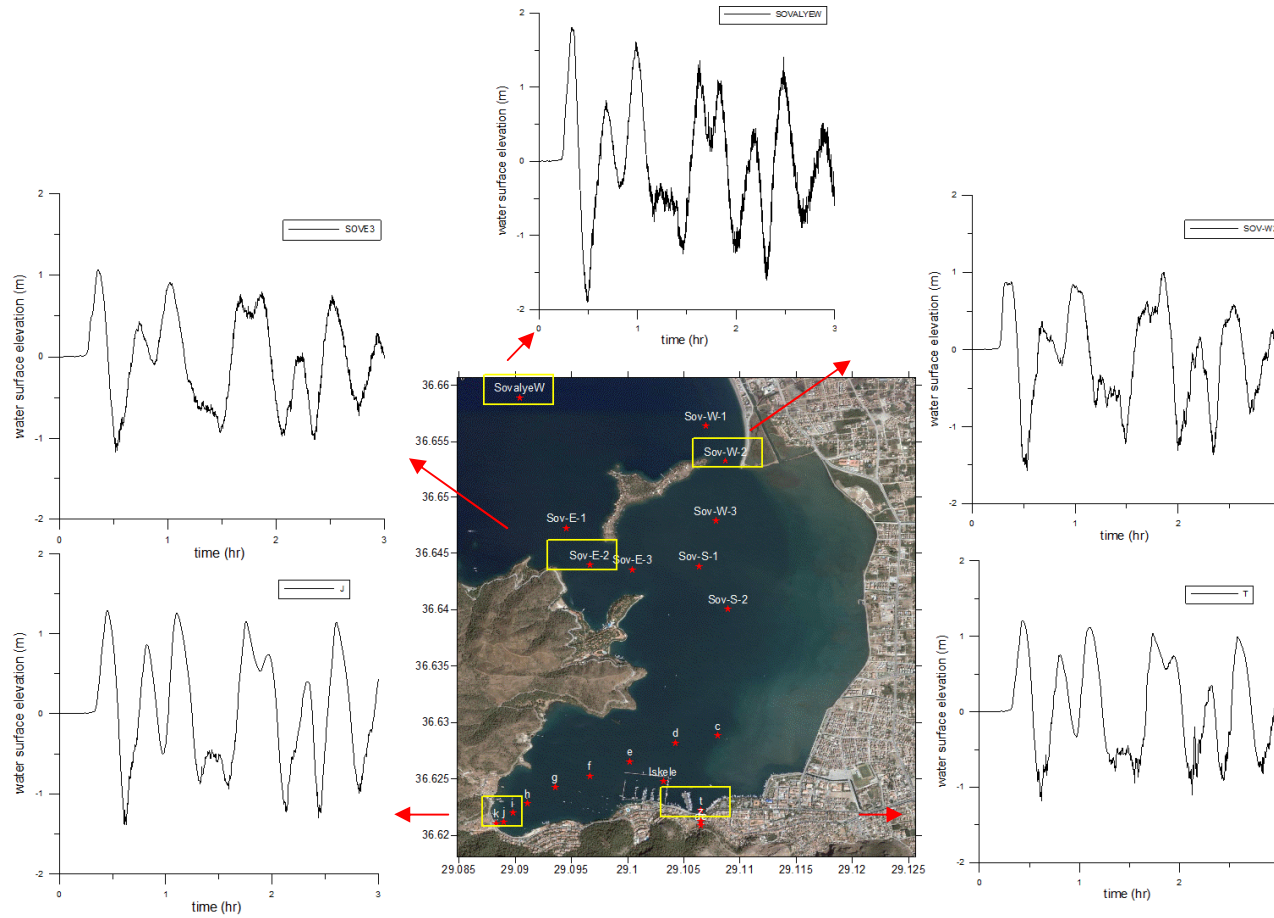


Figure 20: Gauge locations in the Domain D and time histories of water surface elevations for gauges

4.3.2.1.2 Tsunami simulation of WCS3

The same procedure is also valid for the simulation of WCS3. For the propagation of this scenario, the values in *Table 12* were used. The simulation time step was taken as 60min Output time intervals of the simulation was 60sec. The results of the simulations were given in the following subsections. The maximum values for each grid were mapped with *SURFER 8* [®]. The time histories of water surface fluctuations were drawn in *GRAPHER*.

Propagation of WCS3 Scenario

Domain B

Distributions of wave propagations for different simulation time steps and maximum positive and maximum negative tsunami amplitudes were given in *Figure 19*. Maximum positive and maximum negative tsunami amplitudes are **1.78m** and **-2.02m** respectively in the Domain B at the point of 30m deep located in front of the “Sovalye” Island.

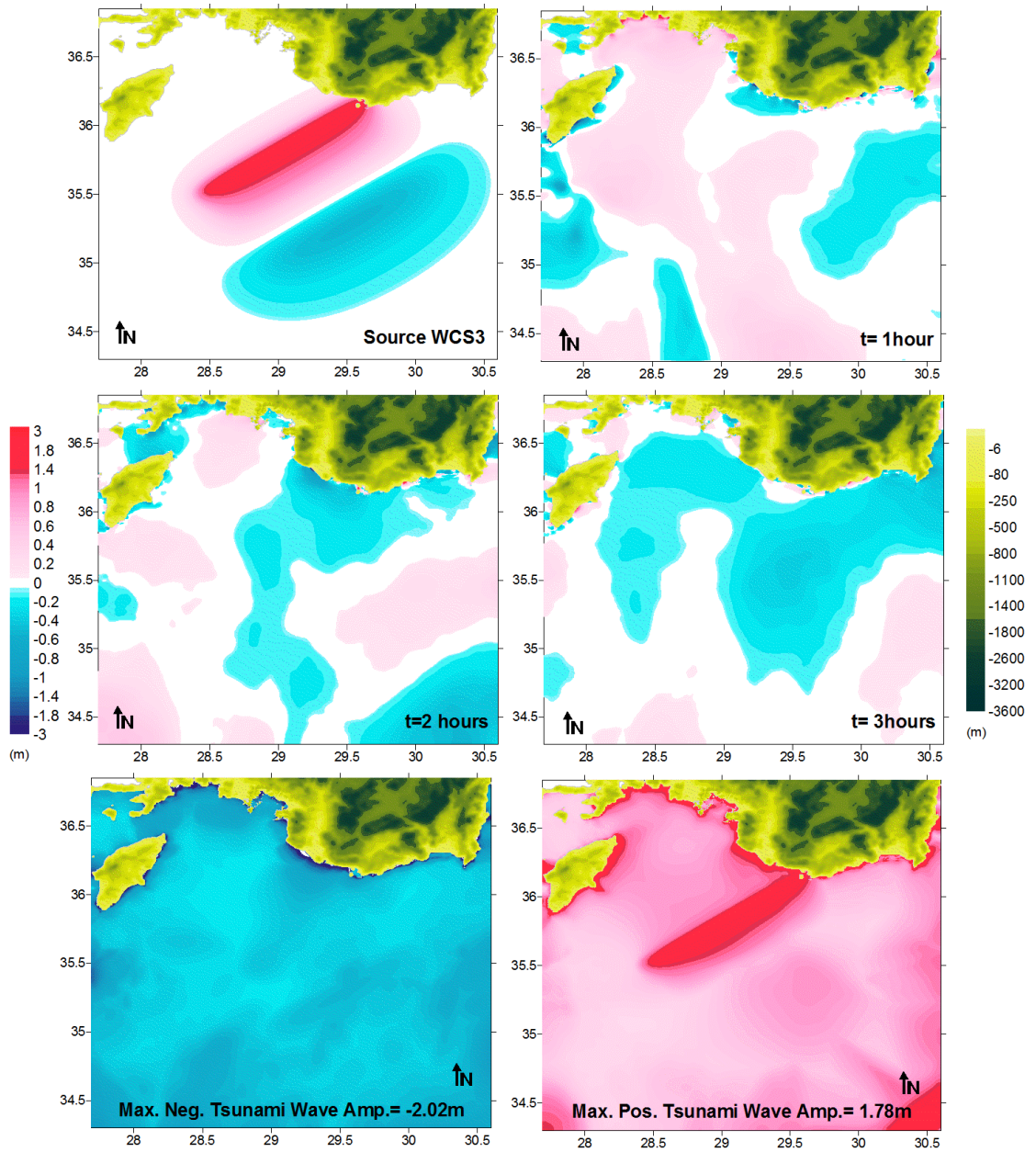


Figure 21: The sea state at different time steps ($t=0, 60, 120$ and 180 min), and max. (+) and max. (-) tsunami wave amplitudes in the Domain B

Domain C

Distributions of wave propagations for different simulation time steps and maximum positive and maximum negative tsunami amplitudes were given in *Figure 22*. Maximum positive and maximum negative tsunami amplitudes are **1.58m** and **-1.75m** respectively in the Domain C in front of the “Sovalye” Island.

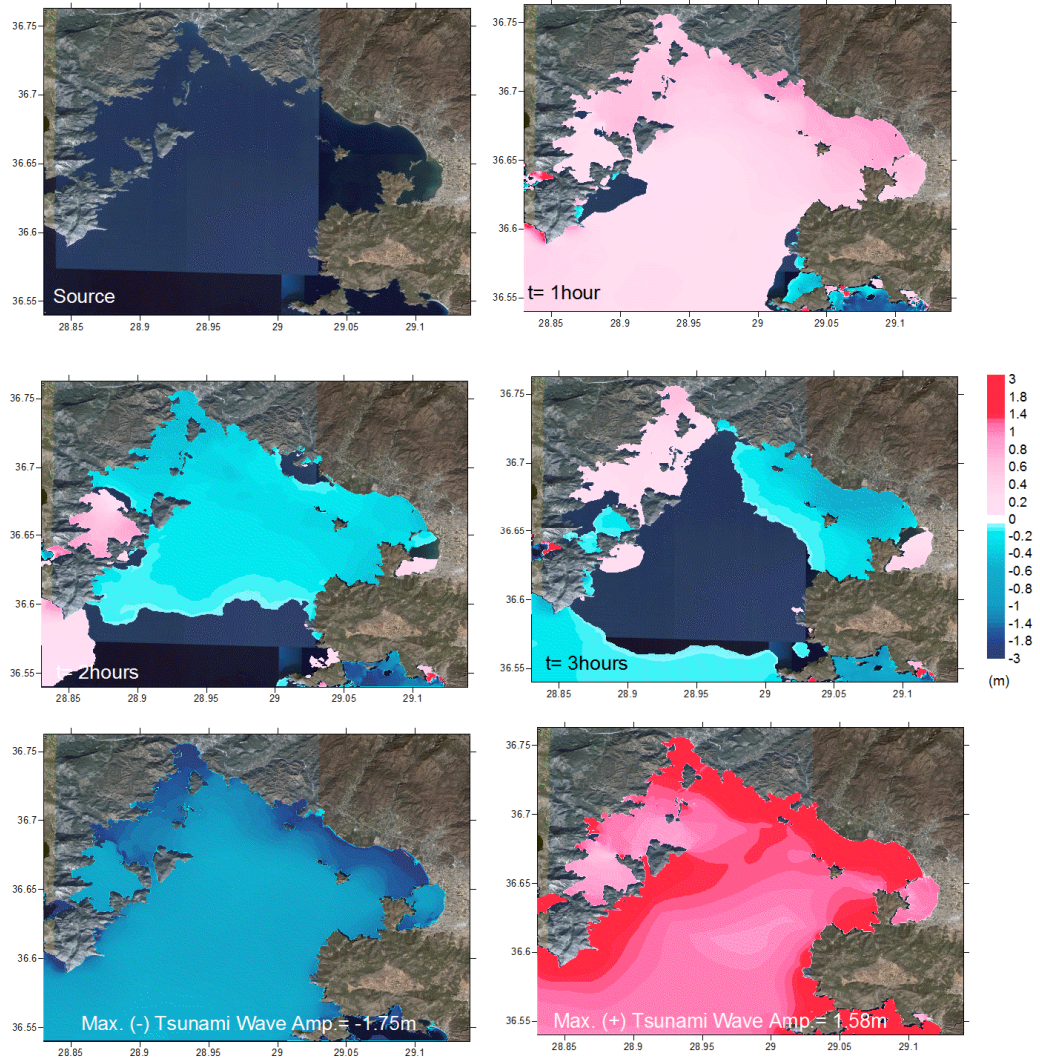


Figure 22: The sea state at different time steps (t=0, 60, 120 and 180 min), and max. (+) and max. (-) tsunami wave amplitudes in the Domain C.

Domain D

Distributions of wave propagations for different simulation time steps and maximum positive and maximum negative tsunami amplitudes were given in *Figure 23*. Maximum positive and maximum negative tsunami amplitudes are **1.41m** and **-1.58m** respectively in the Domain D at the gauges in front of “Sovalye” Island.

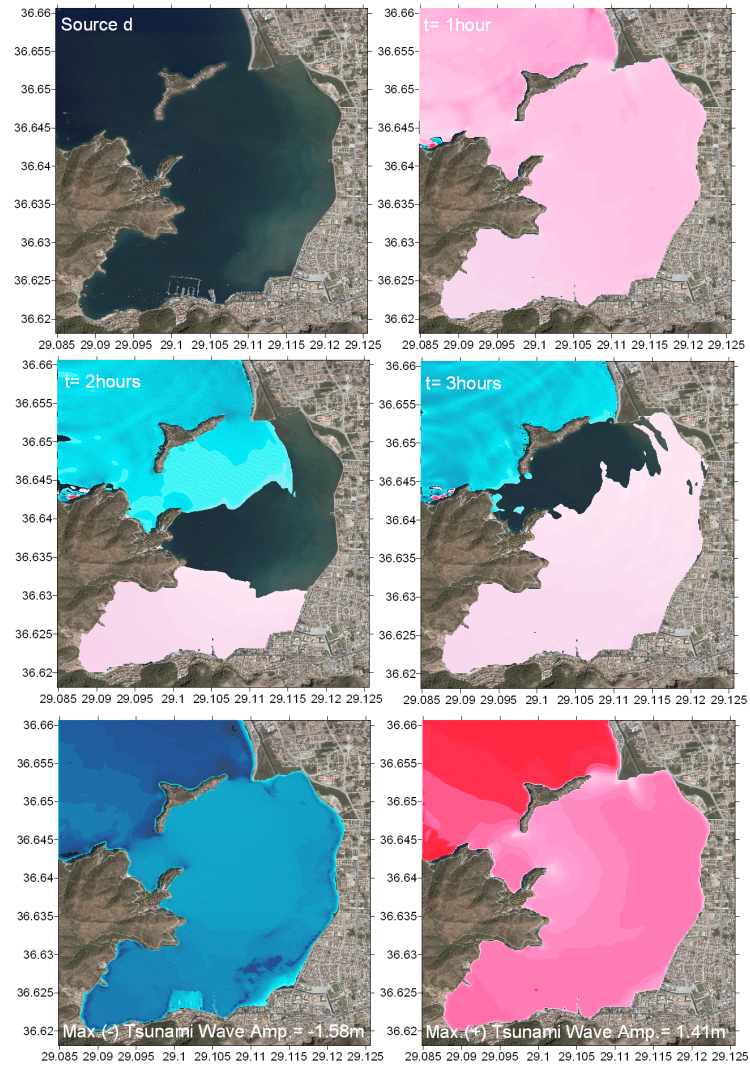


Figure 23: The sea state at different time steps (t=0, 60, 120 and 180 min), tsunami amplitudes in the Domain D.

Gauge Locations

The same gauges were selected in order to compare the results of different scenarios. At the entrance of the bay, in Domain C, the maximum positive and maximum negative water surface elevations for the gauges **j** and **k** are **1.78m**, **1.67m**, and **-2.51m**, **-2.13m** respectively. First wave arrives to the Fethiye Bay in 7min after tsunami occurred. Results were given in *Figure 24* and *Figure 25*.

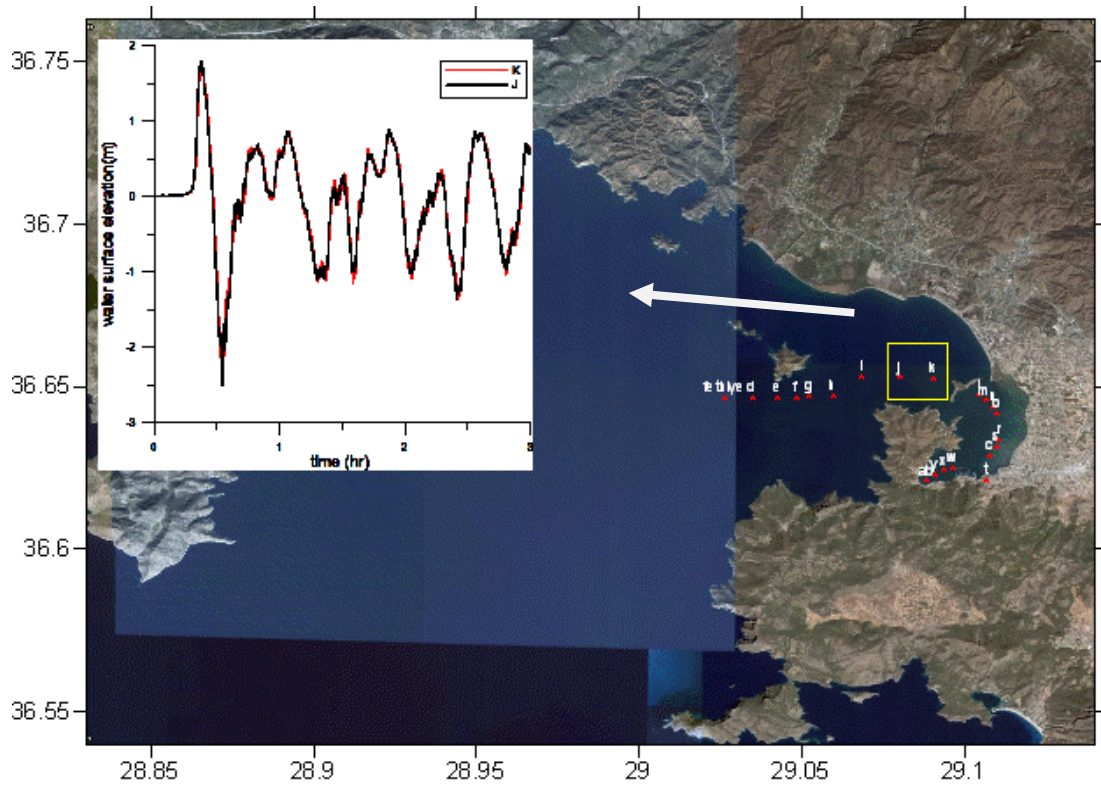


Figure 24: Gauge locations at Domain C and time histories for the gauges j and k.

In the Domain D of scenario WCS3, at the gauge SovalyeW, maximum positive and maximum negative tsunami wave amplitudes are **1.41m** and **-1.58m** respectively.

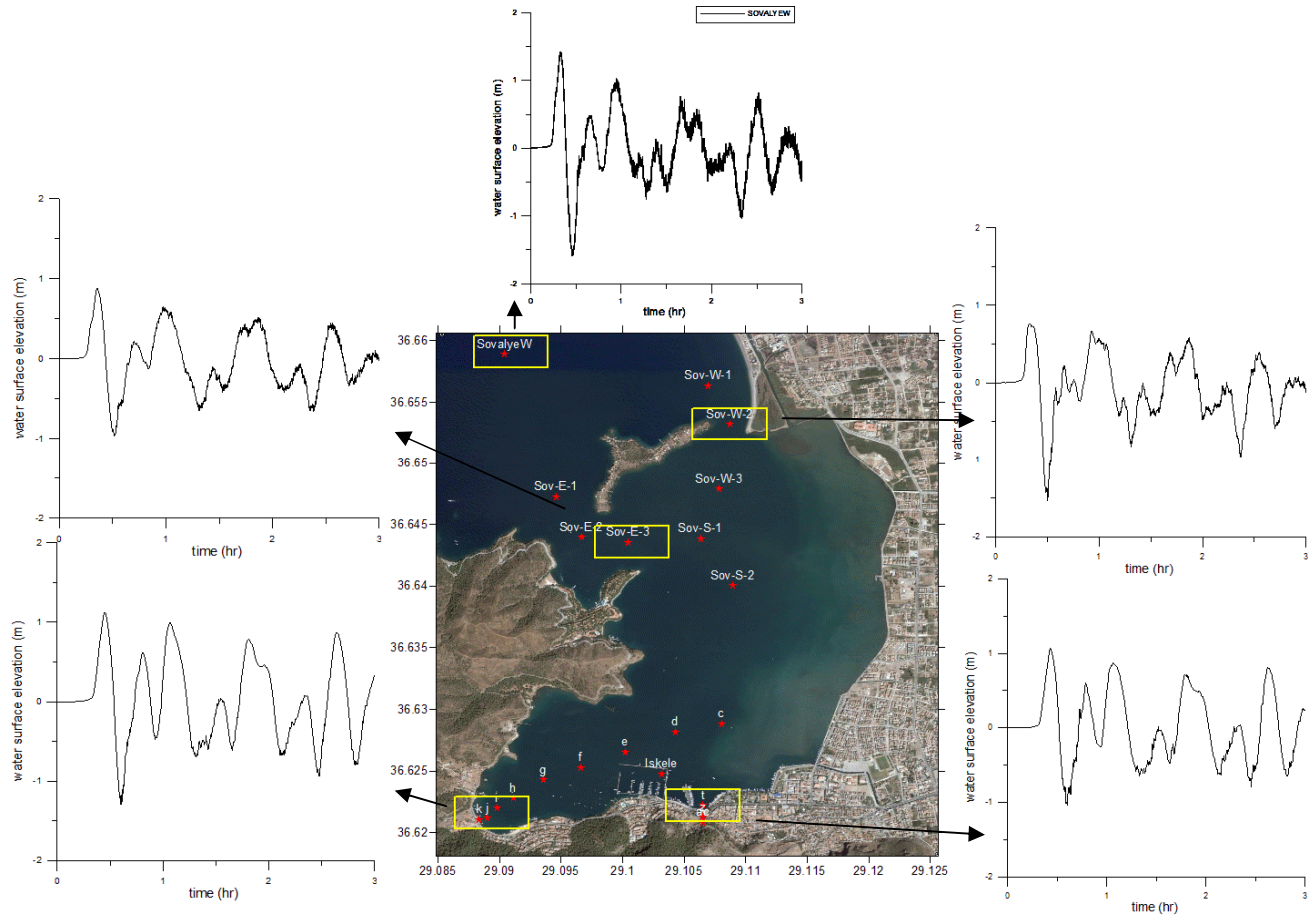


Figure 25: Gauge locations at Domain D and time histories for the gauge SovalyeW

4.3.2.1.3 Tsunami Simulation of WCS4

The simulation of WCS4 followed the same procedure. The propagation of the tsunami waves were performed according to rupture parameters of the source WCS4. Snapshots were taken for 1, 2 and 3 hours. Maximum positive and maximum water surface elevations in the nested domains were plotted in *SURFER 8*. Water surface elevation values for specific gauge points were given to be able to compare the results of simulations done by using different scenarios.

Propagations of WCS4 Scenario

The same grid sizes and domains were used in the propagation of this scenario. The maximum values for each grid were mapped with *SURFER 8*[®].

Domain B

Distributions of wave propagations for different simulation time steps ($t=0, 60, 120$ and 180 min), and maximum positive and maximum negative tsunami amplitudes were given in *Figure 26*. Maximum positive and maximum negative tsunami amplitudes are **2.08m** and **-1.10m** respectively in the Domain B at a point of 30m deep located in front of the “Sovalye” Island.

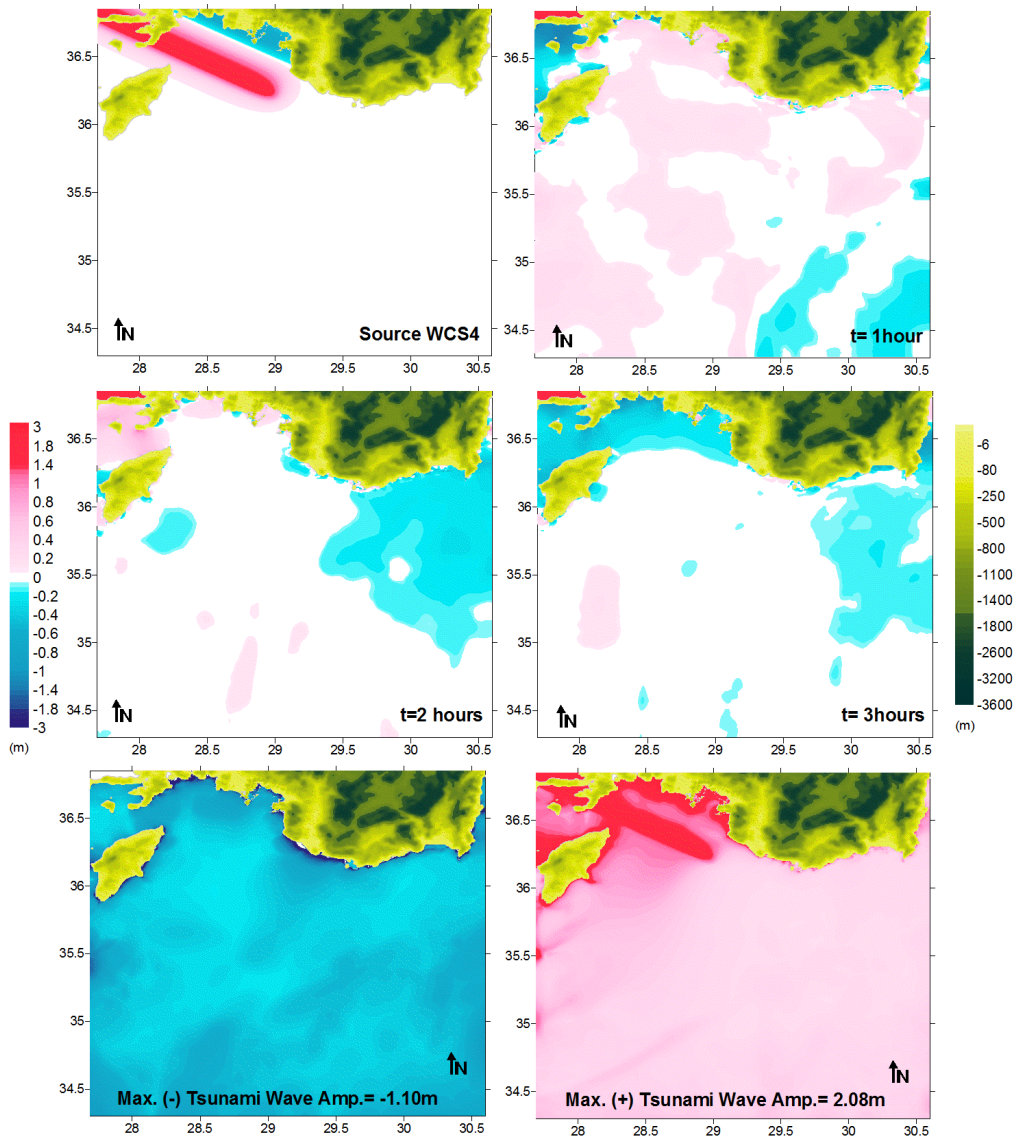


Figure 26: The sea state at different time steps, max. (+) and max. (-) tsunami wave amplitudes in the Domain B

Domain C

Distributions of wave propagations for different simulation time steps and maximum positive and maximum negative tsunami amplitudes were given in *Figure 27*. Maximum positive and maximum negative tsunami amplitudes are **1.90m** and **-1.00m** respectively in the Domain C in front of the “Sovalye” Island.

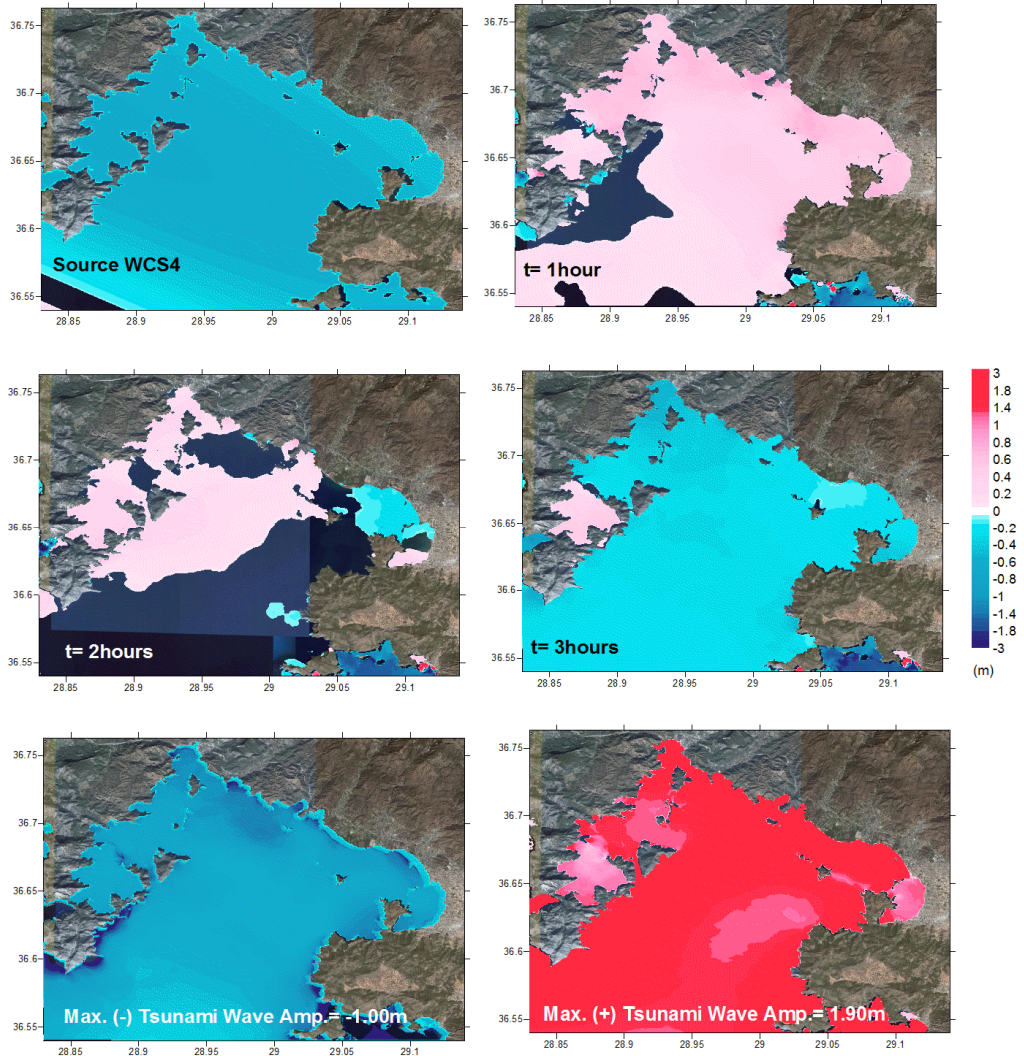


Figure 27: The sea state at different time steps (t=0, 60, 120 and 180 min), max. (+) and max. (-) tsunami wave amplitudes in the Domain C.

Domain D

Distributions of wave propagations for different simulation time steps ($t=0$, 60, 120 and 180 min), and maximum positive and maximum negative tsunami amplitudes were given in *Figure 28*. Maximum positive and maximum negative tsunami amplitudes are **1.78m** and **-0.87m** respectively in the Domain D.

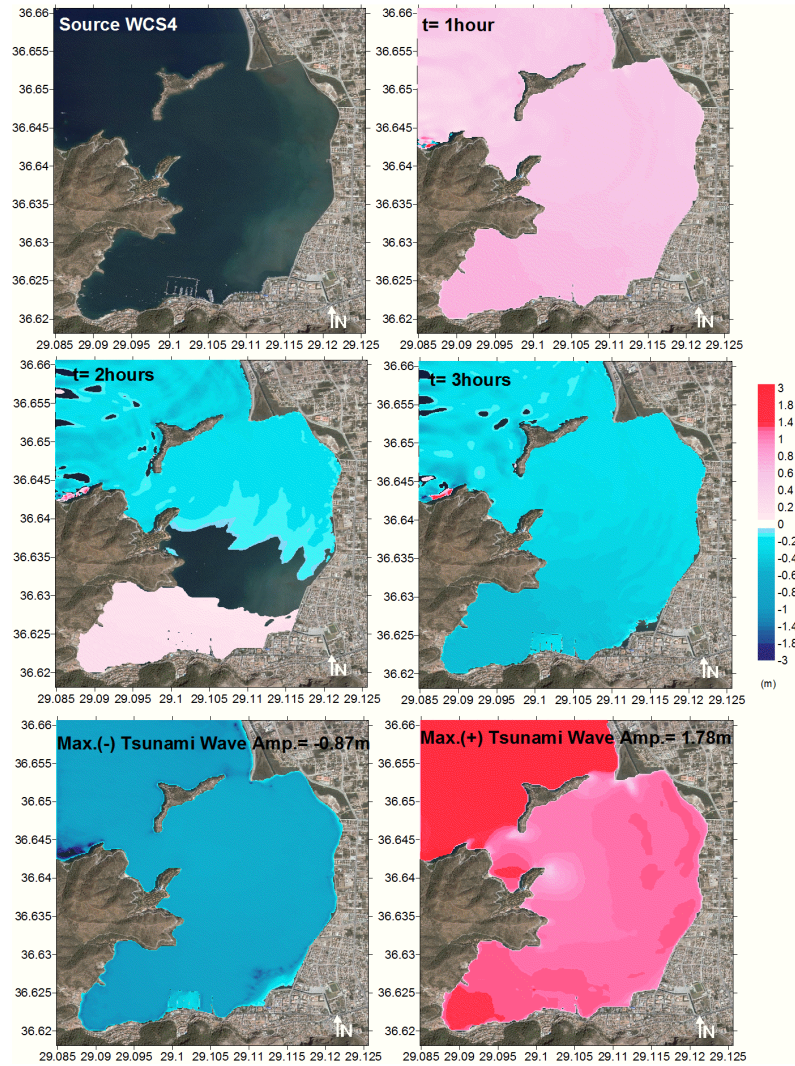


Figure 28: The sea state at different time steps, max. (+) and max. (-) tsunami wave amplitudes in the Domain D.

Gauge Locations

The same gauges were selected in order to compare the results of different scenarios. At the entrance of the bay, in Domain C, the maximum positive and maximum negative water surface elevations for the gauges **j** and **k** are **2.42m**, **2.18m**, and **-1.31m**, **-1.49m** respectively. *Figure 29* and *Figure 30* give the location of the gauges and the graph of water surface elevations at these gauges.

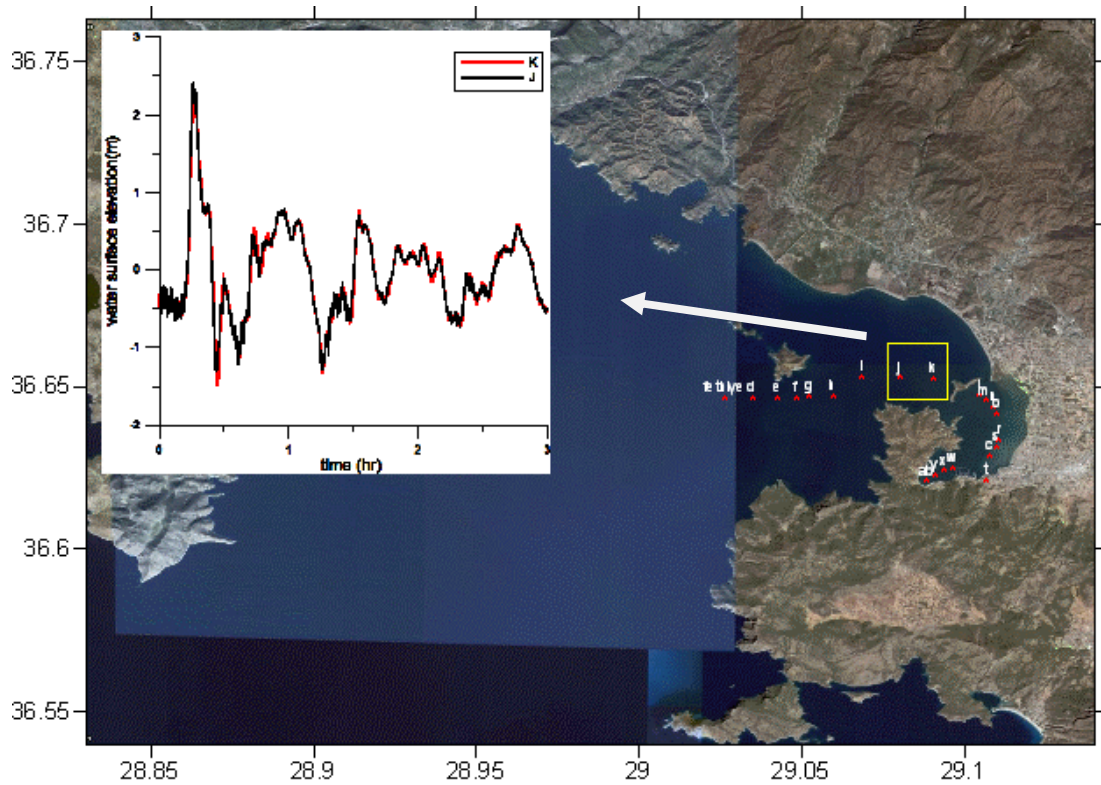


Figure 29: Gauge locations at Domain C and time histories for the gauges j and k

In Domain D of WCS4, the maximum positive and maximum negative water surface elevations for the gauge SovalyeW is **1.78m** and **-1.90m**.

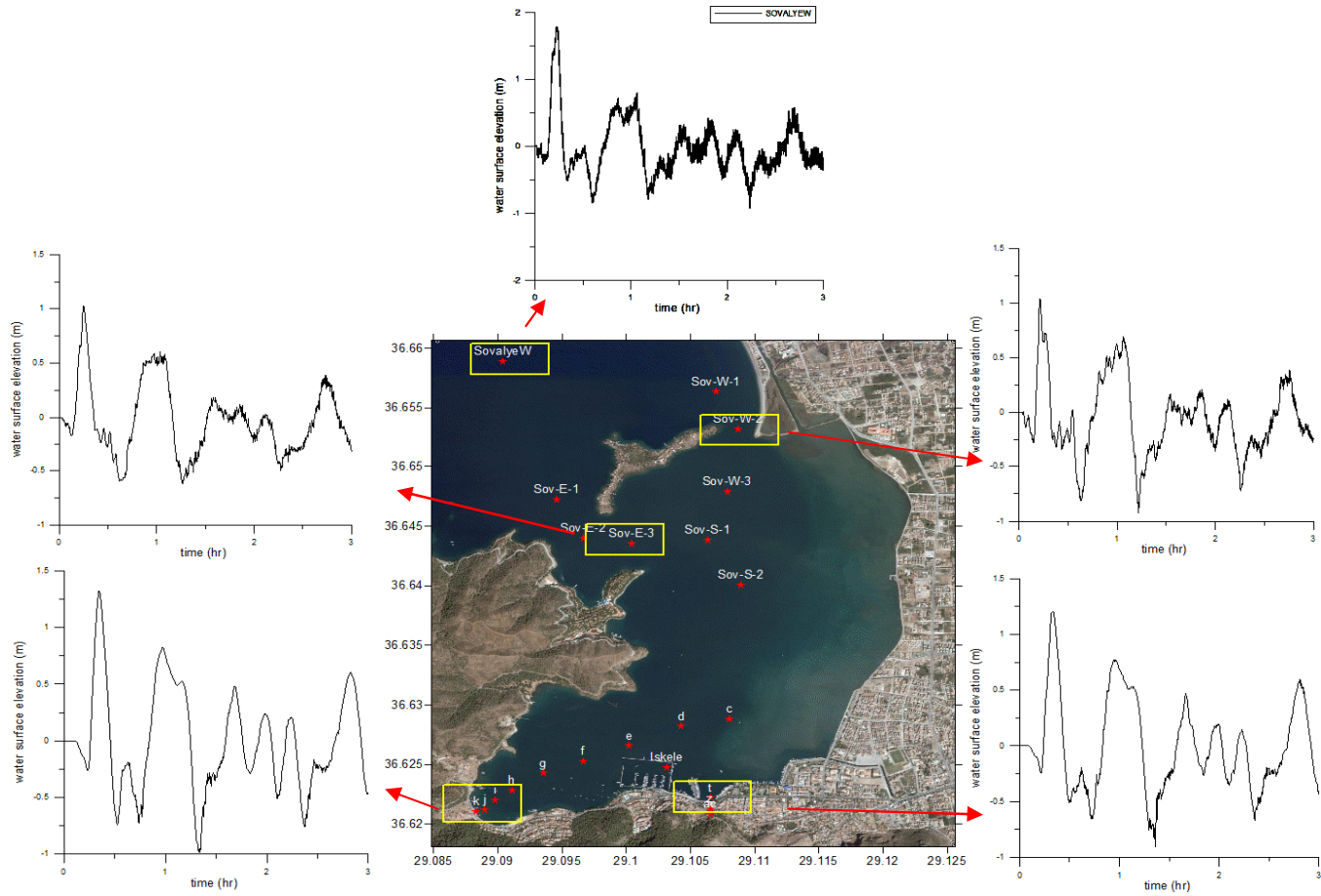


Figure 30: Gauge locations at Domain D and time histories for the gauge SovalyeW

4.3.2.1.4 Tsunami Simulation of Z26-2

Propagation of Z26-2 Scenario

Domain B

Distributions of wave propagations for different simulation time steps ($t=0, 60, 120$ and 180 min), and maximum positive and maximum negative tsunami amplitudes were given in *Figure 31*. Maximum positive and maximum negative tsunami amplitudes are **3.72m** and **-3.58m** respectively in the Domain B at the point of 30m deep located in front of the “Sovalye” Island.

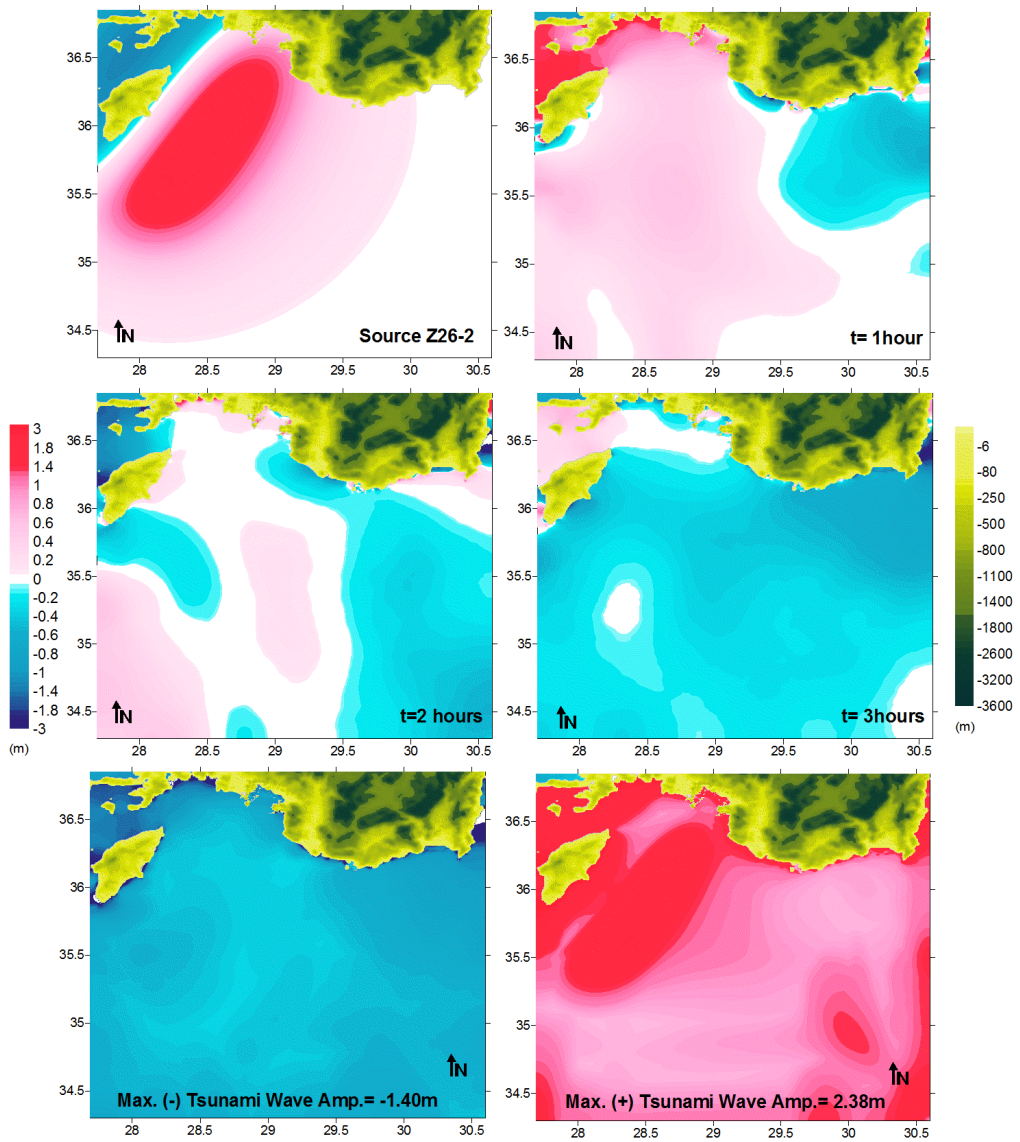


Figure 31: The sea state at different time steps and max. (+) and max. (-) tsunami wave amplitudes in the Domain B.

Domain C

Distributions of wave propagations for different simulation time steps ($t=0$, 60, 120 and 180 min), and maximum positive and maximum negative tsunami amplitudes were given in *Figure 32*. Maximum positive and maximum negative tsunami amplitudes are **2.10m** and **-1.30m** respectively in the Domain C in front of the “Sovalye” Island.

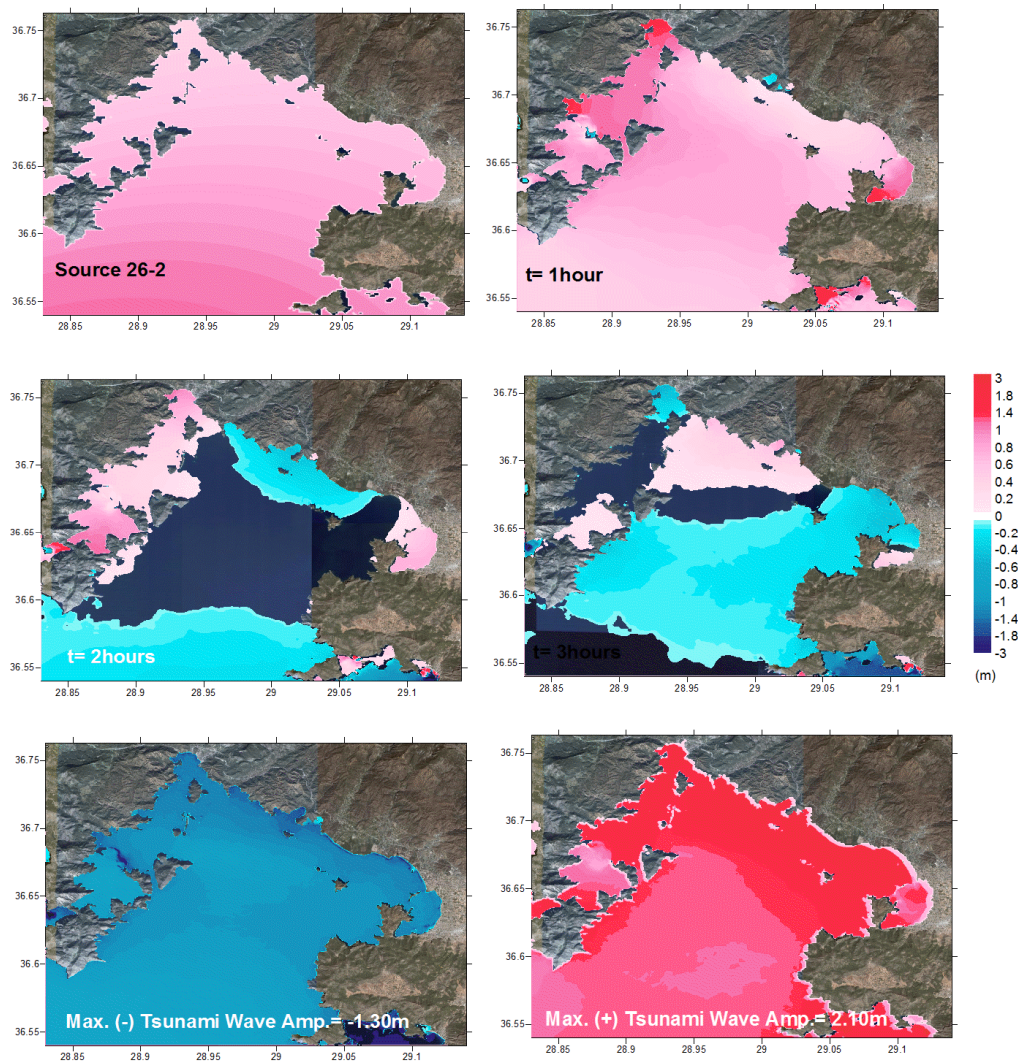


Figure 32: The sea state at different time steps max. (+) and max (-) tsunami wave amplitudes in the Domain C.

Domain D

Distributions of wave propagations for different simulation time steps and maximum positive and maximum negative tsunami amplitudes were given in *Figure 33*. Maximum positive and maximum negative tsunami amplitudes are **1.90m** and **-1.16m** respectively in the Domain D.

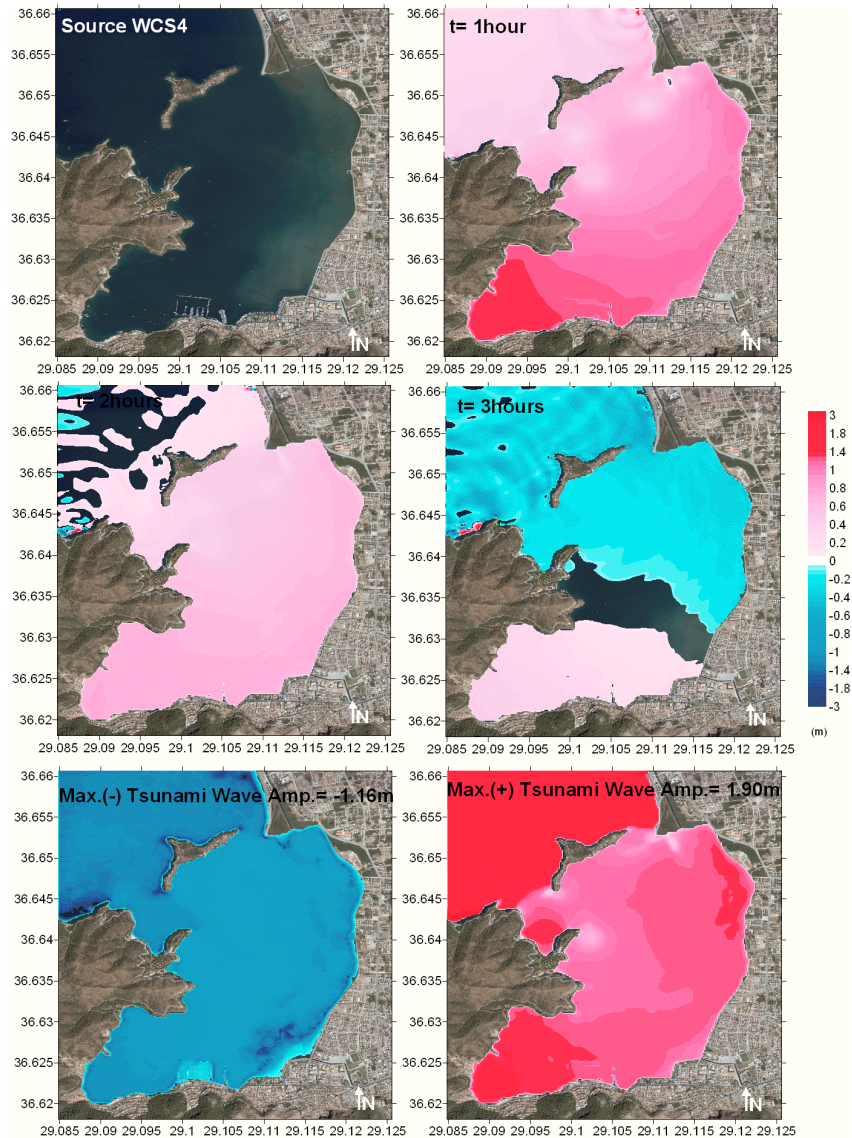


Figure 33: The sea state at different time steps (t=0, 60, 120 and 180 min), max. (+) and max (-) tsunami wave amplitudes in the Domain D

Gauge Locations

In Domain C of WCS4, the maximum positive and maximum negative water surface elevations for the gauges **j** and **k** are **2.02m, 1.90m** and **-1.46m and -1.47m**. The out time hisotries of gauges j and k for Domain C are given with the figure of selected gauges below. The graphs and location of the gauges were given in *Figure 34 and 35*.

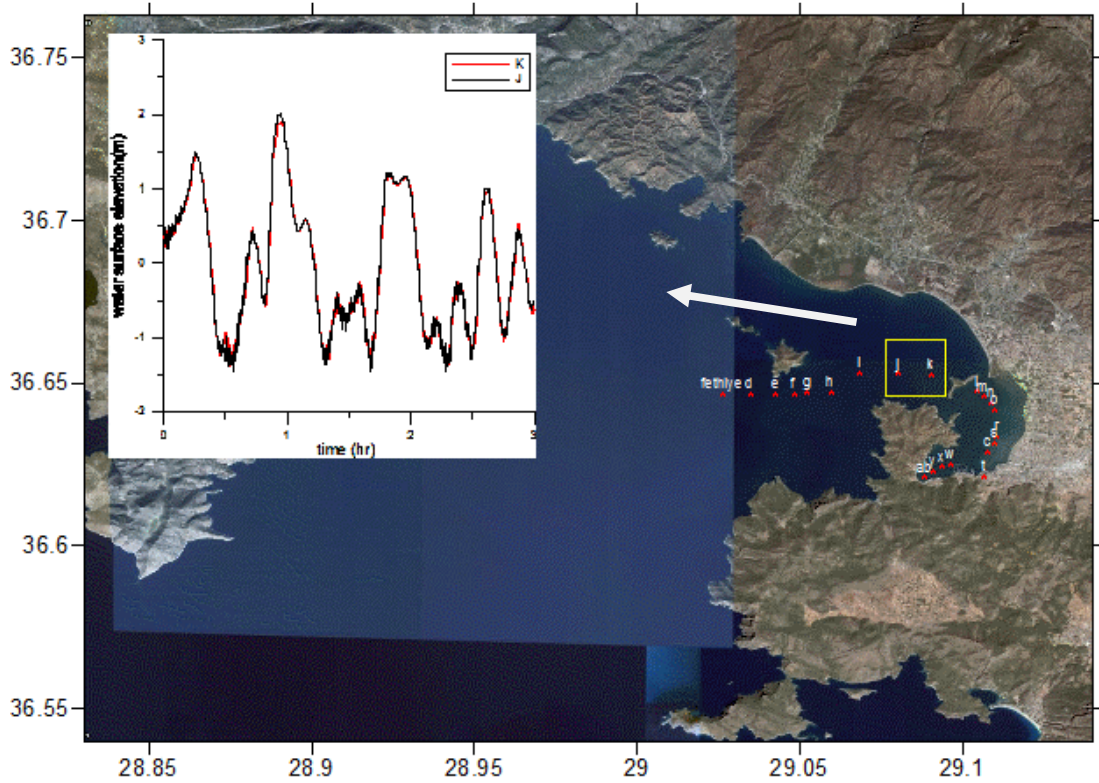


Figure 34: Gauge locations at Domain C and time histories for the gauges j and k.

In Domain D of Z26-2, the maximum positive and maximum negative water surface elevations for the gauge SovalyeW is **1.81m** and **-1.90m**

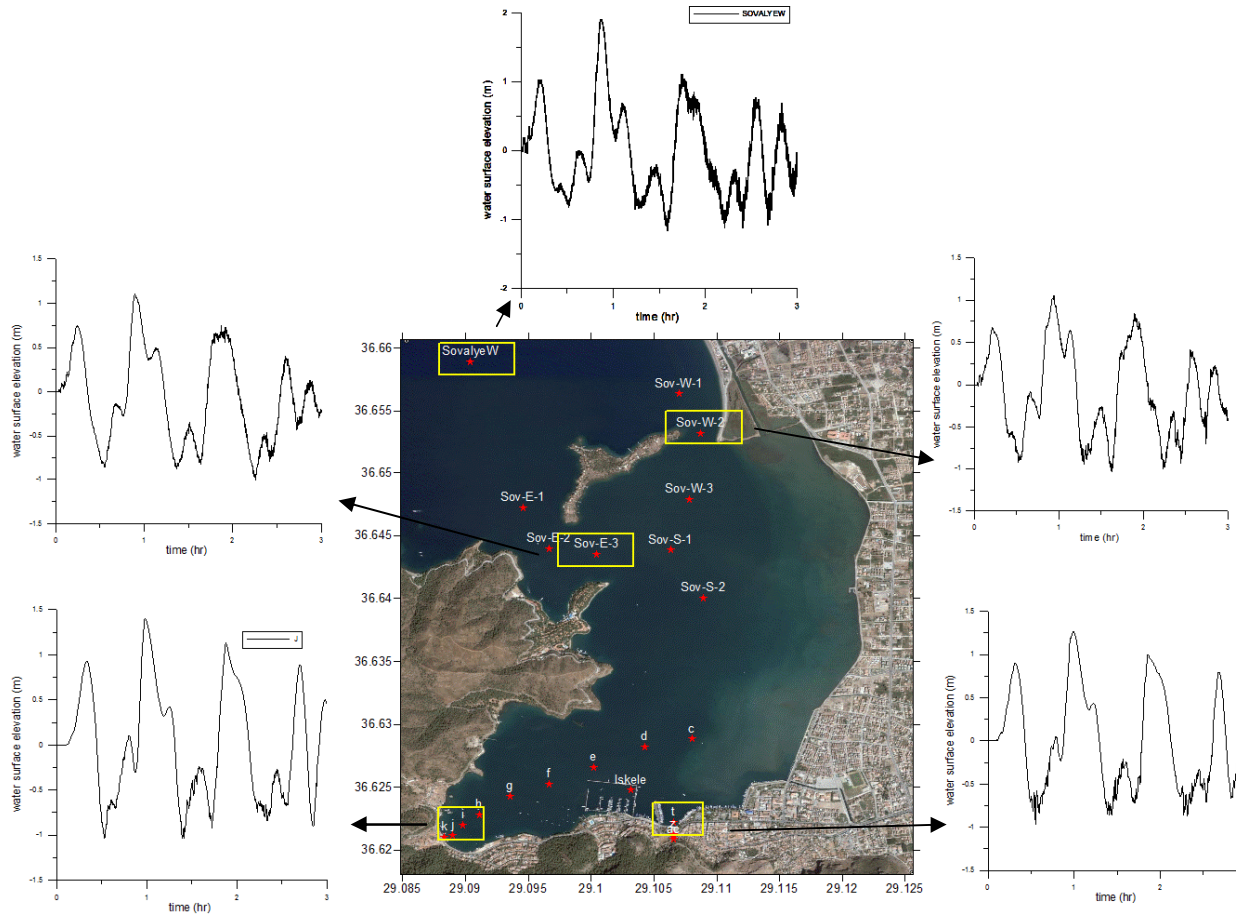


Figure 35: Gauge locations at Domain D of Z26-2 and time histories for the gauges

CHAPTER 5

SUMMARY OF TSUNAMI SOURCES AND SIMULATIONS

Inundation refers to the horizontal distance the wave penetrates inland. Depending on land use, either run-up or inundation are relevant, and most often both

Inundation is one of the most important aspects of tsunami impact. Inundation maps should give all relevant and necessary information in a way that novice users can also understand them. An inundation map includes a line corresponding to the maximum penetration of tsunami wave triggered by the event under study (Synolakis, 2002).

In recent years, the trend of executing the mapping progress using Geographic Information Systems (GIS) has led to the development of information generated from the inundation mapping.

The brief summary of the processes done in the case study of Fethiye are given in *Figure 34*.

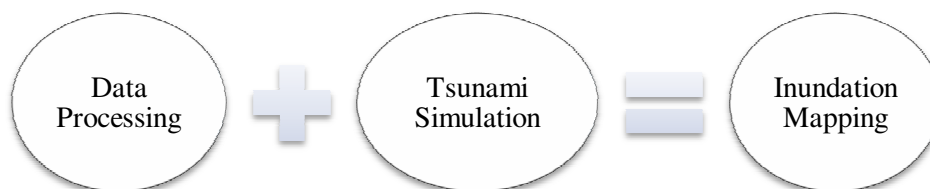


Figure 36: Brief Summary of the applied processes

In *Table 6*, the water surface elevation values acquired from simulations of WCS1, WCS3, WCS4 and Z26-2 Scenarios were compared.

Table 8: Summary of rupture specific simulations performed for the Fethiye

Summary of Rupture Specific Simulation at Gauge Points							
Sources	Arrival time of initial wave(min)	Arrival time of max. wave(min)	Max.(+) wave amp. (meter)				
			j	Sov E-3	SovalyeW	t	Sov- W2
WCS1	20	30	1.29	1.07	1.81	1.21	1.00
WCS3	20	30	1.13	0.89	1.41	1.07	0.76
WCS4	15	30	1.33	1.03	1.78	1.21	1.04
Z26-2	5	60	1.40	1.10	1.90	1.26	1.05

According to *Table 8*, the water surface elevations are the greatest in zone Z26-2 therefore the most critical scenario is Z26-2. Therefore flow depths and inundations were prepared according to simulation results of Z26-2 for the case study, Fethiye.

CHAPTER 6

INUNDATION MAPPING FOR THE CASE STUDY FETHIYE

The simulation results gave us the propagation and inundation of tsunami waves. The inundation data obtained as a result of simulations were integrated into ArcGIS environment in order to develop inundation map of the Fethiye Bay.

The extent of the city development is through northeastern coasts and associated population at risk depends on the inundation zones of the region. In *Figure 37*, low danger zones were delineated with blue tones; high danger zones were delineated with red tones. The greatest inundation distances occurred in “Sovalye” Island. Since “Sovalye” Island decreases the tsunami wave effect, there will be no significant loss of human lives at the center of the Fethiye. But such a tsunami can cause material losses along Fethiye Bay. The results of the scenario show those 20 residential areas, two historical places, 5 commercial auto parks, 1 mosque and 9 monuments and berthing places at city center would be hit from inundation. Tsunami wave amplitudes and currents would damage the boats inside the bay especially in Ece marina along Fethiye town.

The final inundation maps were given in *Figure 36* and *Figure 37*. These maps provide valuable information for the decision makers to develop mitigation strategies and save lives in future tsunamis. These results are also significant in relocating the public buildings, schools, hospitals and other places which will be important in an emergency case.

Inundation Map of the Fethiye Bay

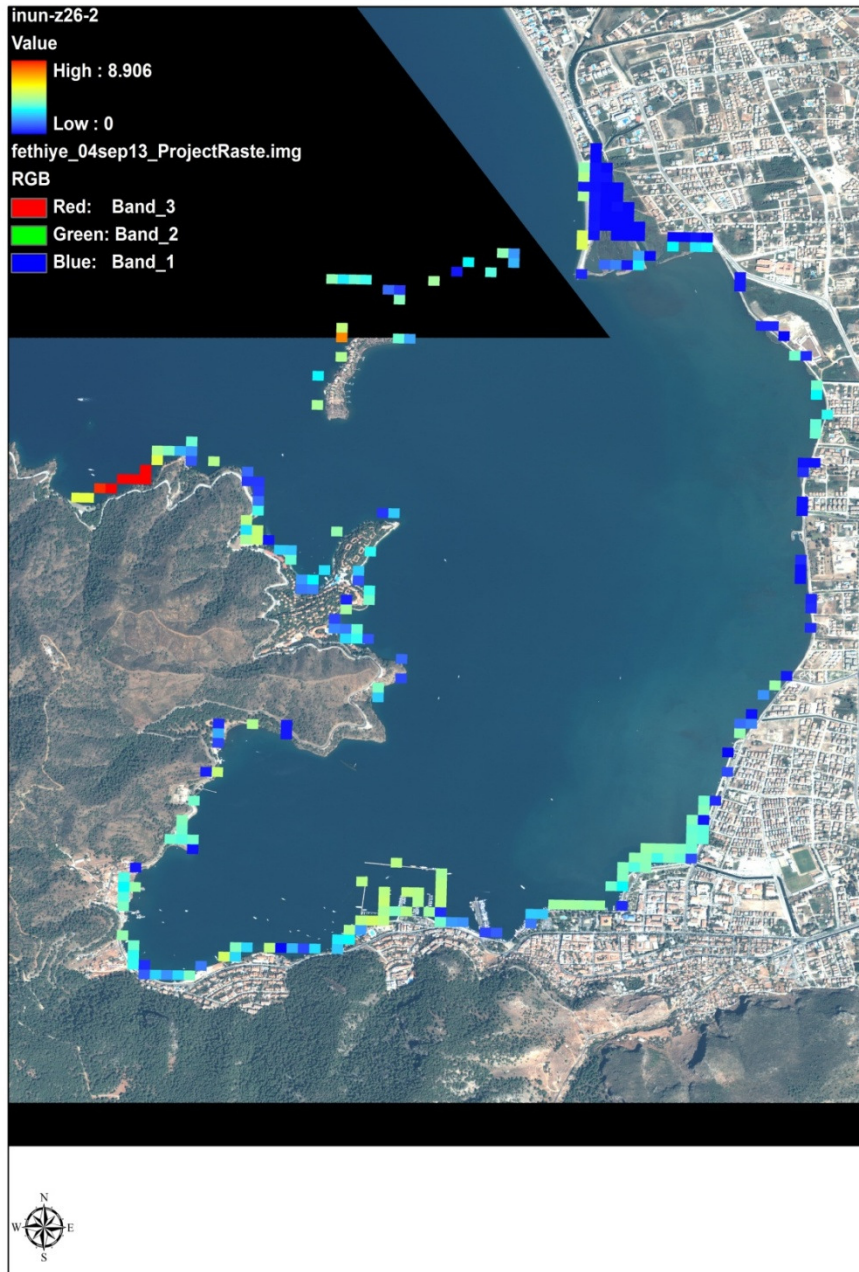


Figure 37: Inundated areas overlaid with Quickbird image in a raster format

Inundation Map of the Fethiye Bay

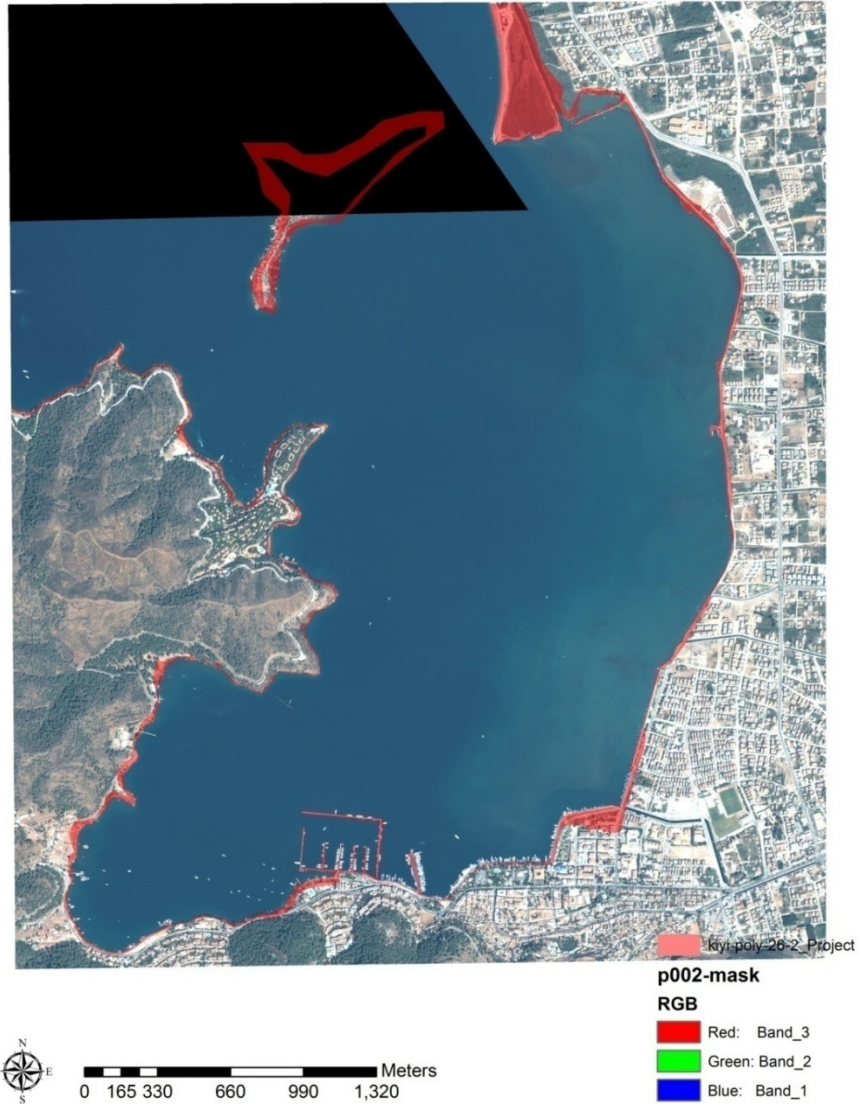


Figure 38: Inundation areas as a result of simulation Z26-2

CHAPTER 7

DISCUSSION OF RESULTS AND CONCLUSION FOR THE FETHIYE BAY

The spatial data and tsunamigenic data were arranged in a geodatabase. A geodatabase was generated (built) that contained both tsunamigenic (water surface elevations and inundation) and spatial data. The heights of the buildings located at the center of the city were also appended to the topography and the effects of these buildings on the simulations and results were also conducted in this thesis. Without building height effect, the waves could penetrate inland more. The grid size of the smallest data was taken as 15m which is accurate and reliable for tsunami inundation maps. From these data, tsunami inundation maps were prepared.

Prasetya et. al. (2008) states that the slope of the ground inland and topography is strongly related with tsunami inundation distance. In their articles, according to numerical model results of 3DD, it is concluded that the gently sloping regions in Banda Aceh have low run ups and greater inundations compared to the areas that have steeper slopes. Since the eastern part of the town has lower slopes, the inundation distance is more. Computational maximum tsunami run up is around 1.5m. The damping effect of “Sovalye” Island causes a wave height decrease in the Bay.

The initiative of the risk analysis covers seven areas such as determining the threat, preparedness, timely and effective warnings, mitigation, public outreach and communication, research, and international coordination. Since risk assessment is included in the first step of the initiative, which is “determining threat”, just this part was analyzed in this thesis. The potential tsunami sources were determined and the realistic models were developed.

CHAPTER 8

GIS-BASED TSUNAMI INUNDATION MAPPING FOR THE ZAKINTOS, KIPARISSIA AND PYLOS TOWNS (TURKEY)

Until this chapter, the processes were applied to Fethiye Bay. Starting with Chapter 8, inundation mapping procedure for Zakintos-Kiparissia-Pylos region was performed by following the same procedure with the case study Fethiye.

8.1 Geological History of Zakintos-Kiparissia-Pylos Region

The western part of the Hellenic Arc, between Zakintos, Kiparissia and Pylos, has been repeatedly affected by large magnitude earthquakes in history that have caused severe destruction and human loss in these areas. These coastal regions are significant for the touristic income of Greece. But the buildings in the coastal zones were not built according to building earthquake standards for the constructions. Therefore they are very vulnerable to forces of earthquakes and tsunamis. This needs to an effective risk management and mitigation planning strategies for Zakintos, Kiparissia and Pylos regions.

The earth's lithosphere beneath the eastern Mediterranean constitutes a broad boundary region between three major tectonic plates, the Eurasian, African, and Arabian plates. The motions of the major plates drive smaller plates, and it is the shapes and motions of these smaller plates that determine the locations and focal mechanisms of earthquakes in the region. Greece is the most seismically active country in Europe, accounting for more than half of the continent's seismic energy release and exhibits the highest seismic activity in the whole Mediterranean area

(Slejko, 2008b). The seismic tectonics of southern Greece is governed primarily by the motion of the Africa plates with respect to the relatively small Aegean Sea plate. Most shallow earthquakes in central and northern Greece (depths less than 50 km) result from interaction between the Eurasia plate and the small Aegean Sea plate, which is moving southwest with respect to the Eurasia plate with a velocity of about 30 mm/year. The boundary between the Aegean plate and the Eurasian plate in central and northern Greece is diffuse. Seismicity is concentrated in east-trending and northeast-trending zones of deformation. The east-trending zones are most prominent in mainland Greece, are characterized by predominantly normal faulting, and have produced earthquakes with magnitudes of about 7. The northeast-trending belts are characterized by predominately strike-slip fault earthquakes. A northeast-trending zone of predominantly strike-slip earthquakes is off the west coasts of Cephalonia and Lefkada, western Greece, and other northeast-trending zones occur beneath the Aegean Sea east of the Greek mainland. (Papadopoulos (2001), Papadopoulos and Fokaefs (2005), Papadopoulos et. al, (2007), USGS, (2008), Zaytsev et. al., (2008))

According to Ambraseys and Jackson (1990), a 100 years' data set of earthquakes in central Greece is inadequate for either a reasonable assessment of seismic hazard or for a confident estimation of maximum magnitude. Nevertheless, it is probable that the maximum magnitude is restricted by the maximum length of fault segments, which appears to be around 15-20 km. The earthquakes of $M_s \geq 5.8$ during 1890-1988 can account for an N-S displacement of around 45-70 cm (with maximum and minimum estimates a factor of two greater and smaller than this) across part of an 1890-1900 triangulation network in central Greece that was resurveyed in 1988. Considering that the contribution of smaller events may increase this displacement by about 50 per cent, this cumulative seismic displacement is similar to that estimated from the geodetic work (of about 100 cm). The western part of the Hellenic Arc between Pirgos and Pylos, western Peloponnesus, is one of the most seismically active areas in the entire Mediterranean region. This area has been repeatedly affected by large magnitude earthquakes that have caused severe destruction and human loss (i.e. 1886 Philiatra M7.3, 1893 Zante-Keri M6.5, 1899 Kiparissia M6.5, 1947 Pylos M7.0, and 1997 Gargaliani M6.6). Some of the largest regional tsunamis

in the Mediterranean Sea have also been observed in association with large earthquakes (i.e. 1630 and 1866, southwestern Hellenic Arc), affecting near-field as well as remote coastal segments in western Peloponnesus, Crete, and as far as Alexandria, Adriatic Sea and east Sicily.

In this chapter, a case study was provided for Zakintos, Kiparissia and Pylos. 13 tsunamigenic earthquake sources were estimated according to seismic report of Slejko, 2009. The simulations of the sources P01 and P04 were performed with NAMI DANCE 4.6 and GIS based inundation maps were created for these scenarios. The aim of this report is to determine characteristics of faults for Western part of Greece, especially for Pylos-Zakinthos (including Philiatra and Kiparissia) area and estimate the possible tsunami sources by using the outputs of the final reports,” Seismic Hazard Assessment” written by Slejko (2008b and 2009)

The method of this report is to collect and enhance reliable data, apply numerical tools and models to this data to estimate the characteristics of probable tsunamis (P01 and P04 Faults) selected from the region and understand the results for the comparison of tsunami’s effects to Pylos-Zakinthos-Kiparissia Region. For further step, the available results of modeling will be integrated to GIS based applications to analyze, organize and display the output in order to be helpful to develop preparedness and mitigation strategies for the region.

The boundaries of the study regions were given in *Table 7*.

Table 9: Boundaries of the study area (Pylos-Zakinthos-Kiparissia)

Coordinate System	GCS_WGS 84	
Longitude	19°E	22.5°E
Latitude	36°N	39°N

8.2 Data Processing

The general bathymetric/topographic data of the region were acquired from different sources as it was done in the data processing stage of the Fethiye case. But in this

case, the available data was limited with Advanced Spaceborne Thermal Emission and Reflection Radiometer (ASTER) image and GEBCO data. The vector map of the region could not be acquired from local authorities. Therefore GIS based applications were used only in organizing, analyzing of the spatial data taken from GEBCO and ASTER. The characteristics of the data used in this study were given in *Table 8* below:

Table 10: Characteristics of the data used

Name	Date	Production Method	Source	Projection
DEM	2005	ASTER 3A orthorectified image	Fethiye Municipality	GCS_WGS_1984
Bathymetry/topography data	2009	GEBCO	METU-OERC	GCS_WGS_1984

High accuracy bathymetric data was needed for the case of the western part of Greece specifically for Zakynthos, Kiparissia, and Pylos regions. Therefore, OERC collected and purchased available bathymetric and topographic data.

Specifically, the followings were completed:

-Collection of bathymetry/topography data with 1 min (1800m grid size) resolution from GEBCO (General Bathymetric Chart of the Oceans) of the British Oceanographic Data Centre.

-Purchase of Advanced Spaceborne Thermal Emission and Reflection Radiometer (ASTER) 3A 60km* 60km, 14 band orthorectified satellite images with a radiometric resolution of 8 bit in 3 different pieces involving different regions from NIK Systems. These three were combined.

-Comparison of new data with the existing METU-OERC archived data which was formerly developed for the previously completed Pylos report, using nautical charts with various scales and resolutions (OERC, 2008b)

The aim of this part of the thesis is to form a database of bathymetry, topography and shoreline data of the region with “xyz” coordinates by using data as accurate and as precise as possible by performing the following steps; i) setting projection system, ii) creating DEM and adding “xyz” coordinates iii) digitizing iv) overlay operations

The coordinate system of all layers in data processing used in the project was converted to same projection system as “GCS_WGS_1984.The satellite image in the file format of “ASTER.3A .dat” was analyzed with software Program” PCI Geomatica”. The satellite images that are combined in the software are orthorectified by using ground control points of the region exported to” .tif “file format.

The dataset formed was transferred to ArcGIS Environment. Digital Elevation Model (DEM) of the regions is obtained. Points with 20m interval are settled at the centre of each cell of DEM. In this way the values of “xyz” coordinates of these points are extracted from DEM in “.dbf” file format.

By changing the visible band coordination given in ASTER Image, the coastal zones of Zakintos, Kiparissia, and Pylos were digitized. Polyline and polygon types of shape files are formed with the same coordinates of image for coastal strip of main land and islands, respectively and a buffer zone of 20m distance is used in the landward of the coastal strip in order to analyze the “xyz” coordinate values in these coastal areas

For the final step of data analysis processing, the buffer zones created with 20m horizontal distance and polygon and polyline shape files were overlaid in ArcMAP 9.3 to extract the points on coastal strip. After collecting and combining the data, the modeling stage of the work was explained in the following sections.

8.3 Estimation of Tsunamigenic Data and Simulations

The valid and reliable tsunamigenic data is needed for the tsunami simulation. In this subsection, first, the way of estimating tsunami source mechanisms were explained. Second, selected worst case tsunami scenarios were simulated by TUNAMI N3

8.3.1 Estimation of Probable Tsunami Source Mechanisms for the Kiparissia-Pylos-Zakintos region

In this thesis, source parameters were estimated with the collaboration of METU, Ocean Engineering Research Center (OERC) and SEHELLARC Partners' report, Slejko, 2009. Since there is no sufficient information available about source parameters of the earthquake taken from the sources of the Slejko report, the dip and slip angles of the faults were justified to give the worst case conditions of tsunami source mechanisms. The fault map showing the surficial seismic zones and their names in the shape of red line in the western part of Greece (*Figure 39*) was taken from the Slejko, 2009 report. By using this fault map, OERC has prepared 12 probable tsunami sources and has estimated rupture characteristics for Zakynthos-Kiparissia-Philiatra-Pylos region by taking into consideration the WP5 (Slejko, 2008b and 2009) reports of SEHELLARC and Okada (1985).

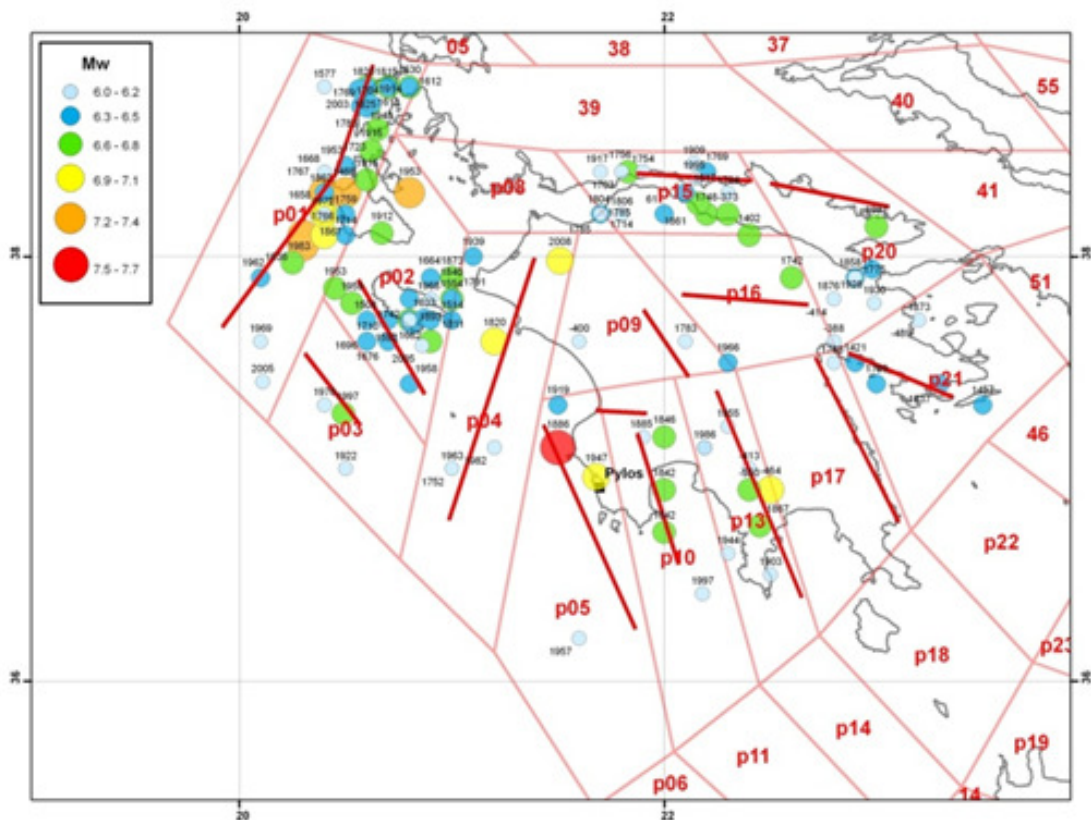


Figure 39: Surficial Seismic Zones. Main faults (red lines), and earthquakes ($M_w \geq 6$) in the SEHELLARC project. (Slejko, 2009)

The estimated rupture parameters have been presented for the review of SEHELLARC partners. The general summary of the rupture parameters were given in *Table 9* below. Their locations and rupture parameters of possible tsunami sources were given in details in the following *figures (40, 41, 42 and 43)* and *Table 12*.

Table 11: Estimated rupture parameters for the Western Greece

	(degree)	(km)	(km)	(km)	(deg.)	(deg.)	(deg.)	(m)	(+)	(-)
Name	Epicenter	Length	Width	Focal Depth	Strike Angle	Dip Angle	Slip Angle	Disp.	Max amplitude	Max amplitude
p01	19.90E 37.90N	130	25	15	25	10	110	6	1.58	-0.95
p02	21.00E 37.50N	66.3	40	15	25	10	110	6	1.90	-0.888
p03	20.60E 37.00N	45.7	20	15	345	10	110	6	1.39	-0.82
p04	20.75E 36.80N	136	30	15	15	10	110	6	1.72	-1.00
p05	21.50E 36.30N	70	20	15	345	10	110	6	1.39	-0.82
p06	22.50E 34.80N	80	45	15	300	10	110	6	1.93	-1.06
p10	22.10E 36.00N	70.3	20	15	345	10	110	6	1.39	-0.83
p11	23.00E 35.00N	100	40	15	320	10	110	6	1.89	-1.07
p12	24.50E 34.25N	120	40	15	290	10	110	6	1.90	-1.09
p13	22.60E 36.10N	110.1	30	15	340	10	110	6	1.70	-0.98
p14	23.20E 35.30N	80	40	15	320	10	110	6	1.87	-1.05
p18	23.30E 35.50N	90	50	15	325	10	110	6	1.99	-1.09

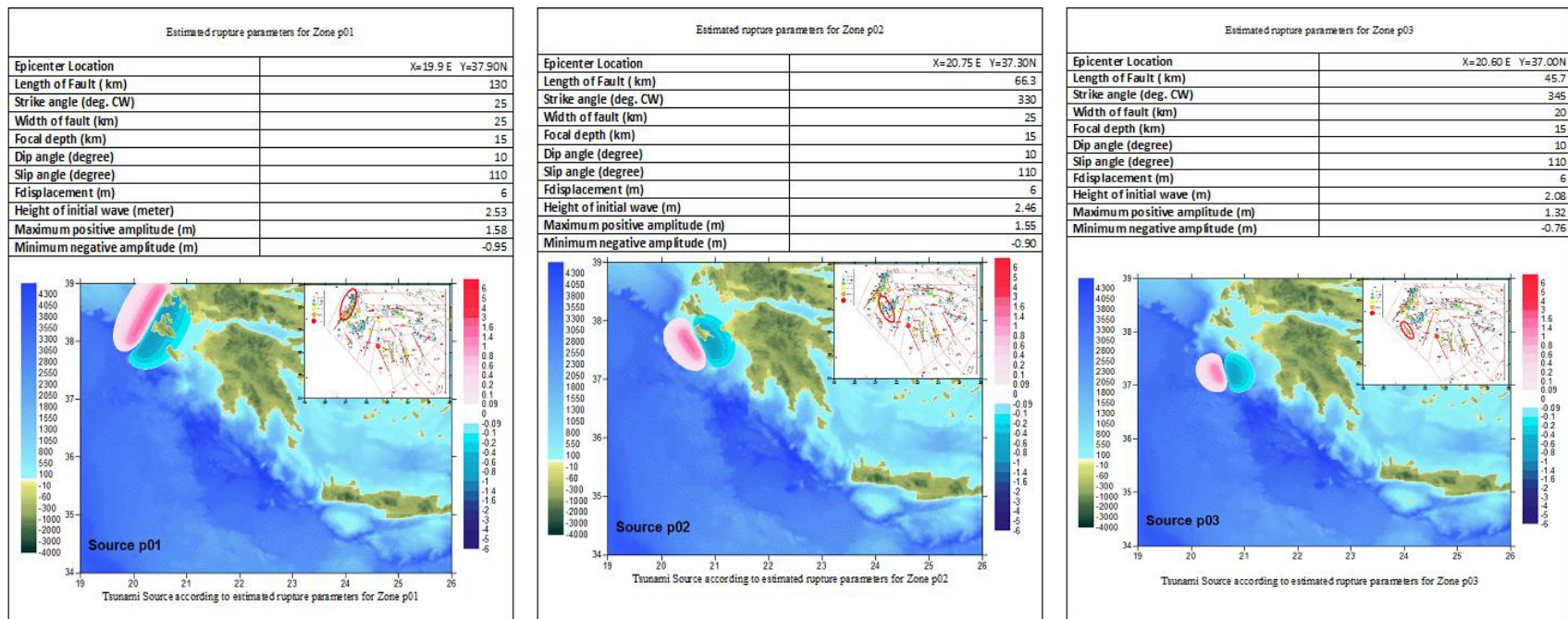


Figure 40: Estimated rupture parameters for the zones p01, p02, p03

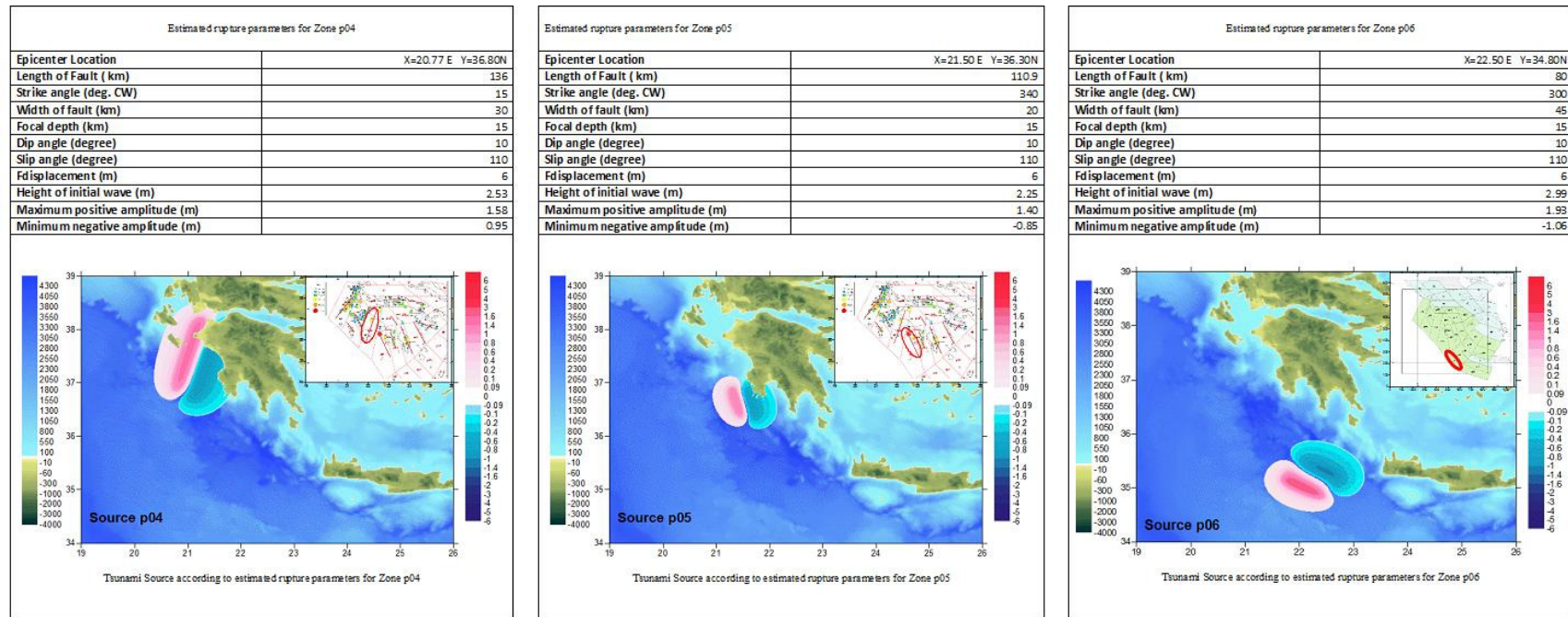


Figure 41: Estimated rupture parameters for the zones p04, p05, p06

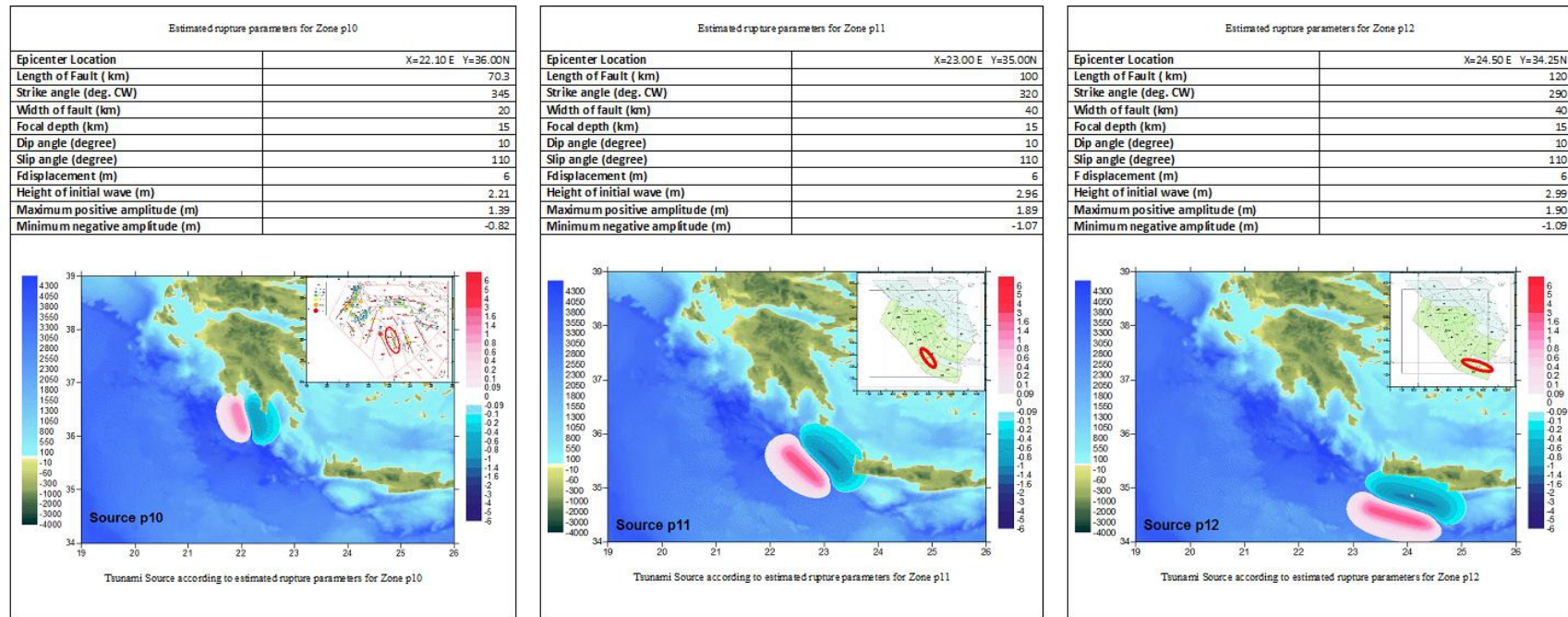


Figure 42: Estimated rupture parameters for the zones p10, p11, p12

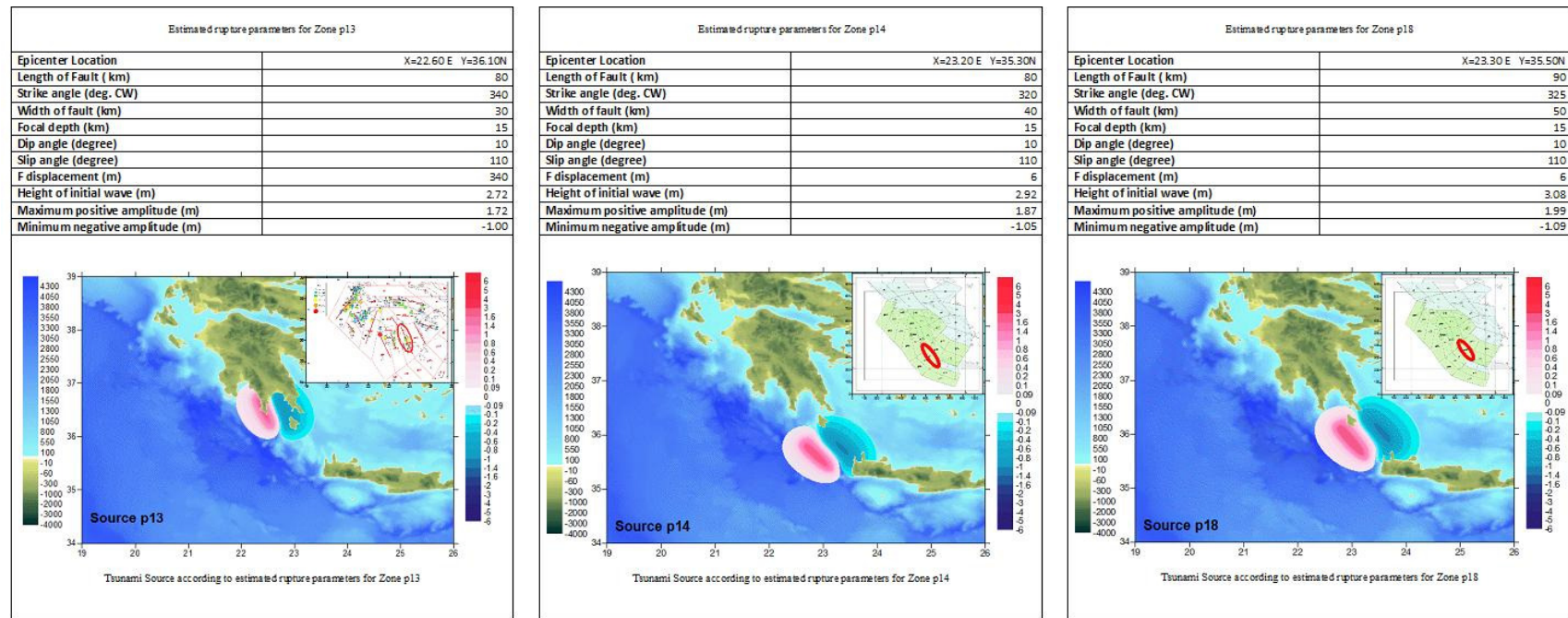


Figure 43: Estimated rupture parameters for the zones p13, p14, p18

8.3.2 Tsunami Simulation for the case region Zakintos-Kiparrisia-Pylos

The initial wave amplitudes and the locations with respect to the study region Zakintos-Kiparrisia and Pylos were investigated and it was found that the most critical tsunami sources are P01 and P04. Therefore the tsunami simulations of these source were decided to be done. The rupture characteristics of faults P01 and P04 were used to generate the initial wave parameters of possible tsunami around Pylos-Zakintos-Kiparrisia areas with *TUNAMI N3*[®] Simulation program. Tsunamigenic data were taken from Slejko (2009) report which is a result of the discussions made by geologists in the SEHELLARC annual meeting in June 2009.

8.3.2.1 Tsunami Simulation of P01

The simulations of nested domains are done with *TUNAMI N3*[®] Program for P01 and P04 at duration of 90 minutes as a nested grid to understand the coastal wave amplifications of tsunami at certain locations. This time was enough to see the distribution of water surface elevations and coastal amplifications. Domain B covers western coast of Greece with 180 m grid size. Domain C was formed near Zakynthos, Kiparrisia, Philiatra, Pylos and neighboring areas with 60m grid size and the D Domains cover Zakynthos, Kiparrisia, Philiatra, Pylos harbors and towns with 20m grid size. These study domain's locations were mapped in *Figures 44, 45 and 46*. The coordinates of the domains were shown in *Table 12*. The simulation time step was taken as 12 sec. The output files of TUNAMI N3 were integrated into *SURFER 8* and *GRAPHER 8* Golden Software Programs. The distribution of water surface elevations were presented only for t=0, t=16, t=32, t=48, t=80min for each domain and regions by using *SURFER 8*[®]. The distributions of maximum positive and negative water amplitudes values for each grid were also mapped with *SURFER 8*[®]. Gauges were placed to specific locations to be able to compare the maximum positive and maximum negative wave amplitude values at each domain coming from P01 and P04 simulation results. The graphs of the gauges were drawn in *GRAPHER 8*.

Table 12: Study Domains

Name	Domains			Boundaries (degree)	Grid Size (m)	Output Time Intervals (sec)	Simulation Duration (min)
	B	C	D				
Greece	B			19E 26E 34N 39N	180	6	90
Philiatra, Kiparissia		C		21.52 E 21.69E 37.12N 37.28N	60	6	90
			D	21.65E 21.66E 37.25N 37.26N	20	6	90
Pylos		C		21.65E 21.66E 37.25N 37.26N	60	6	90
			D	21.65E 21.66E 37.25N 37.26N	20	6	90
Zakinthos		C		21.65E 21.66E 37.25N 37.26N	60	6	90
Zakinthos			D	21.65E 21.66E 37.25N 37.26N	20	6	90

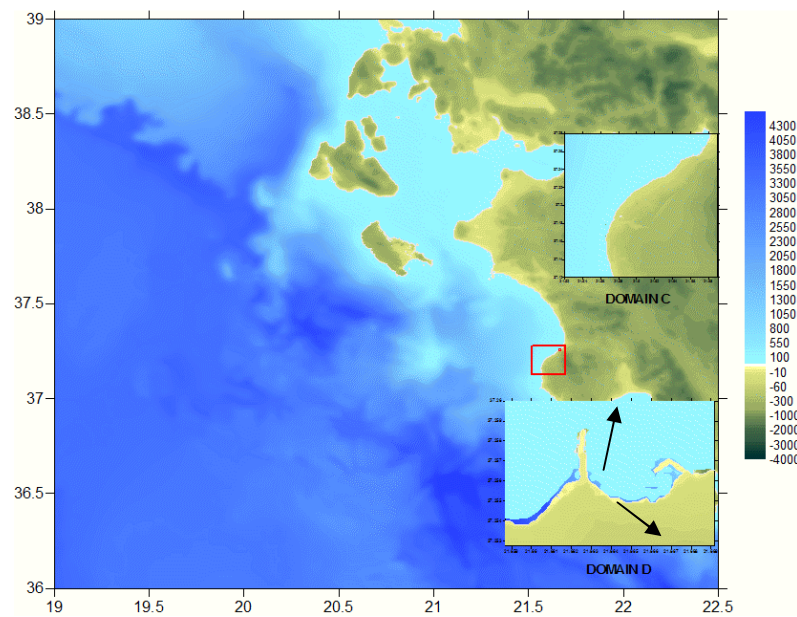


Figure 44: The structure of nested Domains (Domain B, Domain C and Domain D) for the simulation of Kiparissia-Philiatra Region

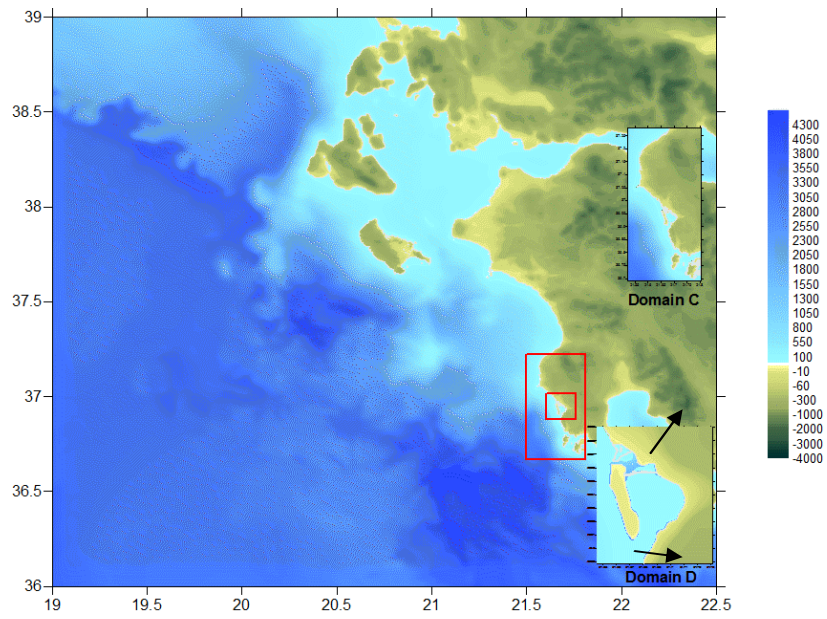


Figure 45: The structure of nested Domains (Domain B, Domain C and Domain D) for the simulation of Pylos Region

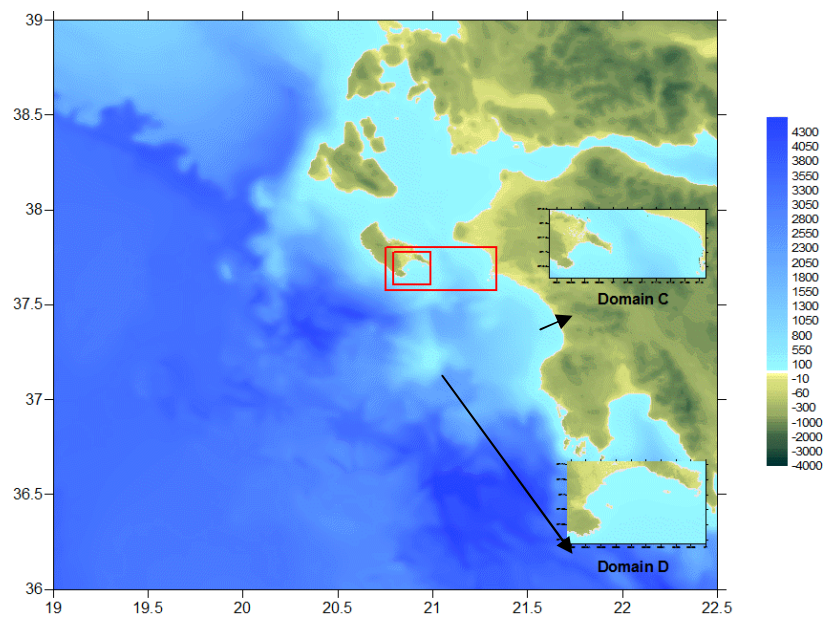


Figure 46: The structure of nested Domains (Domain B, Domain C and Domain D) for the simulation of Zakynthos Region

Propagation of the P01 Scenario in Kiparissia-Philiatra Region

Domain B

In order to compare the time histories of water surface elevations near Kiparissia-Philiatra, several gauge points are selected and the water surface elevations, time of arrival of waves to these points Domain B.

Wave propagation of the selected tsunami with estimated rupture parameters was simulated. Maximum positive wave amplitude is **6.34m** and maximum negative wave amplitude is **-5.83m** in the Domain B. Figure 47 is a summary of wave propagation in Domain B.

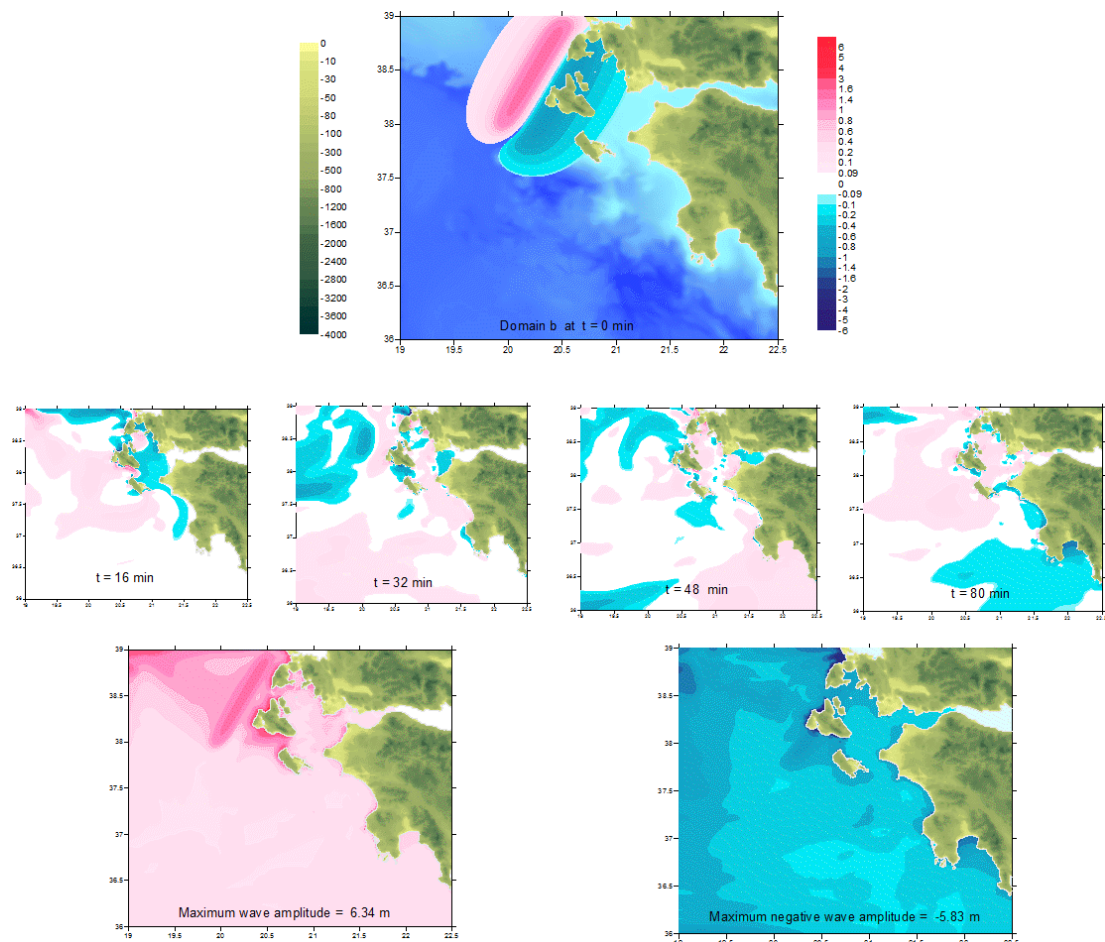


Figure 47. The sea state at different time steps and maximum positive and maximum negative tsunami amplitudes in the Domain B (Kiparissia-Philiatra)

Domain C

Wave propagation of the selected tsunami with estimated rupture parameters was simulated. Maximum positive wave amplitude is **2.0m** and maximum negative wave amplitude is **-1.80m** in the Domain C.

Gauge Locations at Domain C

In order to compare the time histories of water surface elevations near Kiparissia-Philiatra, several gauge points are selected and the water surface elevations, time of arrival of waves to these points are shown in *Figure 48*. **1.5m** positive and **-1.5m** negative water amplitudes occur at Kiparissia7 Gauge point. The wave first arrives at point nearly 24 minutes after the rupture.

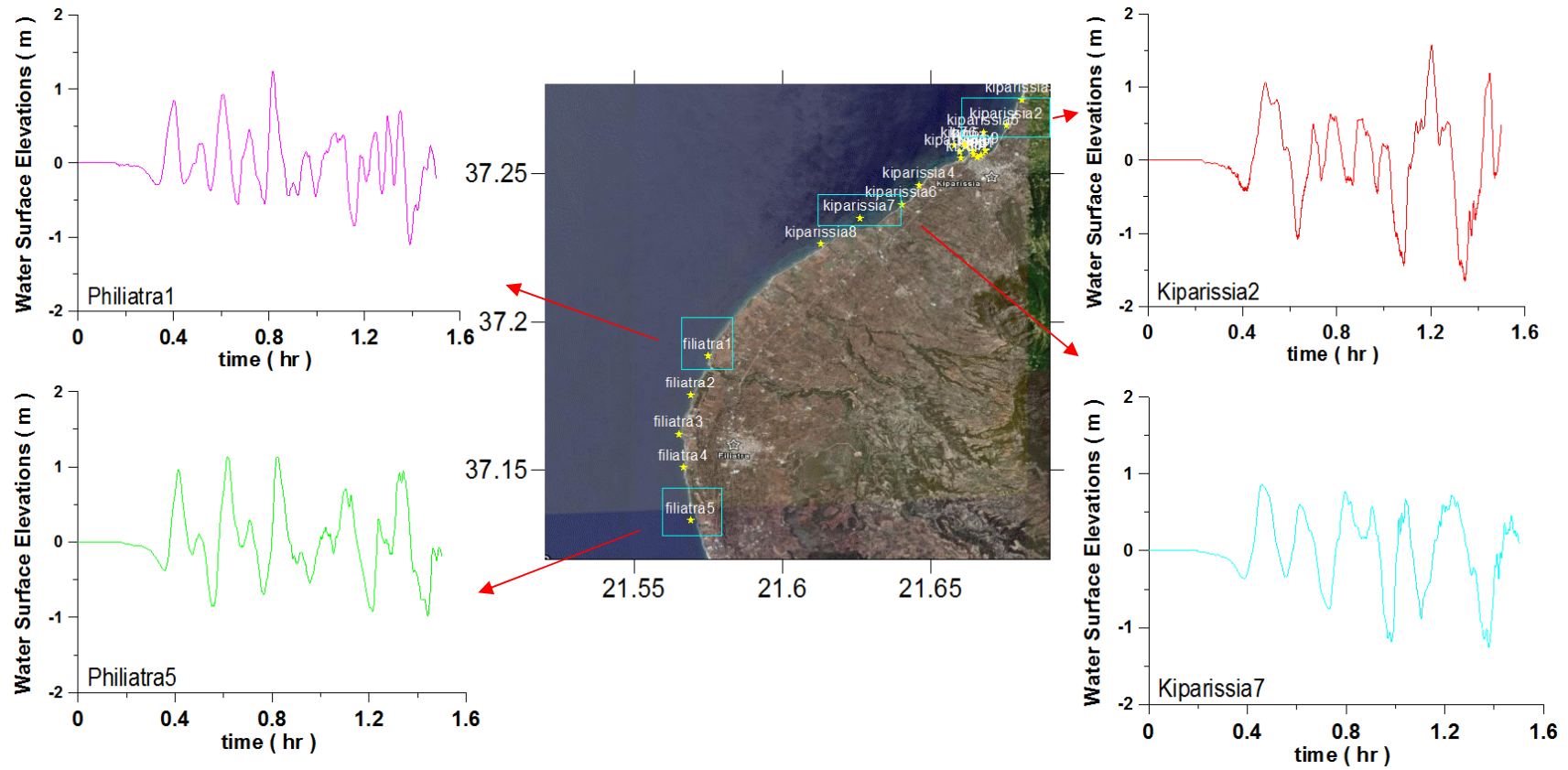


Figure 48: The time histories of water surface elevations (in hours) at selected gauge points at Domain C

Domain D

The sea state at different time steps ($t=0, 16, 32, 48$ and 80 min), maximum positive and maximum negative tsunami amplitudes in the Domain D were given in *Figure 49*. According to this figure, maximum positive and maximum negative amplitudes are **1.7m** and **-1.9m** respectively.

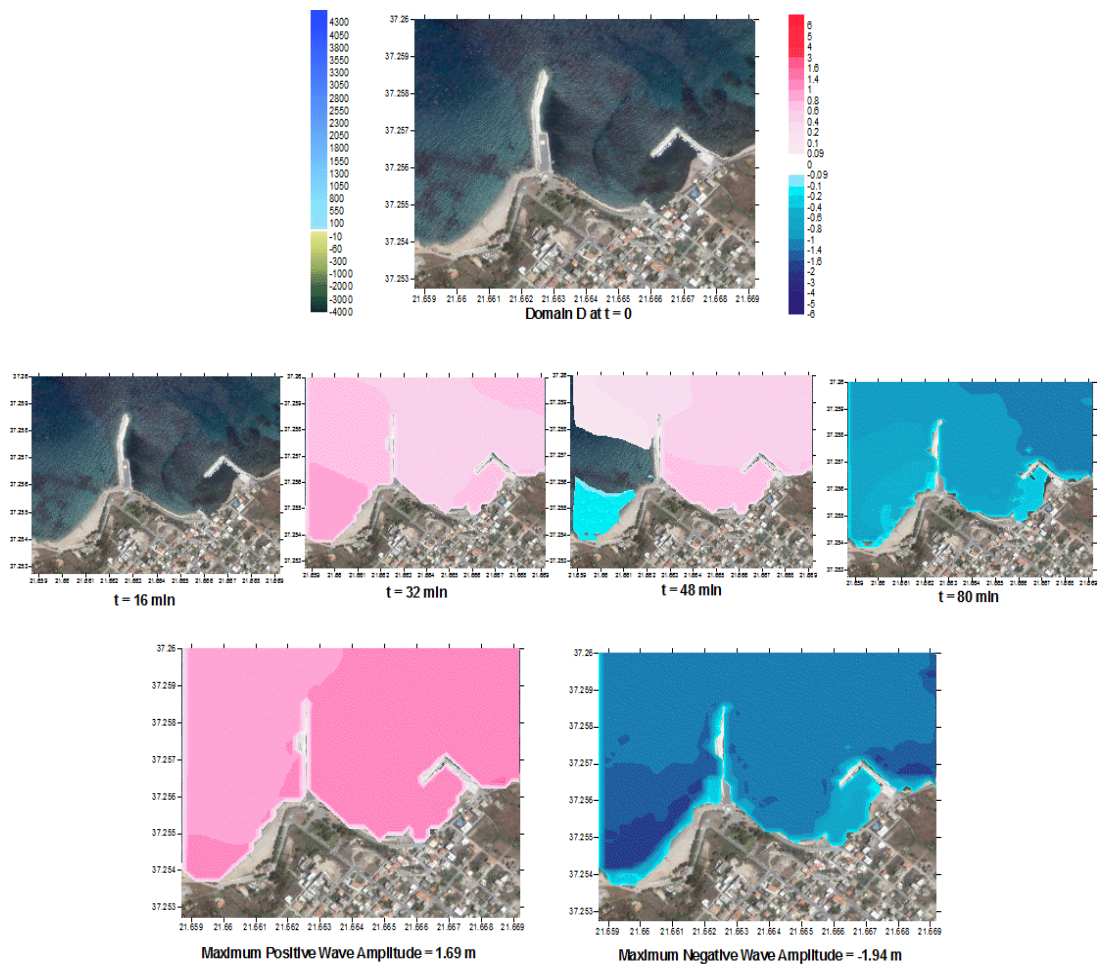


Figure 49: The sea state at different time steps and maximum positive and maximum negative tsunami amplitudes in the Domain D (Kiparissia-Philiatra)

Gauge Locations at Domain D

Several gauge points are selected and the water surface elevations, time of arrival of waves to these points are shown in *Figure 50*. As it is seen from the figure, the maximum positive water amplitude of tsunami is **1.20m** at gauge kip2, while maximum negative amplitude is **-1.70m** at kip8.

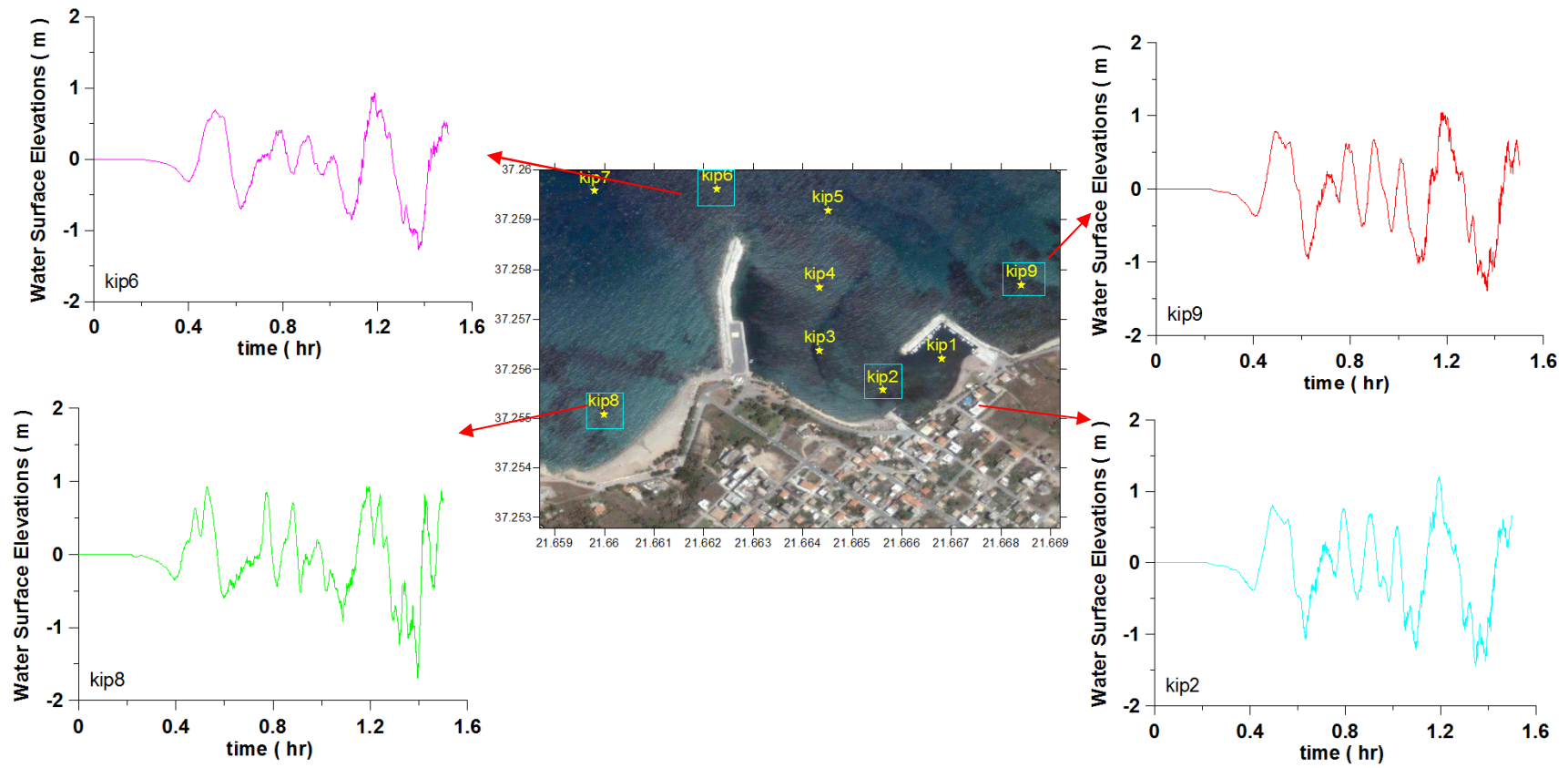


Figure 50: The time histories of water surface elevations at selected gauge points at Domain D

Propagations of P01 Scenario in Pylos Region

Domain B

Since the propagation of the tsunami is same for Domain B given in simulation of Kiparissia-Philiatra region, the simulation and propagation of the tsunami was only shown for Domain C and Domain D at this section.

Domain C

Wave Propagation of the selected tsunami with estimated rupture parameters was simulated for Domain C at Pylos Region. Maximum positive wave amplitude is **2.30m** and maximum negative wave amplitude is **-2.64m** in the Domain C.

Gauge Locations at Domain C

Several gauge points are selected which are shown in *Figure 51* as well as Domain D near Kiparissia-Philiatra Region. As it is seen from the *Figure 52*, the maximum positive water amplitude of tsunami is **0.44m**, while maximum negative amplitude is **-0.43m**. The water surface elevations, time of arrival of waves to these points are shown in *Figure 53*. The wave first arrives at point nearly 36 minutes after the rupture.

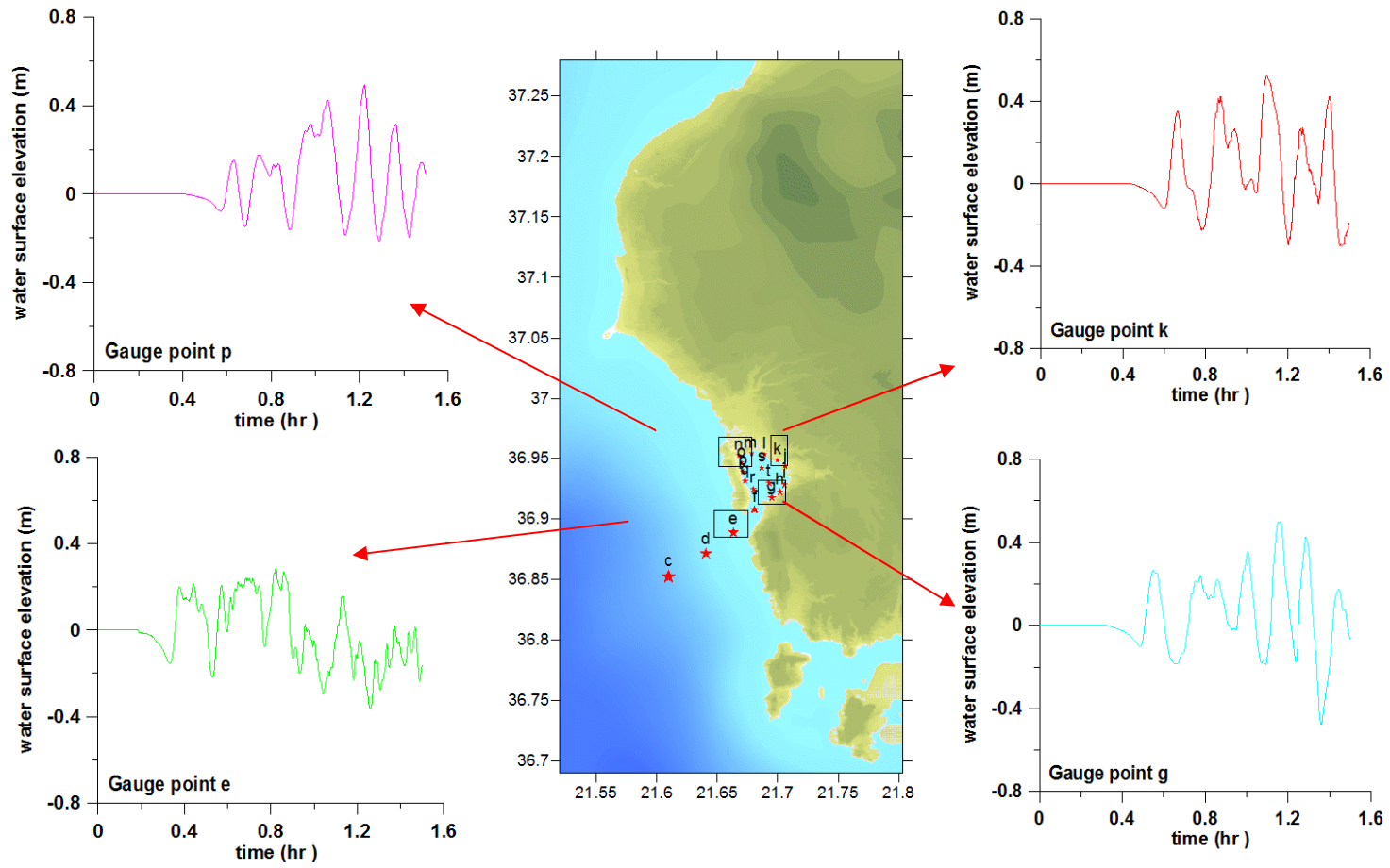


Figure 51: The time histories of water surface elevations (in hours) at selected gauge points at Domain C

Domain D

The sea state at different time steps ($t=0, 16, 32, 48$ and 80 min), maximum positive and maximum negative tsunami amplitudes in the Domain C are given in *Figure 52* below. According to this figure, the maximum positive amplitude of tsunami is **1.78m**, and maximum negative amplitude is **-2.68m**.

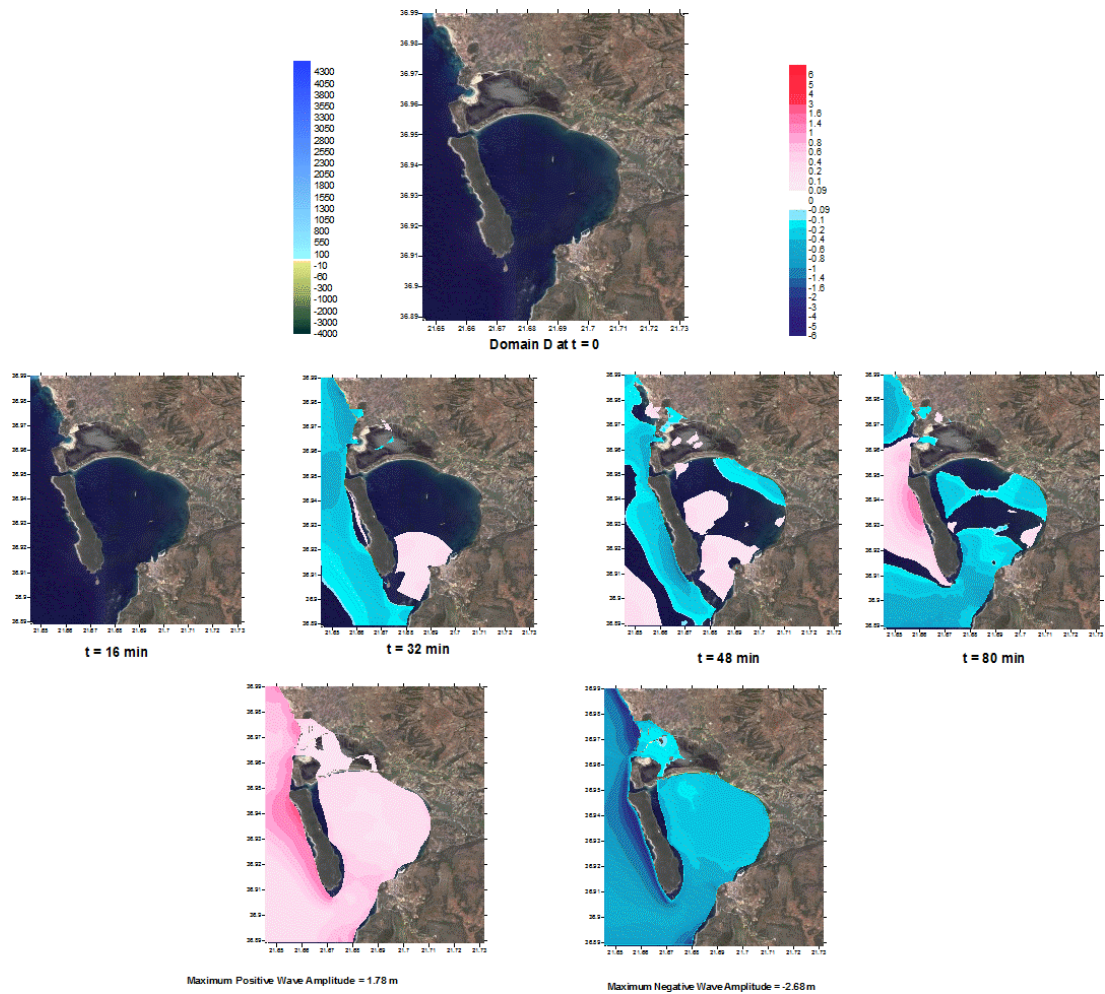


Figure 52: Propagation of tsunami for specific times ($t=16, 32, 48$ and 80 min), max (+) and max (-) tsunami wave amplitudes

Gauge Locations at Domain D

Several gauge points are selected which are shown in *Figure 53*. The maximum positive amplitude of tsunami is **0.42m**, while maximum negative amplitude is - **0.63m**. The water surface elevations, time of arrival of waves to these points are also shown in *Figure 53*.

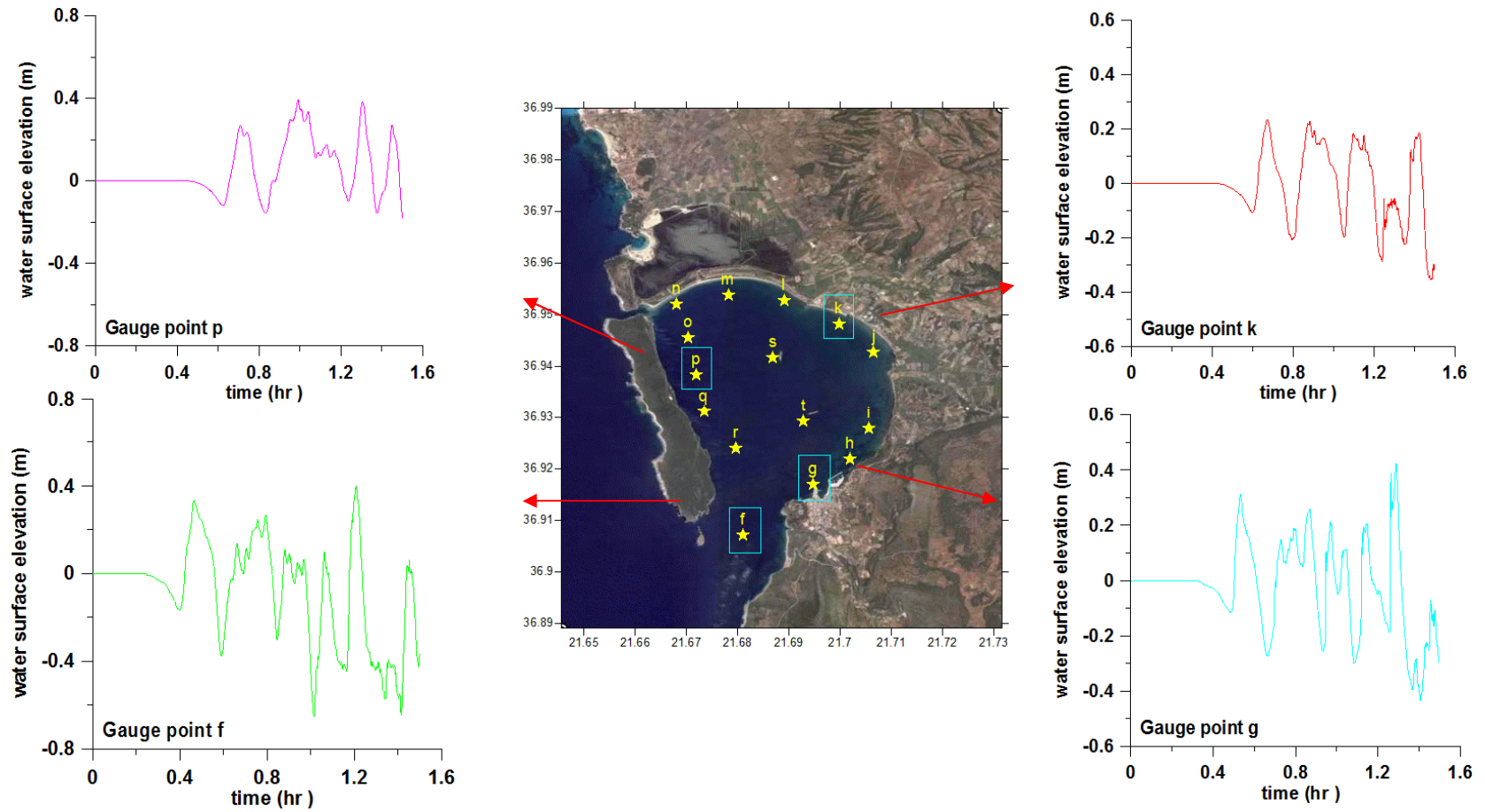


Figure 53: The time histories of water surface elevations (in hours) at selected gauge points at Domain D, Pylos

Propagation of P01 Scenario for Zakynthos Region

Domain B

Wave Propagation of the selected tsunami with estimated rupture parameters was simulated for Zakynthos Region with given domains and the same source P01. Since the propagation of the tsunami is same for Domain B given in simulation of Kiparissia-Philiatra region, the simulation and propagation of the tsunami for Zakynthos region was only shown for Domain C and Domain D at this section.

Domain C

The maximum positive and maximum negative tsunami amplitudes in the Domain C were simulated. The maximum positive amplitude of tsunami is **4.26m**, and maximum negative amplitude is **-2.36m**.

Gauge Locations at Domain C

Several gauge points are selected which are shown in *Figure 54*. The maximum positive amplitude of tsunami is **1.246m**, while maximum negative amplitude is **-1.70m** for selected gauge points. The water surface elevations, time of arrival of waves to these points were shown in *Figure 54*.

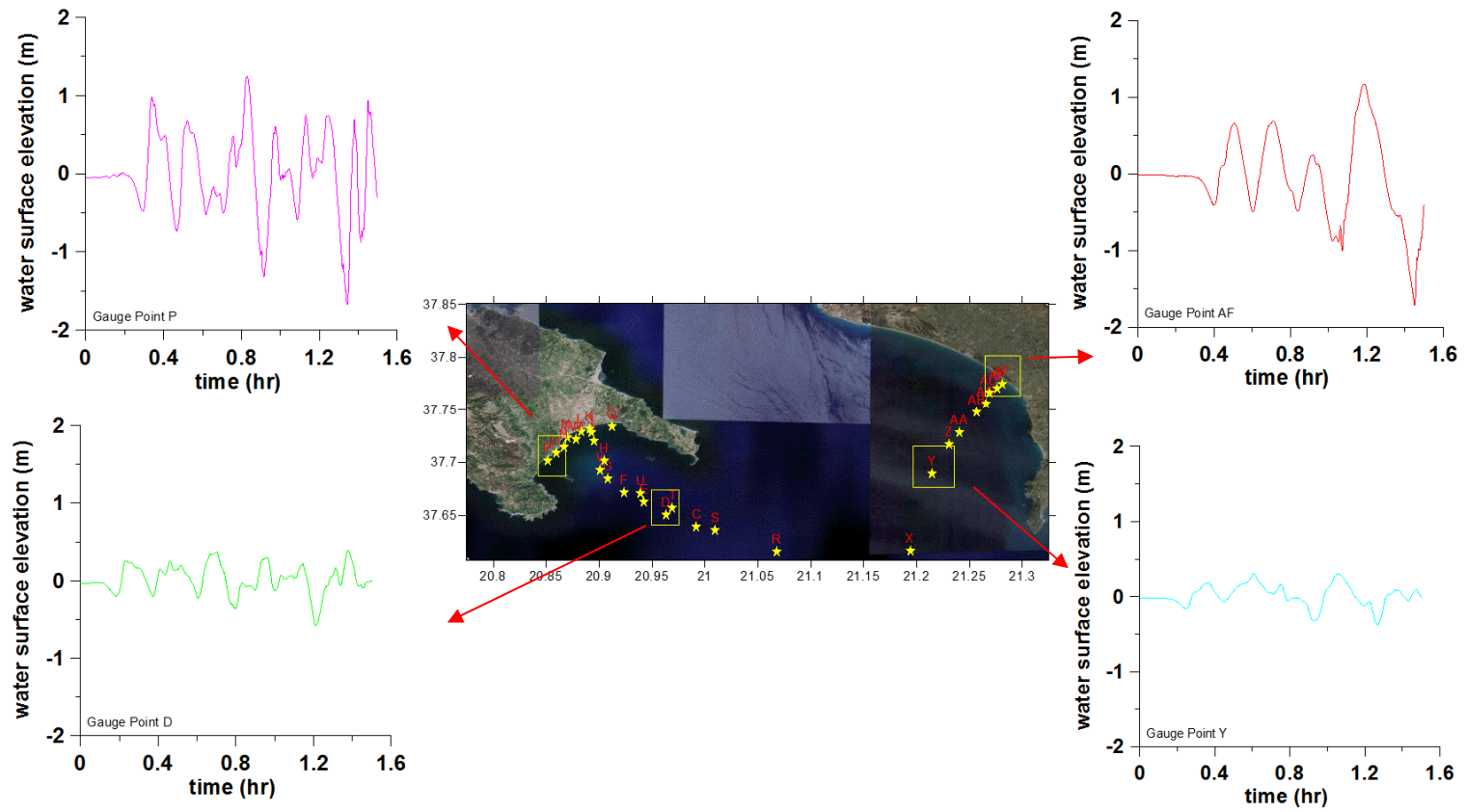


Figure 54: The time histories of water surface elevations (in hours) at selected gauge points at Domain C, Zakynthos

Domain D

The sea state at different time steps ($t=0, 16, 32, 48$ and 80 min), maximum positive and maximum negative tsunami amplitudes in the Domain D are given in *Figure 55* below. According to this figure, the maximum positive amplitude of tsunami is **1.89m**, and maximum negative amplitude is **-2.00m**.

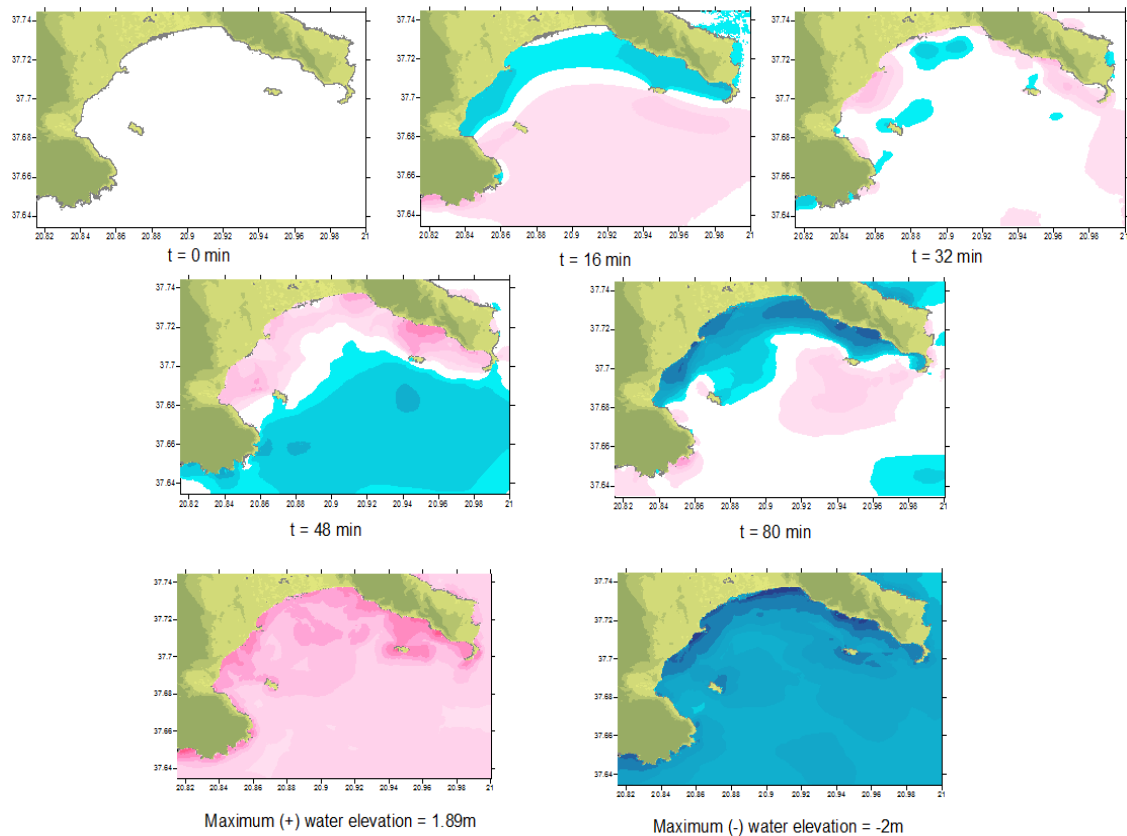


Figure 55: Propagation of tsunami for specific times, maximum positive and maximum negative wave amplitude in the Domain D

Gauge Locations at Domain D

Several gauge points that are selected are shown in *Figure 56*. The maximum positive amplitude of tsunami is **0.97m**, while maximum negative amplitude is -

1.43m. The water surface elevations, time of arrival of waves to these points are shown in *Figure 56*.

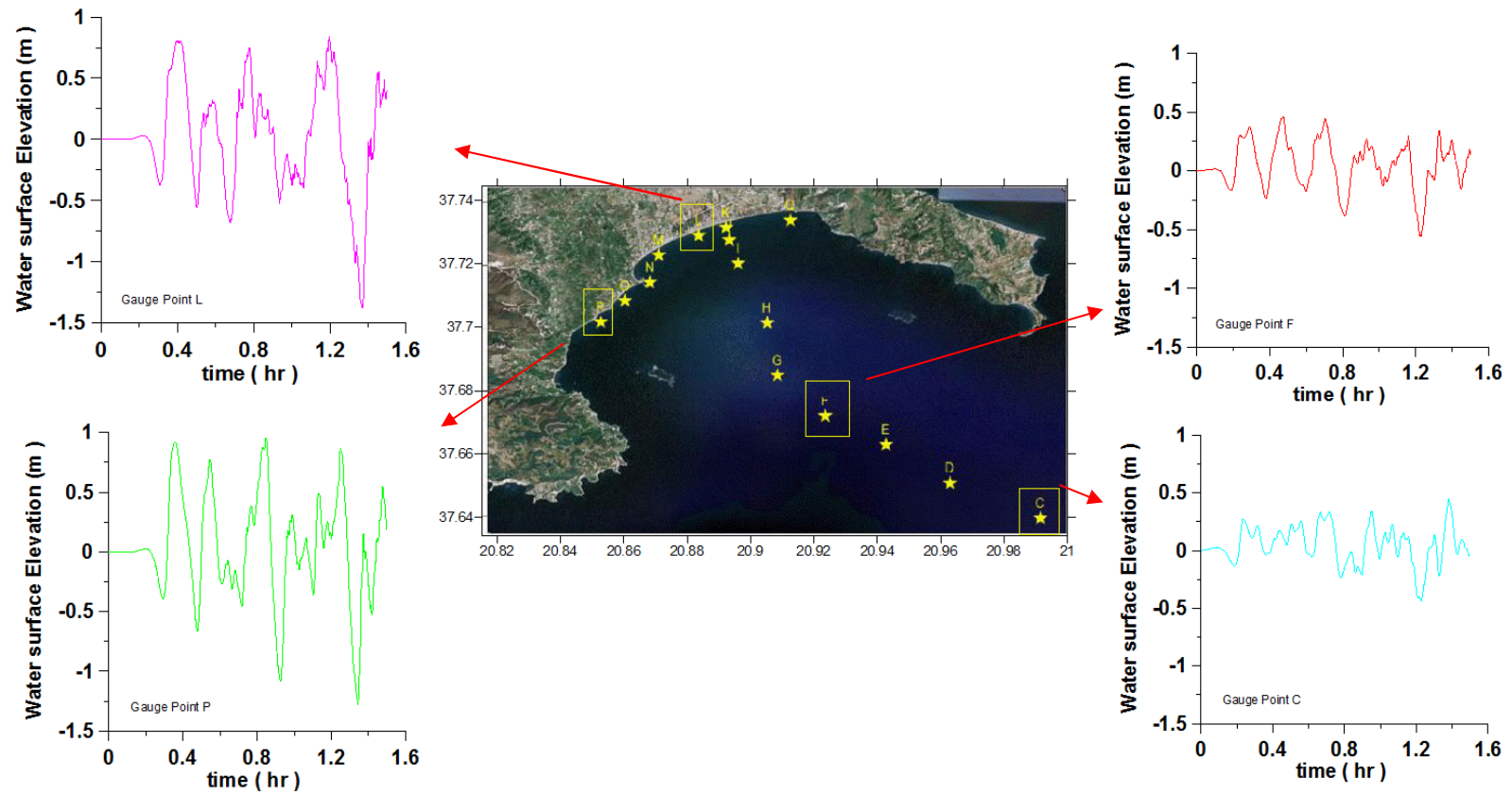


Figure 56: The time histories of water surface elevations (in hours) at selected gauge points at Domain D, Zakynthos

8.3.2.2 Tsunami Simulation of P04

If an earthquake in this region generates tsunami, the probable characteristics of tsunami source can be estimated by the following rupture characteristics. By using the rupture characteristics at *Table 9*, the initial wave parameters were generated with *TUNAMI-N3*

Propagation of P04 scenario in Kiparissia-Philiatra Region

Domain B

Wave Propagation of the selected tsunami with estimated rupture parameters was simulated. Maximum Positive wave amplitude is **5.69m** and maximum negative wave amplitude is **-4.47m** in the Domain B.

Domain C

Maximum positive wave amplitude is **4.94m** and maximum negative wave amplitude is **-3.62m** in the Domain C

Gauge Locations at Domain C

In order to compare the time histories of water surface elevations near Kiparissia-Philiatra, several gauge points are selected and the water surface elevations, time of arrival of waves to these points are shown in *Figure 57*. **4.1m** positive and **-2.2m** negative water amplitudes occur at Philiatra 1 Gauge point. The wave first arrives at point nearly 12 minutes after the rupture.

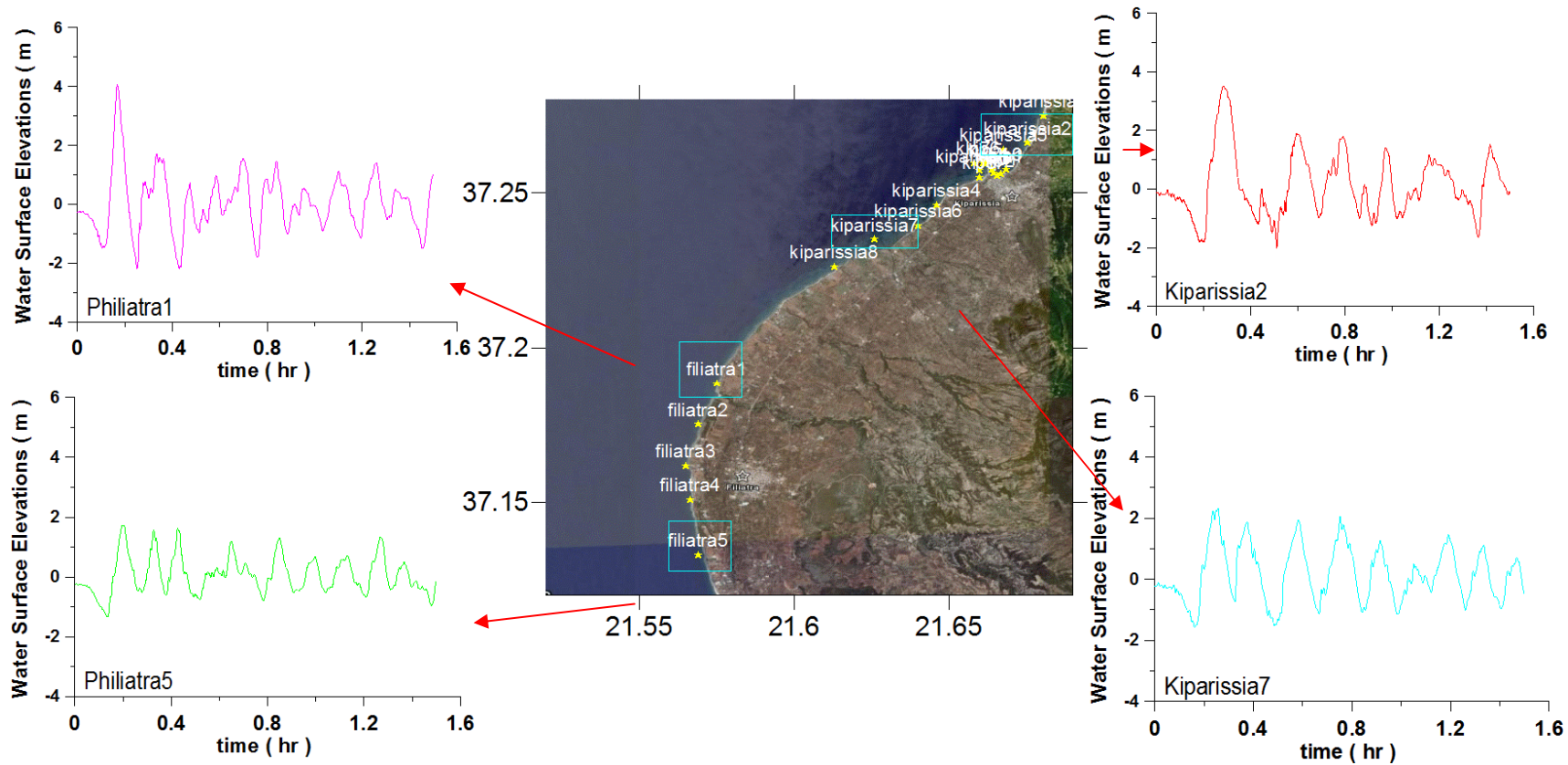


Figure 57: The time histories of water surface elevations (in hours) at selected gauge points at Domain C

Domain D

The sea state at different time steps ($t=0, 16, 32, 48$ and 80 min), maximum positive and maximum negative tsunami amplitudes in the Domain D were given in *Figure 58*. Maximum positive and maximum negative tsunami amplitudes in the Domain D (Kiparissia-Philiatra) are **2.62m** and **-2.14m** respectively.

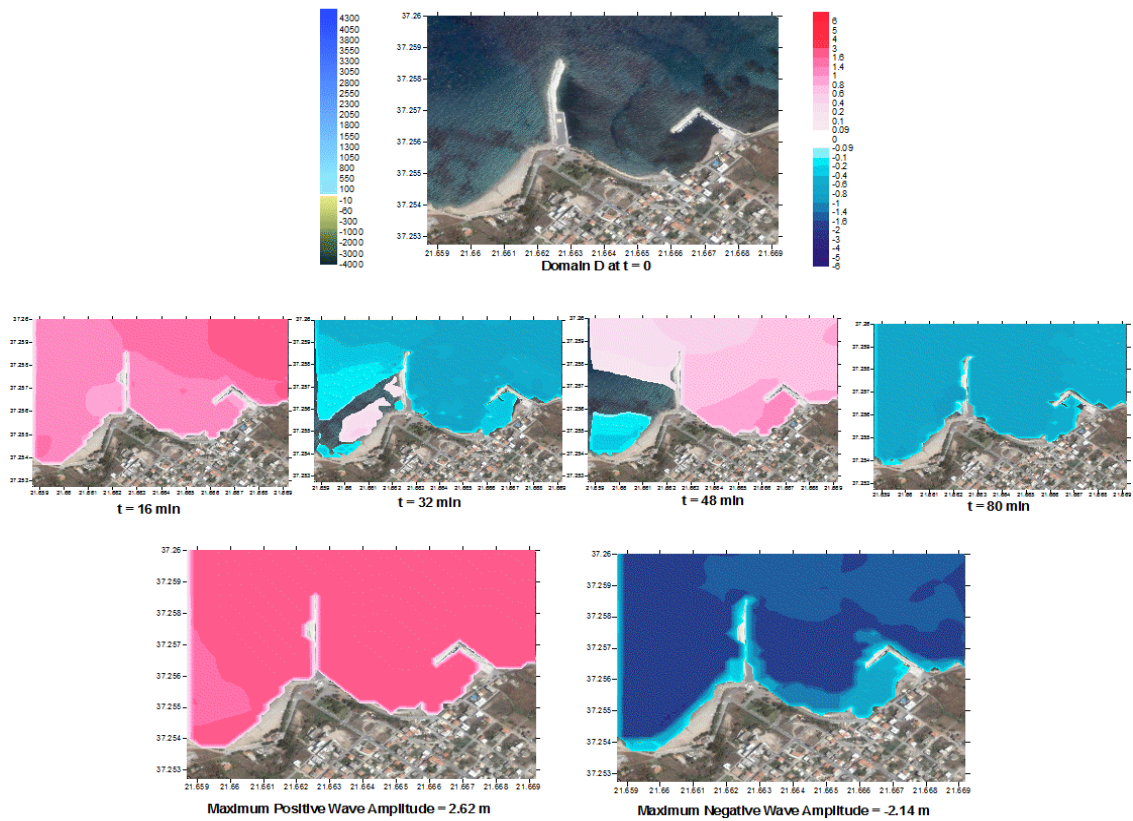


Figure 58: The Sea State at Different Time Steps and max (+) and max (-) tsunami amplitudes in the Domain D

Gauge Locations at Domain D

Several gauge points are selected and the water surface elevations, time of arrival of waves to these points are shown in *Figure 59*. As it is seen from the figure, the maximum positive water amplitude of tsunami is **2.30m** at gauge kip2, while maximum negative amplitude is **-1.90m** at kip8.

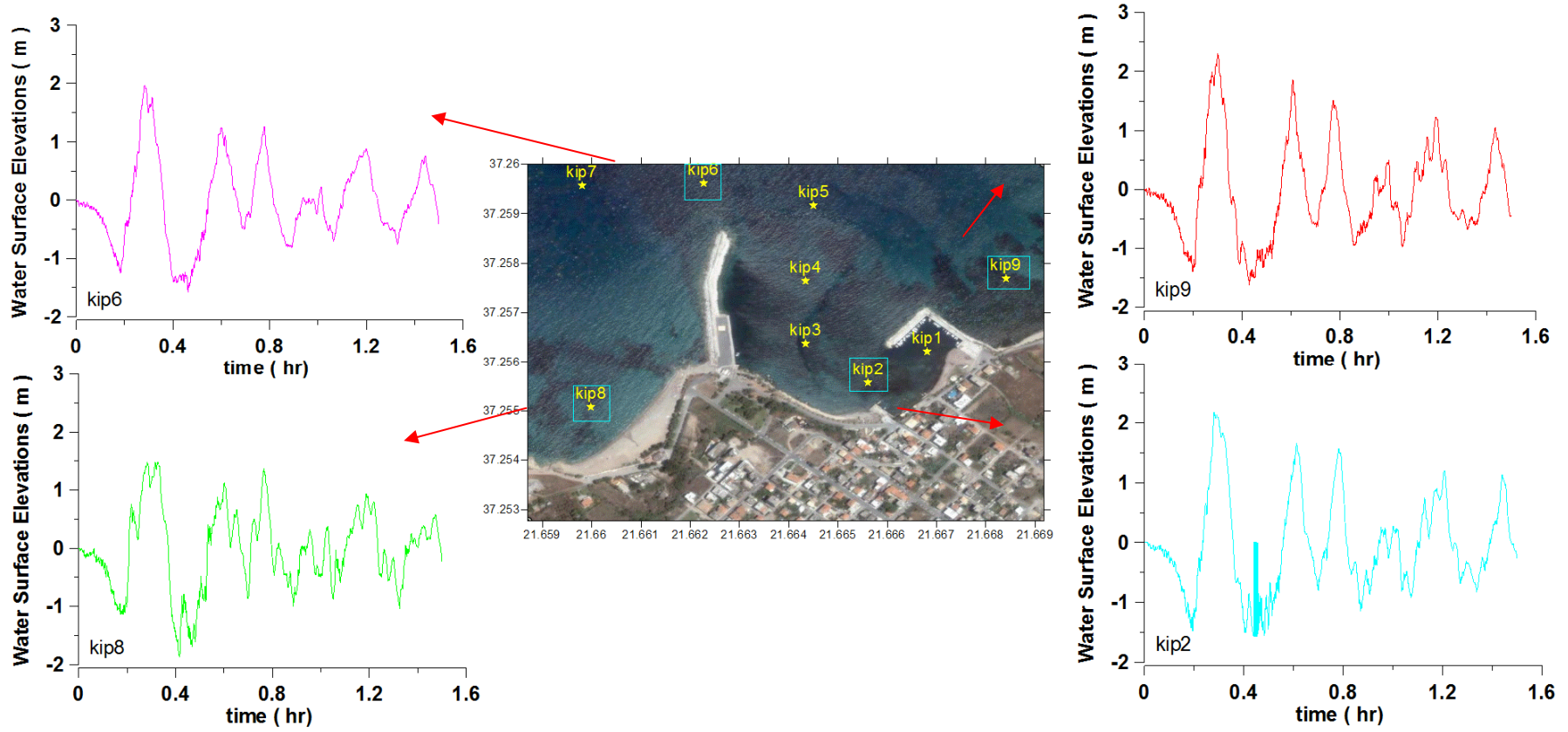


Figure 59: The time histories of water surface elevations at selected gauge points at Domain D

Propagation of P04 Scenario in Pylos Region

In this section, simulation of tsunamigenic earthquake scenario was made with the same source P04 and Domain B, but different C and D domains selected specifically for the Pylos Region.

Domain B

Since the propagation of the tsunami is same for Domain B given in simulation of Kiparissia-Philiatra region, the simulation and propagation of the tsunami is only shown for Domain C and Domain D in this section.

Domain C

Maximum positive wave amplitude is **5.63m** and maximum negative wave amplitude is **-4.57m** in the Domain C.

Gauge Locations at Domain C

Several gauge points were selected which were shown in *Figure 60*. As it is seen from the figure, the maximum positive water amplitude of tsunami is **1.62m**, while maximum negative amplitude is **-0.80m** at gauge point e. The water surface elevations, time of arrival of waves to these points are shown in *Figure 60*. The wave first arrives at point nearly 36 minutes after the rupture.

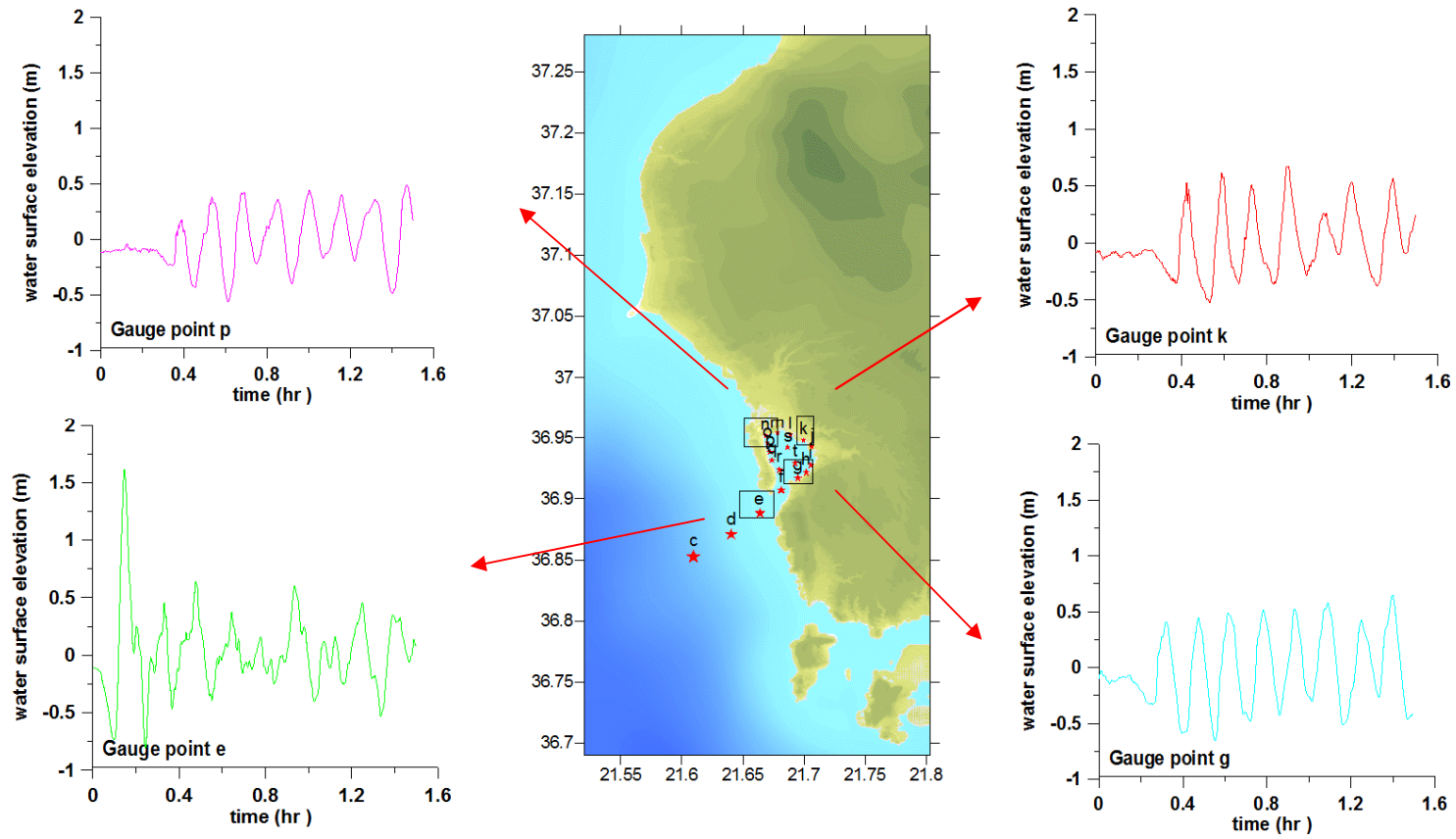


Figure 60: The time histories of water surface elevations (in hours) at selected gauge points at Domain C

Domain D

The sea state at different time steps ($t=0, 16, 32, 48$ and 80 min), maximum positive and maximum negative tsunami amplitudes in the Domain C are given in *Figure 61* below. According to this figure, the maximum positive amplitude of tsunami is **3.82m**, and maximum negative amplitude is **-2.68m**.

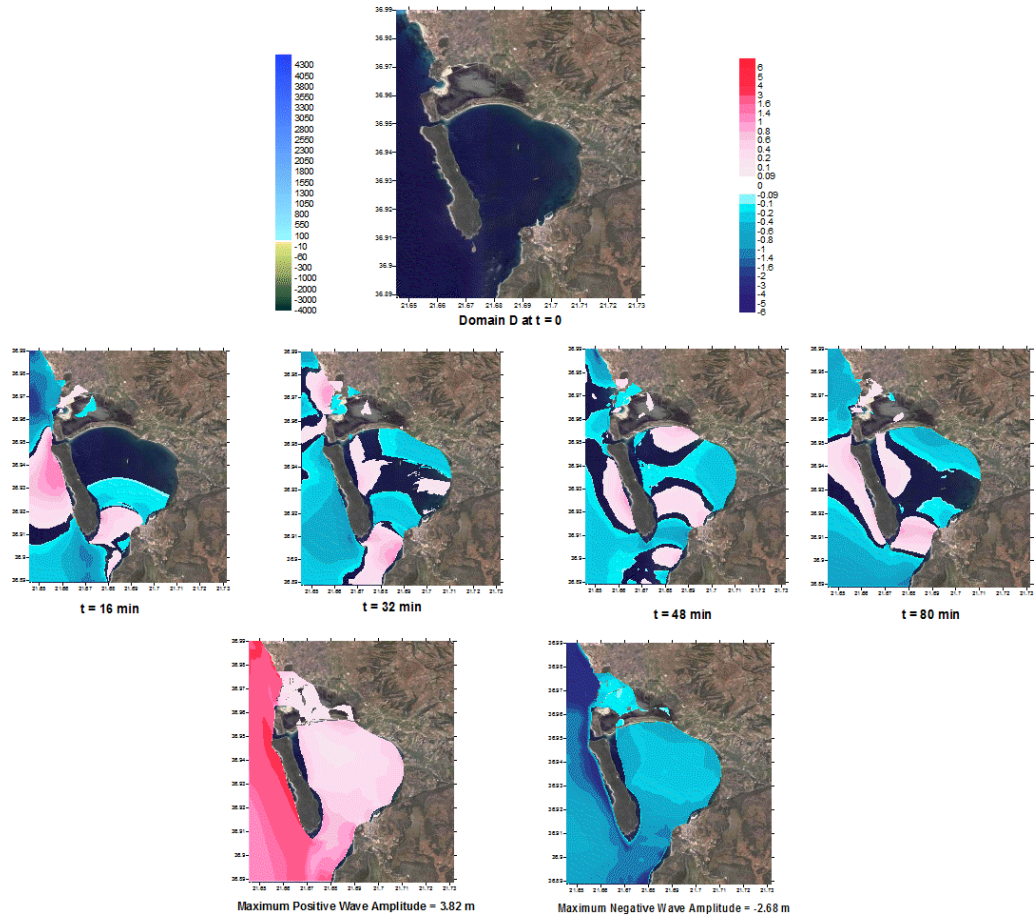


Figure 61: Propagation of tsunami for specific times. Distributions of max. (+) and max. (-) tsunami wave amplitude.

Gauge Locations at Domain D

Several gauge points are selected which are shown in *Figure 62*. The maximum positive amplitude of tsunami is **0.77m**, while maximum negative amplitude is - **1.00m** at gauge point f. The water surface elevations, time of arrival of waves to these points are shown in *Figure 62*.

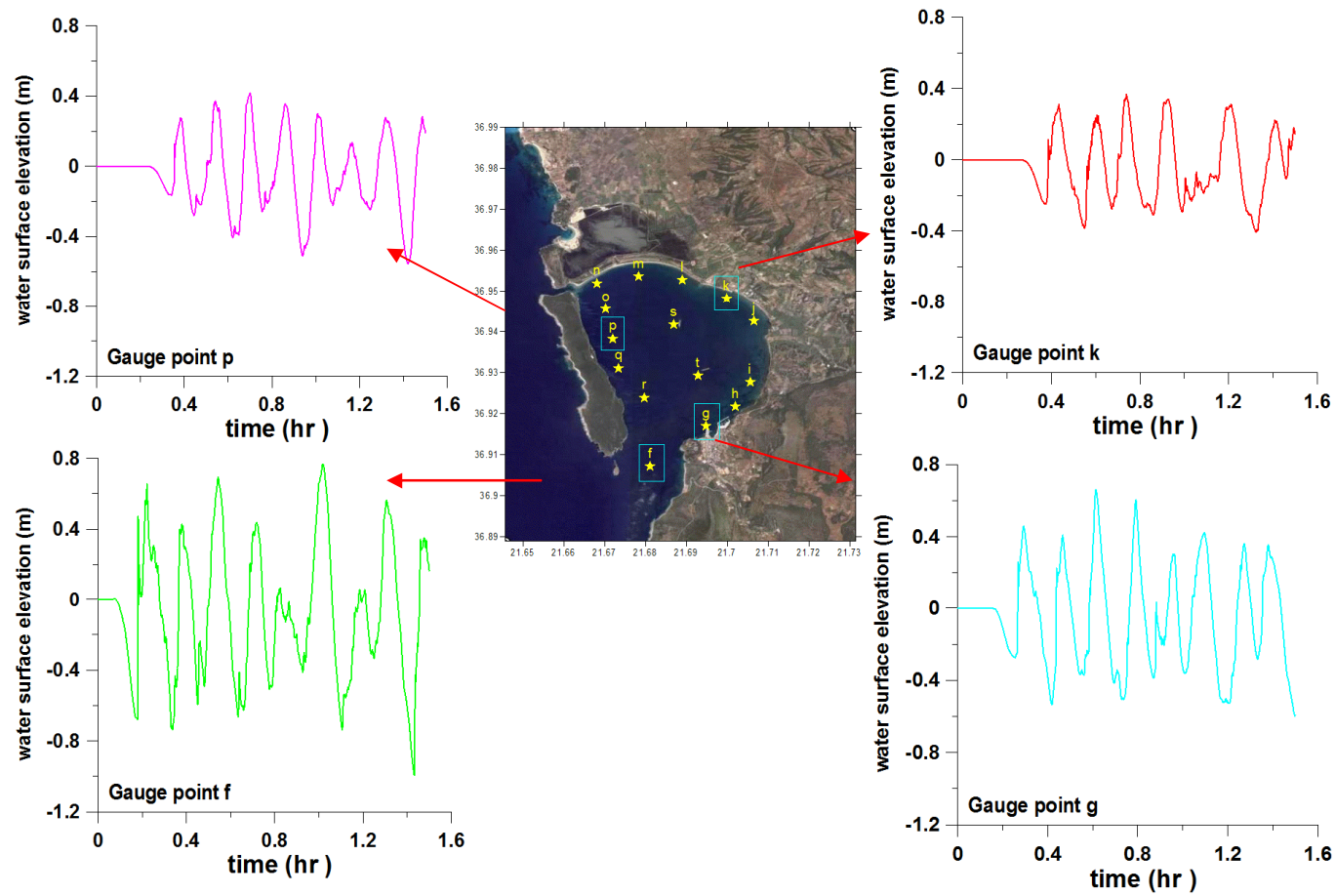


Figure 62: The time histories of water surface elevations (in hours) at selected gauge points at Domain D, Pylos

Propagation of P04 Scenario in Zakintos Region

Domain B

Wave propagation of the selected tsunami with estimated rupture parameters was simulated for Zakintos Region with given domains and the same source P04. The propagation of the Domain B is same with the simulation of Pylos and Kiparissia-Philiatra

Domain C

The maximum positive amplitude of tsunami is **8.14m**, and maximum negative amplitude is **-4.63m**.

Gauge Locations at Domain C

Several gauge points are selected which are shown in Figure 58. The maximum positive amplitude of tsunami is **2.70m** at gauge point p, while maximum negative amplitude is **-2.40m** at gauge point for selected gauge points. The water surface elevations, time of arrival of waves to these points are shown in *Figure 58*.

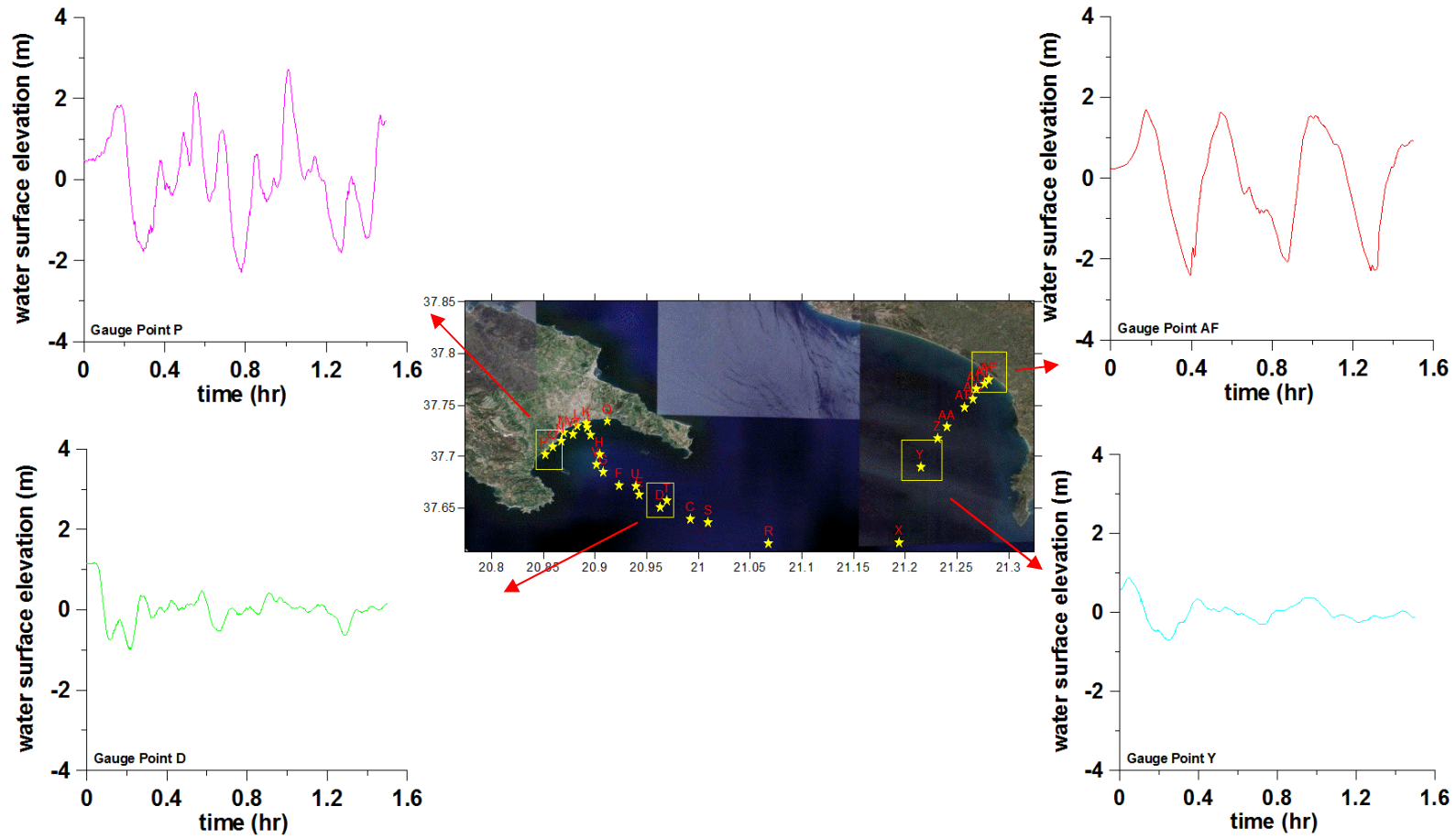


Figure 63: The time histories of water surface elevations (in hours) at selected gauge points at Domain C, Zakynthos

Domain D

The sea state at different time steps ($t=0, 16, 32, 48$ and 80 min), maximum positive and maximum negative tsunami amplitudes in the Domain D are given in *Figure 59* below. According to this figure, the maximum positive amplitude of tsunami is **2.58m**, and maximum negative amplitude is **-3.92m**.

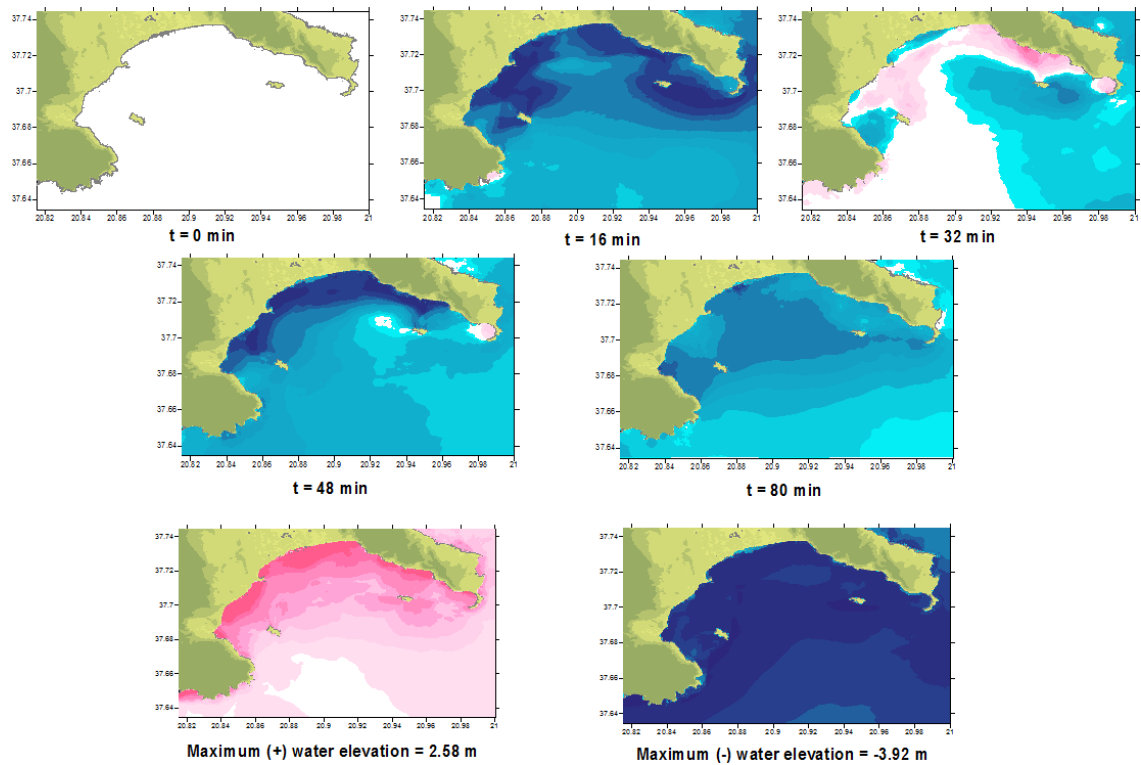


Figure 64: Propagation of tsunami for specific times. Max (+) and max (-) wave amplitude.

Gauge Locations at Domain D

Several gauge points were selected which are shown in *Figure 60*. The maximum positive amplitude of tsunami is **1.98m** at gauge point P, while maximum negative amplitude is **-2.78 m** at gauge point L. The water surface elevations, time of arrival of waves to these points are shown in *Figure 60*.

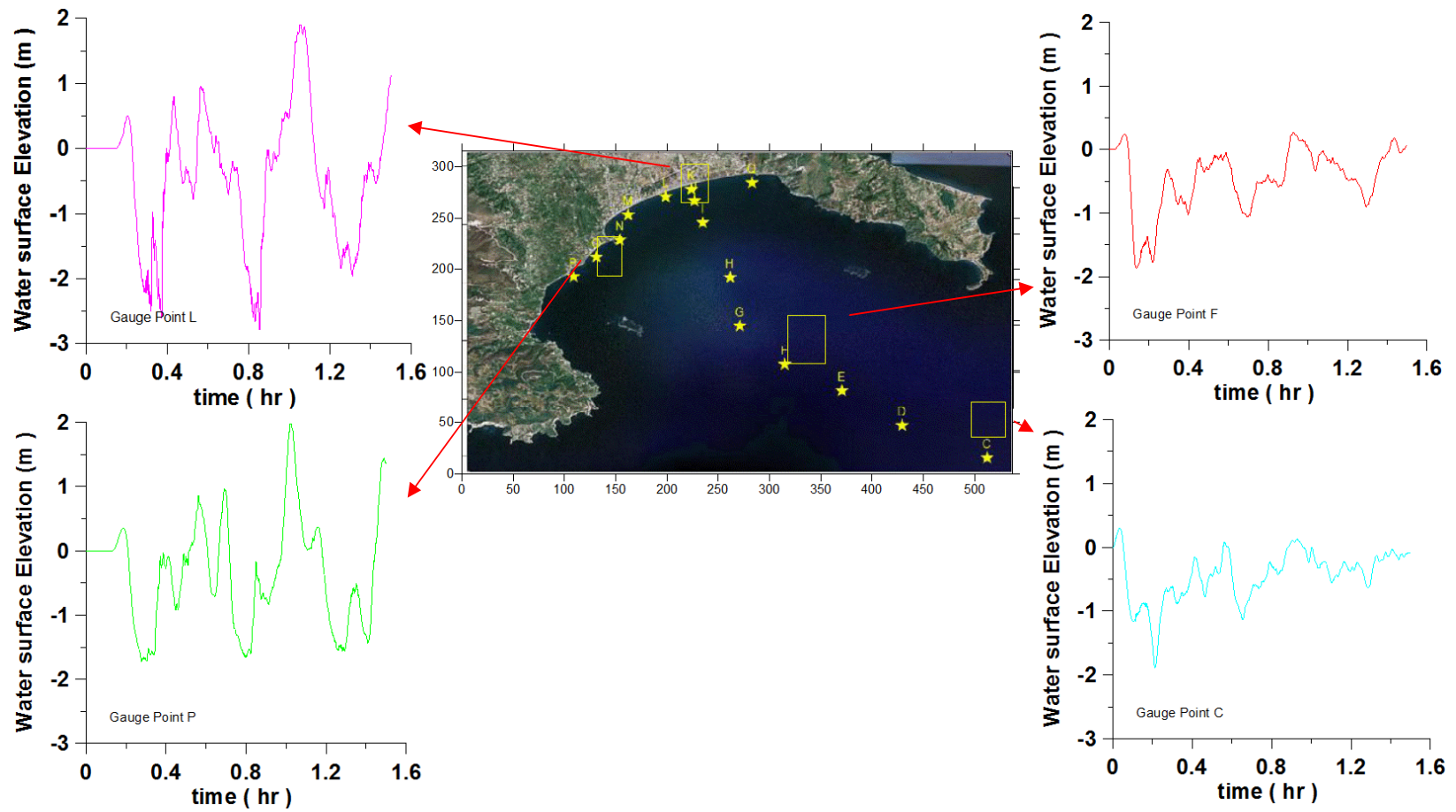


Figure 65: The time histories of water surface elevations (in hours) at selected gauge points at Domain D, Zakynthos

CHAPTER 9

SUMMARY OF THE SIMULATIONS P01 AND P04 SCENARIOS

The summary of the processes done for the simulations of surficial seismic zones P01 and P04 in previous chapters were given in this chapter as a table format.

Table 14 shows the rupture parameters and location of tsunamigenic source P01.

Table 13: Summary of the P01 Scenario-Input Values

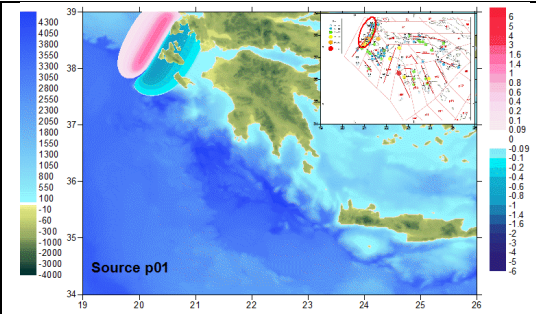
 <p>Source p01</p>	Epicenter Location	X=20.2 E Y=38.20N
	Length of Fault (km)	80
	Strike angle (deg. CW)	25
	Width of fault (km)	25
	Focal depth (km)	15
	Dip angle (degree)	10
	Slip angle (degree)	110
	isplacement (m)	6
	Height of initial wave (m)	2.49
	Maximum positive amplitude (m)	1.57
	Minimum negative amplitude (m)	-0.92

Table 15 shows the rupture parameters and location of tsunamigenic source P04.

Table 14: Summary of the P04 Scenario-Input Values

	Epicenter Location	X=20.765E Y=36.790N
	Length of Fault (km)	136
	Strike angle (deg. CW)	15
	Width of fault (km)	25
	Focal depth (km)	15
	Dip angle (degree)	10
	Slip angle (degree)	110
	Displacement (m)	6
	Height of initial wave (m)	2.53
	Maximum positive amplitude (m)	1.58
	Minimum negative amplitude (m)	-0.95

Table 15: Summary of the water surface elevations at selected gauge point

Regions and Sources	Domains	Gauges and water surface elevations			
		Philiatra1	Philiatra5	k2	k7
P01- Kiparissia- Philiatra	C	1.25	1.15	1.5	0.95
P04- Kiparissia- Philiatra	C	4.06	1.74	3.53	2.32
		e	p	k	g
P01-Pylos	C	0.27	0.45	0.55	0.52
P04-Pylos	C	1.62	0.49	0.67	0.65
		p	d	af	y
P01- Zakynthos	C	1.25	0.43	1.15	0.25
P04- Zakynthos	C	2.72	1.16	1.70	0.89
		kip6	kip8	kip9	kip2
P01- Kiparissia- Philiatra	D	0.94	0.97	1.01	1.15
P04- Kiparissia- Philiatra	D	1.97	1.49	2.30	2.19
		p	k	f	g

Table 16: Summary of the water surface elevations at selected gauge point
(cont.)

P01-Pylos	D	0.4	0.22	0.4	0.4
P04-Pylos	D	0.42	0.37	0.77	0.66
		L	P	f	c
P01- Zakynthos	D	0.56	0.89	0.4	0.35
P04- Zakynthos	D	1.91	1.98	0.27	0.30

Table 16 is the summary of the selected gauges in Domain C and Domain D for the scenarios. These gauges were arranged according to the city centers of the case studies ylos, Zakintos, Kiparissia and Philiatra. The results of Scenarios P01 and P04 were compared and it was seen that P04 was giving most critical results at these regions and domains.

With a high resolution bathymetric data, visualization of numerical modeling results as inundation maps in GIS allow quantitative evaluation of the inundation from a probable or historical tsunami.

The tsunami risk analysis, modeling, and mitigation measures are necessary for better preparedness and proper mitigation measures. Given the intense coastal landuse and recreational activities along the coast, even a small hazard may pose high risk.

Inundation distances are in the range of 10m along the western Greece coasts.

In the following figures, the flow depth distributions were given as a quantitative value. The yellow zones are low danger zones and the red ones are the high danger zones.

Flow depths were given quantitatively in *Figure 66, Figure 67 and Figure 68*.

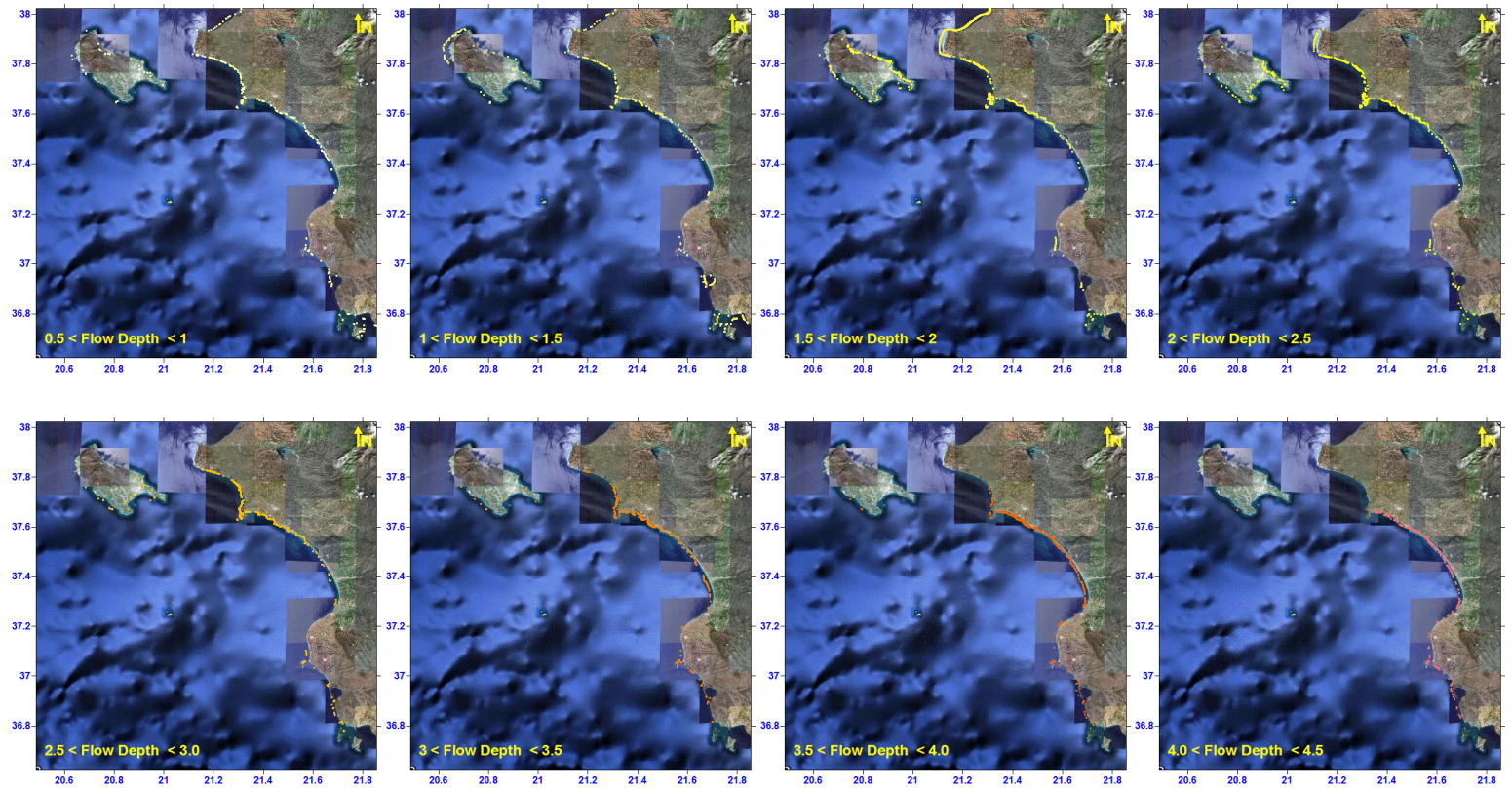


Figure 66: Flow depth distribution from 0.5 to 4.5 for the simulation of P01 in Western Greece

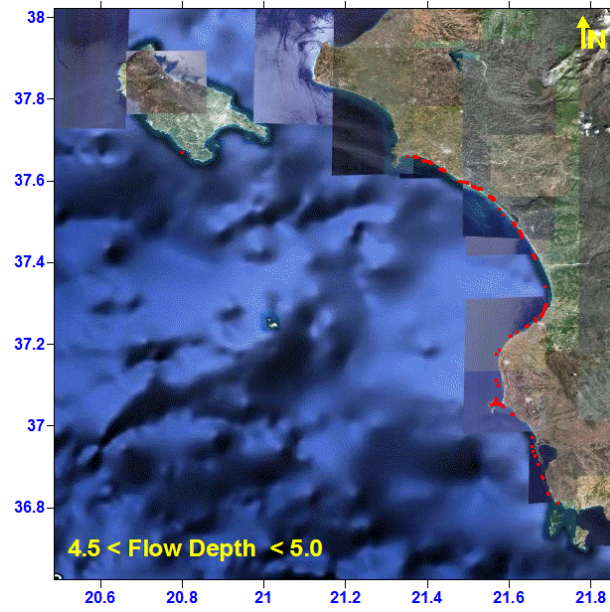


Figure 67: Flow depth distributions between 4.5 and 5

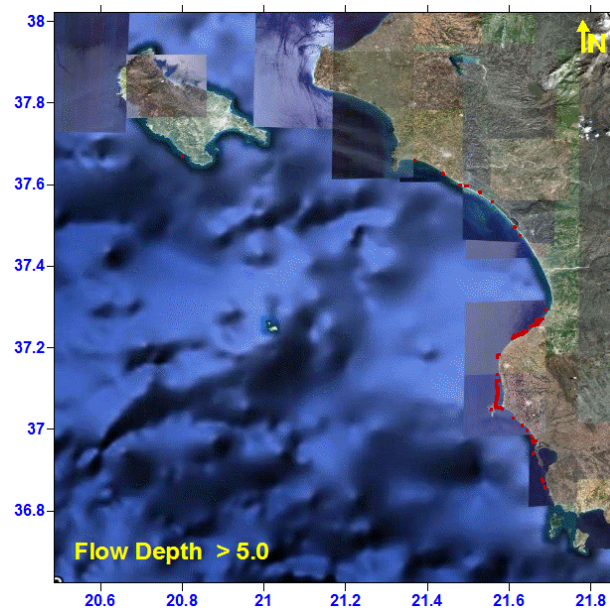


Figure 68 : Flow depth distributions greater than 4.5

As it is seen in *Figure 67* and *Figure 68*, Pylos, Kiparissia and Philiatra regions are located in high danger zones.

CHAPTER 10

DISCUSSION OF RESULTS AND CONCLUSION FOR THE SIMULATIONS OF PYLOS-ZAKINTOS-KIPARISSIA

The rupture characteristics of historical earthquakes that triggered tsunamis cannot be determined accurately by using only available instrumental seismic data. In order to perform tsunami modeling, the rupture characteristics are the most important input parameters as well as the high resolution bathymetric data and the fine grid simulations. The reliable and best possible higher resolution bathymetric data from ASTER satellite images at the near shore and land areas and the direct measurements of depth at the deep water area in SEAHELLARC Project have developed.

In this case study, the tsunami generation mechanisms and estimated the tsunami sources related to surficial zones described and characterized in Slejko (2008b) were evaluated. These sources are considered to be the possible tsunami sources in earthquakes that may occur in the region. They were also considered to be effective for the Pylos area and other additionally selected areas (Kiparissia, Philiatra and Zakynthos). These sources have been named as p01, p02, p03, p04, p05, p06, p10, p13 (from Slejko 2008b). However earthquakes occurring in other zones may also be capable of generating tsunamis. These may cause coastal effects at the nearest shoreline and should also be considered separately for those coastal areas.

Two complete simulations of the sources P01 and P04 were performed and the results were presented.

Model accuracy can be degraded by errors in the initial conditions set for the sea surface and water velocity, due to inadequate physics, and bathymetry/topography computational grid, due to inadequate spatial coverage, resolution and accuracy, including the difficult issues encountered in merging data from different sources. But for the case study region Kiparissia-Pylos-Philaitra and Zakintos, the data was adequate for good results.

Population at risk depends on the inundation zones of the region. Computational maximum tsunami flow depth is maximum in the Kiparissia-Philaitra region. In Pylos, the natural breakwater protects the city from tsunami waves. Therefore, there may be no significant loss of human lives

The author hopes that the simulations of a range of plausible scenarios will motivate better assessments of site-specific tsunami hazard along the western Greece coasts especially for Kiparissia- Philaitra and Pylos regions located in high danger zones and help accelerate hazard mitigation activities in the region.

CHAPTER 11

SUGGESTIONS FOR THE FUTURE

GIS Analysis can be done to be able to access essential community facilities which significantly impaired due to transportation infrastructure damage during an earthquake or tsunami.

The evacuation processes can be estimated with the output of this thesis. Detailed risk assessment can be done for emergency purposes.

Tsunami forecasting tools based on latest modeling techniques can guide emergency managers during tsunami events. It is impossible to provide a warning forecast for the closest coasts. But even a late forecast will still provide valuable assessment guidance to emergency managers responsible for critical decisions regarding response, recovery and search-and-rescue.(Titov,2005). Therefore an early warning system should be deployed for the Mediterranean Sea before facing with devastating events that can cause loss of human and materials.

If a tsunami warning system establishes to the Mediterranean, the scenarios of tsunamis can be increased and the results of the simulations of these scenarios can be used in case of an emergency. When the next great earthquake strikes the western Greece, the communities of Greece must more adequately be prepared.

REFERENCES

- Alptekin** Ö., Nabalek J. L., and Toksöz N. “3 Eylül 1968 Bartın Depreminin kaynak mekanizması ve Karadeniz’in aktif tektonigi hakkında düşünceler” *Deprem Arastırma Bülteni*, 50, 5–28, (1985)
- Altinok** Y. and Ersoy Ş., “Tsunamis observed on near the Turkish Coast”, Kluwer Academic Publishers, *Journal of Natural Hazards* 21, 185-199, (2000)
- Altinok**, Y. and Ersoy S., “Tsunamis in the Aegean Sea and near surroundings”, *International Earth Sciences Colloquium on the Aegean Region*, Izmir, pp.215–222, (1995)
- Altinok**, Y., Ersoy S., Yalciner, A.C., Alpar B. And Kuran U., “Historical Tsunamis in the Sea of Marmara”, *International Tsunami Symposium*, Session 4, Paper 4-2, Seattle, pp: 527-535, (2001)
- Ambraseys** N. N. and Jackson J. A., “Seismicity and associated strain of central Greece between 1890 and 1988”, *International Geophysical Journal*, 101, 663–708, (1990)
- Ambraseys**, N.N. “Catalogue of Tsunamis in the Eastern Mediterranean from Antiquity to Present Times”, *Annali di Geofisica*, Vol. 32, pp. 113-130, (1962)
- Borrero** J. C., Sieh K., Chlieh M., Synolakis C.E., “Tsunami Inundation Modeling for Western Sumatra”, *PNAS*, vol:103, 19673-19677, (2006)
- Chandrasekar** N., Immanuel J.L., Sayaham J. D., Rajamanickam M., Saravanan S. “Appraisal of Tsunami Inundation and Run-up along the coast of Kanyakumari District, India”, *GIS Analysis*, (2007)

Cita M.B., Rimoldi B., “Geological and Geophysical Evidence for a Holocene Tsunami Deposit in the Eastern Mediterranean Deep-Sea Record”, *J. Geodynamics*, Vol.24. No:1-7 pp. 293-304, (1997)

Cox D., “Tsunami Inundation with macro-roughness in the constructed environment”, *ICCE 2008*, Hamburg, (2008)

Dawson A.G., Lockett P., Shi S., “Tsunami Hazards in Europe”, *Environment International*, 30 (2004) 577-585, (2003)

Galanopoulos, A.G. “Tsunamis Observed on the Coasts of Greece from Antiquity to Present Time”, *Annali di Geofisica*, Vol. 13, pp. 369-386, (1960)

Goto, C. and Ogawa, Y., “Numerical Method of Tsunami Simulation With the Leap-Frog Scheme”, Translated for the TIME Project by Prof. Shuto, N., Disaster Control Res. Cent., Faculty of Eng., Tohoku Univ. Sendai, Japan, (1991)

Guidoboni, E., Comastri, A., and Traina, G., “Catalogue of Ancient Earthquakes in the Mediterranean Area up to the 10th Century”, *Istituto Nazionale di Geofisica*, Rome (1994).

Hart D.E., Knight G.A., “Geographic Information System Assessment of Tsunami Vulnerability on a Dune Coast”, *Journal of Coastal Research*, vol:25, pp.131-141
ITIC, General Tsunami Terms, 2005, Mediterranean”, *Bulletin of the Seismological Society of America*, Vol. 52, pp. 895-913, (2009)

Jackson, J. and McKenzie, D., “Active tectonics of the Alpine-Himalayan Belt between Turkey and Pakistan”, *Geophysical Journal*. **77**, 185–264, (1984)

Jackson, J. and McKenzie, D.: The relationship between plate motion and seismic moment tensors and the rates of active deformation in the Mediterranean and Middle East, *Geophys. J.***93**, 45–73, (1988).

Johnson R. (2000), “GIS Technology for Disasters and Emergency Management”, ESRI White Paper.

Karnik, V. “Seismicity of the European Area”, Vol. 2, Reidel, Dordrecht, Holland (1971).

Ketin, I. and Abdüsselamoglu, S., “Bartın Depreminin etkileri”, *TJK Bülteni* XII(1–2) 66–77, (1969).

KOERI, “Earthquake Database of Bosphorus University, Kandilli Observatory and Earthquake Research Institute” , (2004)

Kuran, U. and Yalçın, A. C., “Crack propogations earthquakes and tsunamis in the vicinity of Anatolia”,

METU-OERC, (2008a), “Wednesday, February 20, 2008 at 18:27:11 SOUTHERN GREECE Earthquake Simulation Analysis of Possible Tsunami in the Region Effecting Pylos Area”, SEAHELLARC Internal Report on June 28, 2008.

METU-OERC, (2008b), Bathymetry and Topography Data Processing, Tsunami Modelling and Visualization for Western Coast of Greece, SEAHELLARC Interim Report for the Second Annual Meeting in Pylos, June, 2008

Murty, T. S., “Seismic Sea Waves Tsunamis”, *Department of Fisheries and the Environment Fisheries and Marine Service*, Scientific Information and Publication Branch, Ottawa, Canada, (1977).

Nikonov, A., “Tsunami – a threat from the south?” *Search and Development, Science in Russia* 6 13–19, (1997).

Okada, Y., “Surface Deformation Due to shear and Tensile Faults in a Half-space”, *Bulletin Seismological Society America*, 75, 1135-1154, (1985).

Papadopoulos G. A., Daskalaki E., Fokaefs A., and Giraleas N., “ Tsunami hazards

in the Eastern Mediterranean: strong earthquakes and tsunamis in the East Hellenic Arc and Trench system”, *Nat. Hazards Earth Syst. Sci.*, 7, 57–64, (2007)

Papadopoulos G.A., “Tsunamis in the East Mediterranean, A Catalogue for the Area of Greece and Adjacent Seas”. In: *Proc. Joint IOC-IUGG International Workshop Tsunami Risk Assessment Beyond 2000: Theory, Practice & Plans*, Moscow, pp 34–43, (2000).

Papadopoulos G.A. and Fokaefs A., (2005), “Strong Tsunamis in the Mediterranean Sea; A re-evaluation”, *ISET Journal of Earthquake Technology*, Paper No. 463, Vol. 42, No. 4, pp. 159-170, (2005)

Papadopoulos G. A. and Chalkis, B. J., “Tsunamis observed in Greece and the surrounding area from antiquity to the present times”, *Marine Geol.* **56** (1984), 309–317.

Papadopoulos G. A., “Seismic faulting and nonseismic tsunami generation in Greece”, In: *Proc. IUGG/IOC International Tsunami Symposium, 23–27 August, Wakayama Japan* (1993) pp.115–123.

Papadopoulos G.A. and Chalkis, B.J. (1984). “Tsunamis Observed in Greece and the Surrounding Area from Antiquity up to the Present Times”, *Marine Geology*, Vol. 56, pp. 309-317.

Papadopoulos G.A., (2003), “Tsunami Hazard in the Eastern Mediterranean: Strong Earthquakes and Tsunamis in the Corinth Gulf, Central Greece”, *Natural Hazards* 29:437-464

Pınar A., “Rupture Process and Spectra of Some Major Turkish Earthquakes and Their Seismotectonic Implications”, *PhD Thesis*, Bogaziçi Üniversitesi, Istanbul (1995).

Poirier J. P. and Taher, M. A., “Historical seismicity in the near and middle east, North Africa, and Spain from Arabic documents (VII–XVIIIth century)”, *Bulletin*

Seismological Society Am. 70 2185–2201, (1980)

Prasetya G.S., Healy T.R., Lange W.P., Black K.P., “Extreme Tsunami Run Up and Inundation Flows at Banda Aceh, Indonesia: Are there any solutions to this type of coastal disaster?” *Natural Hazards*, (2008)

Ranguelov B., “Earthquakes and tsunami hazards in the Black Sea”, In: *Abstract Book of the First Congress of the Balkan Geophysical Society*, 23–27 September, Athens (1996), pp. 44–45. *Res.* **65**(4) 1257–1265., (1996)

Sanyal J., Lu X.X., “Application of GIS in flood hazard Mapping: A case study of Gangetic West Bengal, India”, *Natural Hazards*, (2009).

SEHELLARC, WP4-Deliverable D11, D12 and D13 Report-ATLAS, (2009)

Sengör A. M. C., Büyükasıkoğlu S., and Canitez N., “Neotectonics of the Pontides: Implications for ‘incompatible’ structures along the North Anatolian Fault”, *J. Struct. Geol.* **5** 211–216 (1983),

Shebalin N. V., Karnik V. and Hadzievski D., “Catalogue of Earthquakes”, *UNESCO*, Skopje, Yugoslavia, (1974).

Slejjko Dario, “WP5 Seismic Hazard Assessment”, *Interim Report in SEHELLARC Project*, June 2008a.

Slejjko Dario, “WP5 Seismic Hazard Assessment”, *Interim Report in SEHELLARC Project*, June, (2008b).

Slejjko Dario, “WP5 Seismic Hazard Assessment”, *Interim Report in SEHELLARC Project*, (2009)

Soloviev S. L., “Tsunamigenic zones in the Mediterranean Sea”, *Natural Hazards* 183–202, (1990).

Stiros C.S., The AD 365 Crete Earthquake And Possible Seismic Clustering During the Fourth to Sixth Centuries AD in the Eastern Mediterranean, A Review Of Historical And Archaeological Data, *Journal of Structural Geology* 23 (2001) pp: 545-56(2003):

Synolakis C.E., Bernard E.N., Titov V., Kânoğlu U., González F., Standards, Criteria, And Procedures For NOAA, Evaluation of Tsunami Numerical Models, *NOAA Technical Memorandum OAR PMEL-135* (2007),

Synolakis C. E., Liu, P. L. F., Yeh, H. Workshop on Long Wave Runup Models, *NSF in Catalina Island* LA, USA, June 2004. (2004):

Synolakis C.E., Borrero J. Eisner R., “Developing Inundation Maps for Southern California”, *Coastal Disasters*, (2002)

Taymaz T. Yılmaz T., Dilek Y., “The Geodynamics of the Aegean and Anatolia”, *Geological Society of London, Special Publications*, 291,201-230, (2007)

Taymaz T., Yolsal, S., Yalciner, A. C., Understanding Tsunamis, Potential Source Regions and Tsunami- Prone Mechanisms in the Eastern Mediterranean, from the Geodynamics of the Aegean and Anatolia, (Eds. Taymaz. T, Yılmaz Y., Dilek Y.), Geological Society, London, Special Publications, 291., pp: 201-230(2007):

Tinti S., Gavagni I., Piatanesi A., A finite-element numerical approach for modeling tsunamis, *Annali di Geofisica*, Vol XXXVII, N.5, 1994

Tinti S. and Maramai, A. “Catalogue of Tsunamis Generated in Italy and in Côte d’ Azur, France: A Step towards a Unified Catalogue of Tsunamis in Europe”, *Annali di Geofisica*, Vol. 39, pp. 1253-1299. (1996).

Tinti S., Maramai, A. and Graziani, L “The New Catalogue of Italian Tsunamis”, *Natural Hazards*, Vol. 33, No. 3, pp. 439-465.(2004).

Titov V.V., Gonzalez F.I., Bernard E.N., Eble M.C., Mofjeld H.O., Newman J.C. and Venturato A.J., Real-time Tsunami Forecasting: Challenges and Solutions, *Natural Hazards* 35:41-58 (2005)

UNESCO Tsunami Glossary, UNESCO-IOC. IOC Information document No. 1221 Printed by Servicio Hidrográfico y Oceanográfico de la Armada (SHOA) Errázuriz 254 Playa Ancha Valparaíso Chile Published by the United Nations Educational, Scientific and Cultural Organization 7 Place de Fontenoy, 75 352 Paris 07 SP, France UNESCO, (2006),

Wood N.J., Good J.W., “Vulnerability of Port and Harbor Communities to Earthquake and Tsunami Hazards”, *The use of GIS in Community Hazard Planning*, vol:32, pp. 243-269(2003)

Wyss, M. and Baer, M., “Earthquake hazard in the Hellenic Arc”, reprinted from *Earthquake Prediction – An International Review*, Maurice Ewing Series 4, American Geophysical Union(1981), pp. 153–172

Yalciner A.C, Demirbaş E., Pelinovski E.N., Imamura F., Synolakis E.C., “Amplitude Evaluation and Runup of Solitary Waves on a Sloping Plane”, *Kamchatsky Tsunami Workshop*, (2002).

Yalciner A. C., Pelinovsky, E. Zaytsev, A., Kurkin A., Ozer C., and Karakus H., “NAMI DANCE Manual”, *METU, Civil Engineering Department, Ocean Engineering Research Center*, Ankara, Turkey,(2006)

Yalciner A. C., Synolakis, C. E., Gonzales, M., Kanoglu, U., “Joint Workshop on Improvements of Tsunami Models, Inundation Map and Test Sites of EU TRANSFER Project”, Fethiye, Turkey, (2007):

Yalciner A.C., Alpar, B., Altinok, Y., Ozbay, I., Imamura, F., “Tsunamis in the Sea of Marmara: Historical Documents for the Past, Models for Future”, *Marine Geology*, 190, pp: 445-463, (2002)

Yalciner A.C., Imamura, F., Synolakis, E.C., “Simulation of Tsunami Related to Caldera Collapse and a Case Study of Thera Volcano in Aegean Sea”, *EGS XXVII General Assembly, Nice, France, April 2002 Session NH8*, (2002)

Yalciner A.C., Kuran, U., Akyarli, A. And Imamura, F., “An Investigation on the Generation and Propagation of Tsunamis in the Aegean Sea by Mathematical Modeling”, Chapter in the Book, "Tsunami: Progress in Prediction, Disaster Prevention and Warning", in the book series of *Advances in Natural and Technological Hazards Research by Kluwer Academic Publishers* Ed. Yashuito Tsuchiya and Nobuo Shuto, pp 55-71, (1995)

Yalciner A.C., Pelinovsky, E.N., Talipova, T.G., Kurkin, A.A., Kozelkov, A.C., Zaitsev, A.I., “Tsunamis in the Black Sea”, *International Workshop on Local Tsunami Warning and Mitigation*, Petropavlovsky, Kamcahtka, Russia, (2002)

Yalciner, A.C., Karakus, H., Ozer, C., Ozyurt, G., (2005), “Short Courses on Understanding the Generation, Propagation, Near and Far-Field Impacts of TSUNAMIS and Planning Strategies to Prepare for Future Events” Course Notes prepared by METU Civil Eng. Dept. Ocean Eng. Res. Center Ankara, Turkey, for the Short Courses in the University of Teknologi Malaysia (UTM) held in Kuala Lumpur on July 11-12, 2005, and in Technology Development Division, Astronautic Technology (M) Sdn. Bhd (ATSB) Malaysia held in Kuala Lumpur on April 24-May 06, 2006, and in UNESCO Training Course I on Tsunami Numerical Modeling held in Kuala Lumpur on May 08-19 2006 and in Belgium Oostende on June 06-16, 2006

Zaytsev A., Karakus H., Yalciner A. C., Chernov A., Pelinovsky E., Kurkin A., Ozer C., Insel I., Ozyurt G., Dilmen D. I., “Tsunamis in Eastern Mediteranean; Histories, Possibilities and Realities”, VII.th International Conference on Coastal and Port Engineering in Developing Countries, COPEDEC VII, Dubai, Paper No: Z-012008,(2006)

Zerger A., “Examining GIS decision utility for natural hazard risk modeling,Environmental Modeling and Software”, *Elsevier*, pp.287-294. (2002)

